(2)

GL-TR-90-0330

NORSAR Basic Seismological Research, 1 October 1989–30 September 1990

Editor:
S. Mykkeltveit

NTNF/NORSAR
Post Box 51
N-2007 Kjeller, Norway

29 November 1990

Scientific Report No. 7

APPROVED FOR PUBLIC RELEASE; DISTRIBUTION UNLIMITED

GEOPHYSICS LABORATORY
AIR FORCE SYSTEMS COMMAND
UNITED STATES AIR FORCE
HANSCOM AIR FORCE BASE, MASSACHUSETTS 01731-5000

SPONSORED BY
Defense Advanced Research Projects Agency
Nuclear Monitoring Research Office
ARPA ORDER NO. 5307

MONITORED BY
Geophysics Laboratory
F49620-89-C-0038

The views and conclusions contained in this document are those of the authors and should not be interpreted as representing the official policies, either expressed or implied, of the Defense Advanced Research Projects Agency or the U.S. Government.

This technical report has been reviewed and is approved for publication.

JAMES F. LEWKOWICZ
Contract Manager
Solid Earth Geophysics Branch
Earth Sciences Division

JAMES F. LEWKOWICZ
Branch Chief
Solid Earth Geophysics Branch
Earth Sciences Division

FOR THE COMMANDER

DONALD H. ECKHARDT, Director
Earth Sciences Division

This report has been reviewed by the ESD Public Affairs Office (PA) and is releasable to the National Technical Information Service (NTIS).

Qualified requestors may obtain additional copies from the Defense Technical Information Center. All others should apply to the National Technical Information Service.

If your address has changed, or if you wish to be removed from the mailing list, or if the addressee is no longer employed by your organization, please notify GL/IMA, Hanscom AFB, MA 01731-5000. This will assist us in maintaining a current mailing list.

Do not return copies of this report unless contractual obligations or notices on a specific document requires that it be returned.

Unclassified

SECURITY CLASSIFICATION OF THIS PAGE

REPORT DOCUMENTATION PAGE

Form Approved OMB No. 0704-0188

1a. REPORT SECURITY CLASSIFICATION: Unclassified	1b. RESTRICTIVE MARKINGS
2a. SECURITY CLASSIFICATION AUTHORITY	3. DISTRIBUTION/AVAILABILITY OF REPORT: **Approved for public release; Distribution unlimited**
2b. DECLASSIFICATION/DOWNGRADING SCHEDULE	
4. PERFORMING ORGANIZATION REPORT NUMBER(S)	5. MONITORING ORGANIZATION REPORT NUMBER(S): GL-TR-90-0330
6a. NAME OF PERFORMING ORGANIZATION: NTNF/NORSAR; 6b. OFFICE SYMBOL (If applicable)	7a. NAME OF MONITORING ORGANIZATION: Geophysics Laboratory
6c. ADDRESS (City, State, and ZIP Code): Post Box 51, N-2007 Kjeller, Norway	7b. ADDRESS (City, State, and ZIP Code): Hanscom Air Force Base, Massachusetts 01731-5000
8a. NAME OF FUNDING/SPONSORING ORGANIZATION: Defence Advanced Research Projects Agency; 8b. OFFICE SYMBOL (If applicable): NMRO	9. PROCUREMENT INSTRUMENT IDENTIFICATION NUMBER: Contract No. F4962C 89-C-0038
8c. ADDRESS (City, State, and ZIP Code): 1400 Wilson Blvd., Arlington, VA 22209-2308	10. SOURCE OF FUNDING NUMBERS: PROGRAM ELEMENT NO. 62714E; PROJECT NO. 9A10; TASK NO. DA; WORK UNIT ACCESSION NO. BH

11. TITLE (Include Security Classification): NORSAR Basic Seismological Research, 1 October 1989-30 September 1990

12. PERSONAL AUTHOR(S): S. Mykkeltveit (Ed.)

13a. TYPE OF REPORT	13b. TIME COVERED	14. DATE OF REPORT (Year, Month, Day)	15. PAGE COUNT
SCIENTIFIC REP. #7	FROM 89/10/01 TO 90/09/30	1990 November 29	88

16. SUPPLEMENTARY NOTATION

17. COSATI CODES			18. SUBJECT TERMS (Continue on reverse if necessary and identify by block number)
FIELD	GROUP	SUB-GROUP	Source spectral scaling inversion, P-wave focusing effects, wavefield extrapolation of NORSAR array data, seismicity of Norway, symposium report

19. ABSTRACT (Continue on reverse if necessary and identify by block number)

This Annual Technical Report describes the work accomplished under Contract No. F49620-C-89-0038 during the period 1 October 1989 -- 30 September 1990. The report contains five separate contributions (paragraphs 2.1 through 2.5), and in addition abstracts of the investigations submitted as quarterly technical reports during FY90 (paragraph 2.6).

20. DISTRIBUTION/AVAILABILITY OF ABSTRACT	21. ABSTRACT SECURITY CLASSIFICATION	
☐ UNCLASSIFIED/UNLIMITED ☐ SAME AS RPT. ☐ DTIC USERS	UNCLASSIFIED	
22a. NAME OF RESPONSIBLE INDIVIDUAL: James Lewkowicz	22b. TELEPHONE (Include Area Code): (617) 377-3028	22c. OFFICE SYMBOL: GL/LWH

DD Form 1473, JUN 86 — Previous editions are obsolete. — SECURITY CLASSIFICATION OF THIS PAGE: UNCLASSIFIED

In paragraph 2.1, short-period and high-frequency NORESS observations from two aftershock sequences offshore western Norway, with epicentral distances of 424 and 405 km, respectively, have been used in testing a new hedgehog inversion procedure for determination of source spectral scaling characteristics, based on a previously developed spectral ratio method. The two main events analyzed have M_L magnitudes of about 5 while the smallest aftershocks are about 1.5. The observed spectral ratios support ω^2 source models for both of the earthquake sequences, but only if certain constraints are imposed on the scaling parameter that determines the stress drop sensitivity with respect to seismic moment.

P-wave focusing effects at the NORSAR array for Novaya Zemlya explosions are investigated in paragraph 2.2. It is found that the amplitude pattern for Novaya Zemlya explosions shows an order of magnitude variation across the 60 km aperture NORSAR array. The seismometer at site 03C01 records the strongest signals, and it is shown by simple SNR scaling that this seismometer would record detectable signals for Novaya Zemlya explosions of m_b = 2.0--2.5 during normal noise conditions.

A major consideration in selecting the NORESS array site has been the high amplification of short-period P signals from directions to the east. An investigation, described in paragraph 2.3, has been initiated aimed at characterizing the structure responsible for the presumed wave focusing. The data base provided by NORESS itself must be extended for this purpose, and we have started processing data from the large-aperture NORSAR array that encompasses the NORESS site. At this stage a method has been developed to downward extrapolate the observed surface wavefield at NORSAR. The method is posed as an inverse problem taking into account the limited areal extent of sampling at the surface. Preliminary results suggest that the source of focusing at NORESS is far below the Moho.

An important incentive for investigating the natural seismicity of Norway and surrounding areas is that the nuclear explosion monitoring programs need the best possible background information about the seismicity, not only in the areas where such explosions could take place, but also in the areas within local and regional distance from the monitoring stations. In the new Intelligent Monitoring System now installed at NORSAR, such background seismicity can be displayed as overlays. For this purpose, three different catalogues have been prepared, covering the three time periods 1880--1954, 1955--1979 and 1980--1989. The purpose of the contribution in paragraph 2.4 is to document these catalogues, and to outline briefly their seismotectonic context.

Paragraph 2.5 contains a report on the scientific symposium entitled ''Regional Seismic Arrays and Nuclear Test Ban Verification'', held in Oslo, Norway, during 14--17 February 1990. The purpose of the symposium

was to assess the state-of-the-art research on regional seismic arrays and associated topics. In particular, the symposium focused upon the advanced regional arrays NORESS and ARCESS in Norway and their associated data processing facilities, in the light of the potential of such arrays to provide a much improved monitoring capability for a future comprehensive nuclear test ban treaty. In paragraph 2.5, we give a brief review of some of the results presented during the symposium. The majority of the papers presented will be published in a special issue of the *Bulletin of the Seismological Society of America*, scheduled to appear in December 1990. Authors and titles of the 28 papers of the special issue are given.

Preface

Under Contract No. F49620-C-89-0038, NTNF/NORSAR is conducting research within a wide range of subjects relevant to seismic monitoring. The emphasis of the research program is on developing and assessing methods for processing of data recorded by networks of small-aperture arrays and 3-component stations, for events both at regional and teleseismic distances. In addition, more general seismological research topics are discussed.

Each quarterly technical report under this contract presents one or several separate investigations addressing specific problems within the scope of the statement of work. Summaries of the research efforts within the program as a whole are given in annual technical reports.

This Scientific Report No. 7 is the annual technical report for the period 1 October 1989 – 30 September 1990. It contains five separate contributions, and also abstracts for the investigations submitted as quarterly technical reports during FY90.

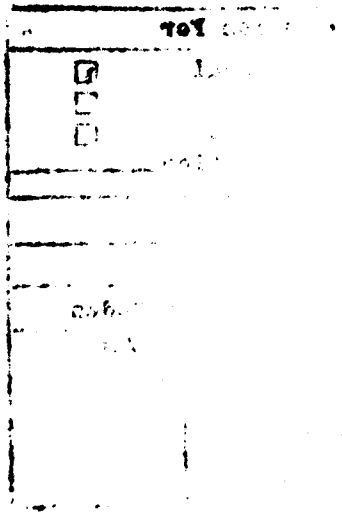

Table of Contents

1 Summary

This Annual Technical Report describes the work accomplished under Contract No. F49620-C-89-0038 during the period 1 October 1989 – 30 September 1990. The report contains five separate contributions (paragraphs 2.1 through 2.5), and in addition abstracts of the investigations submitted as quarterly technical reports during FY90 (paragraph 2.6).

In paragraph 2.1, short-period and high-frequency NORESS observations from two aftershock sequences offshore western Norway, with epicentral distances of 424 and 405 km, respectively, have been used in testing a new hedgehog inversion procedure for determination of source spectral scaling characteristics, based on a previously developed spectral ratio method. The two main events analyzed have M_L magnitudes of about 5 while the smallest aftershocks are about 1.5. The observed spectral ratios support ω^2 source models for both of the earthquake sequences, but only if certain constraints are imposed on the scaling parameter that determines the stress drop sensitivity with respect to seismic moment.

P-wave focusing effects at the NORSAR array for Novaya Zemlya explosions are investigated in paragraph 2.2. It is found that the amplitude pattern for Novaya Zemlya explosions shows an order of magnitude variation across the 60 km aperture NORSAR array. The seismometer at site 03C01 records the strongest signals, and it is shown by simple SNR scaling that this seismometer would record detectable signals for Novaya Zemlya explosions of m_b = 2.0–2.5 during normal noise conditions.

A major consideration in selecting the NORESS array site has been the high amplification of short-period P signals from directions to the east. An investigation, described in paragraph 2.3, has been initiated aimed at characterizing the structure responsible for the presumed wave focusing. The data base provided by NORESS itself must be extended for this purpose, and we have started processing data from the large-aperture NORSAR array that encompasses the NORESS site. At this stage a method has been developed to downward extrapolate the observed surface wavefield at NORSAR. The method is posed as an inverse problem taking into account the limited areal extent of sampling at the surface. Preliminary results suggest that the source of focusing at NORESS is far below the Moho.

An important incentive for investigating the natural seismicity of Norway and surrounding areas is that the nuclear explosion monitoring programs need the best possible background information about the seismicity, not only in the areas where such explosions could take place, but also in the areas within local and regional distance from the monitoring stations. In the new Intelligent Monitoring System now installed at NORSAR, such background seismicity can be displayed as overlays. For this purpose, three different catalogues have

been prepared, covering the three time periods 1880–1954, 1955–1979 and 1980–1989. The purpose of the contribution in paragraph 2.4 is to document these catalogues, and to outline briefly their seismotectonic context.

Paragraph 2.5 contains a report on the scientific symposium entitled "Regional Seismic Arrays and Nuclear Test Ban Verification", held in Oslo, Norway, during 14–17 February 1990. The purpose of the symposium was to assess the state-of-the-art research on regional seismic arrays and associated topics. In particular, the symposium focused upon the advanced regional arrays NORESS and ARCESS in Norway and their associated data processing facilities, in the light of the potential of such arrays to provide a much improved monitoring capability for a future comprehensive nuclear test ban treaty. In paragraph 2.5, we give a brief review of some of the results presented during the symposium. The majority of the papers presented will be published in a special issue of the *Bulletin of the Seismological Society of America*, scheduled to appear in December 1990. Authors and titles of the 28 papers of the special issue are given.

2 Summary of Technical Findings and Accomplishments

2.1 Source spectral scaling inversion for two earthquake sequences offshore western Norway

Introduction

The way in which earthquake source spectral characteristics depend on seismic moment (or magnitude) is important in the many situations in which observations from earthquakes in a certain magnitude range are used for predicting effects from earthquakes in another (usually higher) magnitude range. The discussion of source scaling laws often focuses on the self-similarity principle (Aki, 1967), a departure from which is frequently seen in terms of non-constant stress drop (with seismic moment), and sometimes also in terms of non-exponential frequency-magnitude distributions (Aki, 1987).

The departure from the constant stress drop (CSD) situation invariably means increasing stress drop (ISD) with seismic moment, corresponding to a reduced rate of increase of corner frequencies and a reduced rate of decrease of source radii as magnitude decreases. While the large number of reports on such observations often agree that they start to occur at a magnitude of around 3 and/or a moment of around 10^{21} Nm, similar agreements are less common with regard to explanation (Dyshart *et al.*, 1988). These fall generally in two categories, propagation and/or site effects, and source effects.

A central concept in the first case is the f_{max} (Hanks, 1982), often but not always interpreted as a site effect parameter, appearing for large earthquakes as a second corner frequency and for smaller events as a limiting value for the corner frequency. The second type of explanations may involve concepts such as characteristic barrier spacings and critical minimum crack length, but the reason for the departure from self-similarity could also simply be that the corner frequency of small earthquakes are controlled by the fault zone width rather than by the fault length (Aki, 1987).

Spatially confined earthquake sequences have been used successfully in determination of source spectral characteristics. While earlier studies (Chael, 1987; Chael and Kromer; 1988; Chun *et al.*, 1989) only compared spectral ratio curve shapes to theoretical ones, Boore and Atkinson (1989) extended the method by using independently determined seismic moments, thereby controlling also the absolute levels of the spectral ratios. These studies all find support for an ω^2 high-frequency fall-off, while stress drop (when determined) follows both CSD and ISD models.

The data used in the present paper coincide in part with those used by Chael and Kromer (1988), who analyzed an 1986 aftershock sequence off the

western coast of Norway. In addition, we use data also from an 1989 aftershock sequence not far from the one in 1986. We use essentially the same spectral ratio technique, but depart from earlier studies in that we replace their trial-and-error method with one in which a hedgehog inversion technique is applied. This provides (given that the data are of sufficient quality) more reliable solutions, and better possibilities for analyzing resolution, uncertainties, and trade-offs between parameters.

Data

The data used in this analysis comprise high-frequency (hf) and short-period (sp) recordings at one of the sites in the NORESS regional array in Norway (Mykkeltveit *et al.*, 1990), from two aftershock sequences offshore western Norway in 1986 and 1989. The two sequences, here named A and B, are identified in Table 2.1.1, with origin times, magnitudes and seismic moments. A_0 and B_0 refers to the main events, and we have analyzed six aftershocks in each case, A_1 - A_6 and B_1 - B_6. It is seen from Table 2.1.1 that the magnitudes of the main events are 4.8 and 4.9, while the aftershocks are all in the range 2.8 to 1.4. For sequence B all of the aftershocks occur within 3 days, while sequence A is scattered over a time period of 8 days.

Event A_0 occurred off the west coast of Norway at 62.71°N, 4.69°E, at a distance of 424 km from the NORESS array, and B_0 occurred at 61.97°N, 4.42°E at a distance of 405 km. The distance between the event sequences is 84 km, both of them occurred on the landward side of the continental margin (B closest to the coast), and the focal mechanisms in both cases indicate thrust faulting in response to EW compressional stress. More detailed descriptions of the events are given by Hansen *et al.* (1989), and for more details about the seismotectonics of the region we refer to Bungum *et al.* (1991). There are no indications of significantly different tectonic conditions between the two epicentral areas. Event B_0 has been located, using near-source recordings, very close to (possibly below) the crust-mantle boundary (24-28 km), while A_0 most probably is somewhat shallower (Hansen *et al.*, 1989). In the subsequent analysis, only vertical component data have been used.

For the aftershock data we have, in addition to the high-frequency (hf) data, also used short-period (sp) data from instruments located very close to the hf elements, partly for the purpose of stabilizing the estimates and partly in order to provide records also for aftershocks A_5 and A_6, for which hf records where missing (see Table 2.2.1). The dynamically more limited sp data are reaching clipping level for L_g, but could still be used because we analyze data only between the P_n and the S_n arrivals.

Method of Analysis

The main advantage of spectral ratio methods, which are used in many different types of applications, is that both site effects (including instrument

response) and path effects (earth transfer functions) are removed in taking the ratios. Under certain conditions, source radiation effects are also removed, while earth noise effects are additive and should be dealt with specifically.

The spectral ratio method has been used recently in source scaling investigations by Chael (1987), Chael and Kromer (1988), Chun *et al.* (1989) and Boore and Atkinson (1989), and we refer to these papers for a more detailed description. The relationship for the power spectral ratio $R^2(\omega)$ between the i'th event (aftershock) and the reference event (main shock) r in this case is

$$R^2(\omega) = \left(\frac{M_{0,i}}{M_{0,r}}\right)^2 \left[\frac{1+\left(\frac{\omega}{\omega_{0,r}}\right)^2}{1+\left(\frac{M_{0,i}}{M_{0,r}}\right)^{\frac{2}{\delta}}\left(\frac{\omega}{\omega_{0,r}}\right)^2}\right]^{\gamma} , \tag{1}$$

where ω is angular frequency, ω_0 is corner frequency, and M_0 is seismic moment. The spectral ratios are seen to be controlled here by the two parameters γ and δ, where γ controls the shape of the source spectrum as demonstrated by the following relationship (Aki, 1967; Aki and Richards, 1980) between the far-field displacement spectrum $\Omega(\omega)$ and its low-frequency asymptote $\Omega(0)$ (which in turn scales linearly with seismic moment)

$$\Omega(\omega) = \frac{\Omega(0)}{\left[1+\left(\frac{\omega}{\omega_0}\right)^2\right]^{\frac{\gamma}{2}}} . \tag{2}$$

Values of 2 and 3 for γ correspond to the ω^2 and the ω^3 models, respectively. The parameter δ in equation (1) controls the scaling relation between corner frequencies and seismic moment as follows

$$M_0 {\omega_0}^{\delta} = constant \tag{3}$$

which in turn leads to a proportionality between stress drop $\Delta\sigma$ and $M_0^{(1-\frac{3}{\delta})}$, or alternatively

$$\Delta\sigma_i = \Delta\sigma_r \left(\frac{M_{0,i}}{M_{0,r}}\right)^{(1-\frac{3}{\delta})} \tag{4}$$

where subscripts i and r are defined as for equation (1). Values of 3 and 4 for δ correspond to CSD and ISD (Nuttli, 1983a) models, respectively. Unless an independently determined estimate of the stress drop for the reference event is available, the spectral ratio method only provides the stress drop ratios.

A commonly used realization of the suite of source models allowed by the different combinations of γ and δ is the one due to Brune (1970; 1971), which is an ω^2 CSD model. There are many other models that also relate corner frequencies to stress drop.

Data Analysis

The data have been analyzed in this study essentially as described in detail by Chael (1987), Chael and Kromer (1988) and Chun *et al.* (1989). We have used the data between the arrival of the P_n phase and the arrival of the S_n phase, and computed power spectra using the direct method of power spectral estimation (the Fourier transform of the data multiplied by its complex conjugate), combined with a block-averaging with overlapping blocks for the purpose of spectral smoothing. The approximate stationarity of the P coda makes it possible to estimate power spectra in this way, and the block-averaging is simply one of the ways in which spectral stability is achieved at the expense of frequency resolution.

For both of the events, about 35 sec of data were available between the P_n and the S_n phases. Signal spectra have been estimated, using the block-averaging method, for each of the 10 hf and 12 sp records (see Table 2.1.1), and additional smoothing has been achieved in the frequency domain. The rationale for smoothing the spectra so extensively is that dynamic stability in the present analysis is more important than frequency resolution.

Noise spectra have been estimated in the same way, and for equally long time windows preceding the Pn arrivals (except for event B_1 where only 10 sec of noise were available). These noise spectra are necessary for two reasons, because noise power should be subtracted from signal power (se detailed discussion on this subject by Chun *et al.*, 1989) and because a noise estimate is needed in order to decide which parts of the noise-corrected spectrum that can be used in each particular case.

The signal-to-noise ratios (SNR's) for the main events were around 30 dB for A_0 and 70 dB for B_0, while the aftershocks had SNR values of up to 11 dB for sequence A and 17 dB for B. There were also, however, some low-frequency SNR values in both cases at or below zero, a finding which has been used in determining the exact frequency band of observations to use in each particular case. We have found that subtracting the noise makes a difference only for the weakest ones of the aftershocks.

In earlier analyses of source scaling characteristics using the spectral ratio method it has been common to compare observations only to a suite of theoretical spectral ratio curves, for the purpose of comparing spectral shapes. It is obvious, however, that the availability of independently determined seismic moments can assist in constraining the suite of acceptable models, as pointed out also by Boore and Atkinson (1989). We therefore proceed now with establishing seismic moments for the data analyzed in this study, before starting the source scaling inversion analysis.

The magnitudes used in the present paper have been estimated using a magnitude inversion algorithm recently applied by Alsaker *et al.* (1991), who

used a data base of 741 records from 195 earthquakes in developing attenuation terms and station corrections. The resulting M_L magnitudes are on the average about 0.4 units below those obtained with the earlier scale (Båth *et al.*, 1976). When applied to the data analyzed here, the new scale gives M_L values as shown in Table 2.1.1. While only NORESS data were available for magnitude assessment for sequence A, we could for the B events use up to 6 stations as shown in Table 2.1.1.

Seismic moments were estimated following an inversion algorithm recently applied by Kvamme and Hansen (1991) to essentially the same data base that Alsaker *et al.* (1991) used for the magnitude scale. The inversion algorithm (see also Sereno *et al.*, 1988) utilizes ground motion displacement amplitude spectra, and we have tested it here with different options (for which parameters to determine, always including moments) and different data bases (always including the two aftershock sequences) in order to assess the stability of the results. The seismic moments determined are also in this case shown in Table 2.1.1, and also this time there are many more records available for the B events. The additional station for event A_0 in this case is a NORESS broadband (intermediate period, ip) record that helps to stabilize the moment estimates for the main events The aftershocks were too weak to be recorded on the ip sensors.

The spectral data for the two earthquake sequences have, together with the seismic moments, been used in a simple hedgehog inversion procedure for the purpose of determining simultaneously the scaling parameters γ, δ and $\omega_{0,r}$, with and without a redetermination of the moment ratios. The results of this analysis are shown in Table 2.1.2 and in Figures 2.1.1 and 2.1.2, for sequences A and B, respectively. It is seen there that δ is 3.24 for sequence A (close to an CSD model) while it is 3.80 for sequence B (close to an ISD model). We will return to these results after discussing the method in more detail.

The starting point for the inversion is equation (1), which allows us to estimate the spectral ratios as functions of frequency, given γ, δ, $\omega_{o,r}$ and the moment ratios. The problems with linearizing equation (1) have been circumvented here by using a hedgehog approach (Aki and Richards, 1980), which in fact is particularly appropriate in this case because we have physical limitations that helps us to confine the parameter space to within certain limits. For the parameter γ, it suffices initially to consider only the values of 2 (ω^2-model) and 3 (ω^3-model), the parameter δ can be limited to values centered in the range 3 (CSD) to 4 (ISD), and the corner frequency $f_{0,r}$ (= $\omega_{0,r}/2\pi$) of the main event is bound by the estimated seismic moment. Seismic moments of the order of 10^{16} Nm should correspond to corner frequencies of the order of 1-2 Hz.

Given these parameter space constraints, we computed initially theoretical

spectral ratios using equation (1) for a sufficiently dense grid of parameter combinations within the limits 2-3 for γ, 2.5-4.5 for δ, and 0.5-3.0 for $f_{0,r}$. For each parameter combination we computed the root mean square (RMS) of the deviations between observed and computed log-amplitudes, averaged over all frequencies (with acceptable spectral SNR) and over all of the aftershocks. A proper weighting in frequency domain was obtained by resampling the spectra to an equidistant spacing in log-frequency (20 samples per decade) before the RMS computation (by interpolating at low frequencies and smoothing at high frequencies), while a similar weighting between the events was obtained by using log-amplitudes. In the cases when both hf and sp data were available a weight of 0.5 was given to each of them. In this way, the resulting (properly normalized) RMS values, as computed from log-amplitude differences, can be related directly and easily to average amplitude ratios.

This search in parameter space can either be conducted with a sufficiently dense grid initially, or one can use a coarser grid, determine a minimum, and iterate with gradually finer grids. The difference between these two approaches is only computer time. We have also, however, developed an alternative option under which we for each grid point also search for the moment ratio that gives the best fit between computed and observed spectral ratios. The moment ratio corresponding to the best-fitting parameter combination in the first iteration is then carried into the next iteration, where the grid is a bit narrower, and the procedure continues until a certain convergence criterion is fulfilled (we have used 1% change). In that case the iterations are essential for the results because of the gradual adjustments of the moment ratios. It is this latter option that has been used when obtaining the results shown in Figures 2.1.1 and 2.1.2.

When testing the inversion procedure it soon became clear, when confining the parameters to the initially defined range, that an ω^2-model satisfied the observations much better than an ω^3-model, as found also by most others using the spectral ratio method. We will return to the question of the γ value later, while in the following presenting the results for a fixed γ of 2. Figure 2.1.3 shows, for aftershock sequence B, the results for the first four iterations when inverting also for moment. The two parameters to be resolved are δ and $f_{0,r}$, and contour diagrams are used to depict the RMS levels. There is one more iteration in each of these cases, but without any real change in the location of the minima.

The first impression we get from Figure 2.1.3 is the elongation of the contours, indicating that the resolution is non-uniform. We notice moreover only a very small shift in the locations of the minima over the iterations, with $\delta/f_{0,r}$ changing from 3.70/1.50 to 3.80/1.53. The results are similarly stable for sequence A. From Figure 2.1.3 we also find that the inversion for moment ratios does not really influence the results for the other parameters determined in the inversion.

The results from the present source parameter inversion are summarized in Table 2.1.2, where the new moment values already have been discussed. For the aftershock corner frequencies, equation (3) gives us the relation

$$f_{0,i} = f_{0,r} \left(\frac{M_{0,i}}{M_{0,r}} \right)^{1/\delta} \tag{5}$$

while equation (4) has been used in computing the stress drop ratios. An example of what this could give in terms of stress drops is shown in the last column of Table 2.1.2, where a Brune model (equation (5)) has been used in computing reference event stress drop. It is seen clearly there that a δ-value of 3.24 for sequence A gives only moderately varying stress drops with moment (from 100 to 53%), while a δ-value of 3.80 for sequence B gives a much stronger stress drop variation (from 100 to 10%). As noted earlier, a CSD (constant stress drop) model corresponds to δ= 3.0 and an ISD (increasing stress drop) model to δ= 4.0.

It was mentioned above that a number of options were considered in the initial determination of seismic moments (Kvamme and Hansen, 1991), and we extended this also to testing a number of the resulting solutions in the present inversion. The results were found to be quite stable for all of the parameters except the main event corner frequency, where significant changes were found by using different (but still reasonable) sets of initial moments. Naturally, the seismic moment for the main event was most critical in this respect. While this means that the corner frequency resolution is relatively poor, it is still important to include this parameter in the inversion since the use of a fixed value otherwise easily could bias the results for the other parameters.

It was noted above that the initial solutions were much better for an ω^2 source model as compared to an ω^3-model. In noting, however, that the best fit in the latter case was obtained for simultaneously high values of δ and $f_{0,r}$, we extended the ranges of these parameters beyond their initial limits. What we found then were the results shown in Figure 2.1.4 (sequence *B* only), where the box in the lower-left corner indicates the previously used parameter range. The results are reasonably similar also for sequence *A*, and we find again that the moment-inversion option does not change the results significantly for either of the aftershock sequences. The fit between computed and observed (in terms of RMS) is almost as good as earlier, which means that there is a basic ambiguity between the ω^2 and the ω^3 source models that can be resolved only by invoking independent physical constraints for δ and/or f_0, or by determining γ independently from near-source observations.

When considering only the initial parameter range in Figure 2.1.4 we see that the RMS values are mostly above 1.0, as compared to values around 0.20 when using an ω^2 source model. This was the basis for initially rejecting the ω^3 model. Comparisons between computed and observed spectral ratios (as in Figures 2.1.1 and 2.1.2) also indicate a significantly poorer fit in this case.

The good fit for the ω^3-based solutions in Figure 2.1.4 makes it desirable to investigate this finding further, because of its potential importance with respect to trade-off effects between parameters. We did this by looping the source spectral slope parameter γ between values of 1.5 and 3.0, with results as given in Figure 2.1.5, for both of the earthquake sequences. What we see there is that each of these γ values in fact has one combination of δ and f_0 that gives a very good fit between computed and observed spectral ratios, with corresponding RMS values in the range 0.18-0.21 for sequence A and 0.14-0.21 for B. Even though there for sequence A is a weak RMS minimum for the more commonly accepted δ values (between the dotted lines) we do not attribute any real significance to this, especially when considering that this sequence has less resolving power than B. It is noteworthy, however, that the scaling parameter δ varies quite smoothly and systematically with γ, which in turn increases the confidence of the estimated δ values of 3.24 and 3.80 for the two sequences, given a γ of 2.0.

Discussion

The results obtained in this study are in general consistent with results from earlier studies using the same method. Chael and Kromer (1988), for example, analyzing also earthquake sequence A, found that an ω^2 source model and a γ of 3 (CSD) fitted their observations best. For an ω^2 source model we have found a γ of 3.24 for the same earthquake sequence. The use of seismic moments in this study makes it more interesting to compare results with those of Boore and Atkinson (1989), however, who emphasized the non-uniqueness in the solutions if only spectral ratios are considered. They found, for example, that good spectral ratio fits could be maintained by simultaneously increasing δ and decreasing the stress drop (f_0 in the present case), a finding which corresponds to following the elongated ridges in Figure 2.1.3. Also, when comparing ω^2 to ω^3 models they found that a much higher δ was needed in the latter case, which corresponds to what can be seen from Figure 2.1.4.

Those observations can serve as a useful prelude to one of the main results of this study, namely the basic non-uniqueness demonstrated in Figure 2.1.5. There, a very large range of parameter values is used, and still found to be consistent with observed spectral ratios. In that case it looks as if we have practically no resolving power with respect to the scaling parameter γ.

We can, as mentioned earlier, choose between these solutions only by invoking external constraints on the derived parameters. This applies in particular to δ, where a restriction to the commonly accepted range between 3 (CSD) and 4 (ISD) immediately restricts γ to within the range 1.9-2.3 for earthquake sequence A and 1.7-2.1 for B (see Figure 2.1.5). It is important to note in this respect, however, that McGarr (1986) has found δ values of up to above 6 for earthquake sequences in the same magnitude range as ours, with indications that the largest ones within at least for some of the sequences scale according

to a CSD model (δ of 3). The transition in δ was found to be in the range 10^{14} to 10^{17} Nm, depending on tectonic regime (McGarr, 1984). It is therefore not possible to exclude *per se* the higher δ values in Figure 2.1.5.

Given this non-unique situation, the range of acceptable solutions could of course also be limited if sufficiently reliable near-source observations had been available to allow for a direct estimation of γ (which more often than not results in ω^2 models). Unfortunately, no such data are available in the present case. The corner frequency also enters this discussion, however, since we see from Figure 2.1.4 that $\gamma = 3$ gives about 50% higher f_0 values (3.20 and 2.25 Hz) as $\gamma = 2$ (2.19 and 1.53 Hz), which in turn are somewhat higher than those obtained from the inversion algorithm of Kvamme and Hansen (1991). We therefore have some, albeit not strong, evidence for choosing the solutions resulting from $\gamma = 2$ (and δ = 3-4). The use of this constraint on γ should be kept in mind in the following.

Earthquake sequence *B* has better quality and more resolving power than *A*, which covers a smaller magnitude range. An important additional point in favor of *B* is that many more seismic records than those used in computing spectral ratios in that case have been used in computing magnitude and seismic moments. Another point related to the question of data quality is that the spectral ratio method ideally requires the same epicenter and the same focal mechanism, which of course never happens. While we have not been able to reproduce the high correlation levels found by Chael and Kromer (1988) (who analyzed also sequence *A* but not necessarily the same aftershocks), we have tried to relocate the aftershocks using a master-event technique. Within the limits of the quality of the relative arrival times, however, no significant difference was found. This is not surprising considering the fact that the source radii for the main *A* and *B* events have been estimated to 1–2 km (Hansen *et al.*, 1989). Compared to the hypocentral variations accepted by Boore and Atkinson (1989), for example, the data used in this study are therefore closer to the ideal requirement. An interesting and yet unresolved question in this respect is, by the way, what limits in hypocentral variations can be accepted in studies of this kind?

The hedgehog inversion approach that we have used in the present study clearly requires high-quality data as well as a careful data analysis procedure. The spectral smoothing is an essential part of this procedure. An interesting option in this inversion is that the seismic moments can be (re-)determined along with the scaling parameters, without essentially affecting the resolving power with respect to those parameters. The good correlation that we have observed here for both of the earthquake sequences reflect a high quality in the initial moment determinations.

Given the determination of a preferred γ value (such as 2), this inversion determines simultaneously a set of δ and f_0 values. The shape and the gradi-

ents of the contour levels in such plots provide important information about the resolving power, including trade-off effects between the parameters.

We have chosen in this study to invert for, in addition to δ, the reference event corner frequency f_0 rather than the stress drop. The reason for this is simply that it is the corner frequency which enters the spectral ratio relation (equation (1)), and that a connection to stress drop requires some additional constraint (model) for the relation between corner frequency and stress drop. In using corner frequency, we obtain therefore primarily the stress drop ratios, as shown in Table 2.1.2. It is important to note here that those values (as well as the corner frequency ratios) are quite reliably determined, in contrast to the absolute values of the main event corner frequencies. As an example, the latter values have been used, in the last column of Table 2.1.2, in deriving a set of stress drop values based on the Brune source model.

These stress drop values reflect directly that the corner frequencies determined here are, as mentioned above, somewhat higher than those estimated earlier, using different source spectral approaches (Hansen *et al.*, 1989; Kvamme and Hansen, 1991). While we cannot explain this difference at this stage other than in general terms (lack of near-field observations, differences in models and approaches, resolution problems), there is an important implication with respect to the use of the spectral ratio method. This is that the use of a fixed pre-determined corner frequency, such as one derived from magnitude and some standard model, can easily bring us off scale with respect to the fit between computed and observed spectral ratios. In turn, this can result in biased δ values, equivalent to traversing along the ridge crests in Figure 2.1.3. If we replace the corner frequency with stress drop, the same result holds true.

We have found in this study, when assuming an ω^2 model, that the stress drop scaling parameter δ has values of 3.24 and 3.80 for two earthquake sequences located essentially within similar tectonic environments. An ω^3 model gives a corresponding difference with respect to δ. The potential implication of this is that we may have to accept quite some variation in the stress drop parameter, not only between widely separated main shocks (Hanks, 1977), but even between closely located events and event sequences. Such observations may serve to illustrate why the enduring discussions on the CSD/ISD alternatives (Kanamori and Anderson, 1975; Nuttli, 1983a; 1983b) and on the possible connection between stress drop and tectonic environment (Sommerville *et al.*, 1987; Kanamori, 1988) still are essentially unresolved. The large scatter in the data that has nourished this discussion indicates that the intra-earthquake variability within selected regions (such as California and Fennoscandia) may be as large as the variability between the regions. That means, in turn, that it may be possible to use results about earthquake source properties across regional and tectonic boundaries to a larger extent than previously assumed (cf. Campbell, 1989), and that a large and yet unpredictable variability is still

present in such data, implying large uncertainties with respect to prediction of ground motion. As is well known, such predictions are very sensitive to the stress drop parameter.

A final point here is that the scaling relations derived in this study should not necessarily be assumed to be valid for any magnitude range outside that covered by the present data (M_L 1.5 to 5). Our results favor a single model covering this range, including also, as noted initially, the magnitude (around 3) where departures from a CSD situation often are found to occur, for series of main earthquakes. The results of McGarr (1986) indicates that the CSD/ISD transition for earthquake sequences occurs, if at all, at higher magnitudes. It seems therefore that scaling relations in general should not without good reasons be assumed to be valid for data other than those from which the relations have been derived.

Conclusions

Short-period and high-frequency NORESS observations from two aftershock sequences offshore western Norway, with epicentral distances of 424 and 405 km, respectively, have been used in testing a new hedgehog inversion procedure for determination of source spectral scaling characteristics, based on a previously developed spectral ratio method. This inversion procedure provides insight into resolution properties, uncertainties, and trade-off considerations between source parameters.

The two main events analyzed have M_L magnitudes of about 5 while the smallest aftershocks are about 1.5, with seismic moments in the range 10^{17} to 10^{12} Nm. The observed spectral ratios support ω^2 source models for both of the earthquake sequences, but only if certain constraints are imposed on the scaling parameter (δ) that determines the stress drop sensitivity with respect to seismic moment. In that case, stress drop is found to be almost independent of seismic moment (δ of 3.24) for one of the sequences and increasing with moment (δ of 3.80) for the other. Without such constraints, which may not be justifiable in the case of earthquake sequences, equally good solutions are found for ω^3 models, in which case δ attains values around 5-6, indicating strongly increasing stress drop. External constraints on the source spectral slope and/or corner frequency will similarly help in resolving δ.

The method, which also simultaneously determines corner frequencies (or stress drop if adopting some model relating this to corner frequency) for all of the events, albeit with a poorer resolution, can either use independently determined seismic moments or it can determine these as part of the inversion. Quite similar results are obtained in those two cases, reflecting essentially the quality of the initial moment determinations. The observed variations in stress drop sensitivity between two earthquake sequences, only 84 km apart and occurring in similar tectonic environments, are consistent with the considerable variations that have been observed on a larger scale. Caution is therefore

needed if the scaling relations derived in this study are applied to other events (larger ones and/or series of main events), or to different seismic regions.

H. Bungum
A. Alsaker

References

Aki, K. (1967). Scaling law of seismic spectrum, *J. Geophys. Res.* **72**, 1217–1231.

Aki, K. (1987). Magnitude-frequency relation for small earthquakes: A clue to the origin of f_{max} of large earthquakes, *J. Geophys. Res.* **92**, 1349-1355.

Aki, K. and P.G. Richards (1980). *Quantitative Seismology*, vol. 2, p. 709, W.H. Freeman, San Francisco.

Alsaker, A., L.B. Kvamme, R.A. Hansen, A. Dahle and H. Bungum (1991). The M_L scale in Norway, *Bull. Seism. Soc. Am.* (in press).

Båth, M., O. Kulhanek, T. Van Eck and R. Wahlstrøm (1976). Engineering analysis of ground motion in Sweden, Report No 5-76, Seismological Institute, Uppsala, Sweden, 59 pp.

Boore, D.M. and G.M. Atkinson (1989). Spectral scaling of the 1985 to 1988 Nahanni, Northwest Territories, earthquakes, *Bull. Seism. Soc. Am.* **79**, 1736–1761.

Brune, J.N. (1970). Tectonic stress and the spectra of seismic shear waves from earthquakes, *J. Geophys. Res.* **75**, 497–5009.

Brune, J.N. (1971). Correction, *J. Geophys. Res.* **76**, p. 5002

Bungum, H., A. Alsaker, L.B. Kvamme and R.A. Hansen (1991). Seismicity and seismotectonics of Norway and nearby continental shelf areas, *J. Geophys. Res.* (in press).

Campbell, K.W. (1989). The dependence of peak horizontal acceleration on magnitude, distance, and site effects for small-magnitude earthquakes in California and Eastern North America, *Bull. Seism. Soc. Am.* **79**, 1311–1346.

Chael, E.P. (1987). Spectral scaling of earthquakes in the Miramichi region of New Brunswick, *Bull. Seism. Soc. Am.* **77**, 347–365.

Chael, P.C. and P. Kromer (1988). High-frequency spectral scaling of a main shock/ aftershock sequence near the Norwegian coast, *Bull. Seism. Soc. Am.* **78**, 561–570.

Chun, K-Y., R.J. Kokosky and G.F. West (1989). Source spectral characteristics of Miramichi earthquakes: Results from 115 P-wave observations, *Bull. Seism. Soc. Am.* **79**, 015–030.

Dyshart, P.S., J.A. Snoke, and I.S. Sacks (1988). Source parameters and scaling relations for small earthquakes in the Matsushiro region, southwest Honshu, Japan, *Bull. Seism. Soc. Am.* **78**, 571–589.

Hanks, T.C. (1977). Earthquake stress drops, ambient tectonic stresses and stresses that drive plate motions, *Pure Appl. Geophys.* **115**, 441–458.

Hanks, T.C. (1982). f_{max}, *Bull. Seism. Soc. Am.* **72**, 1867–1879.

Hansen, R.A., H. Bungum and A. Alsaker (1989). Three recent larger earthquakes offshore Norway, *Terra Nova* **1**, 284–295.

Kanamori, H. (1988). Spectral difference between western and eastern U.S. earthquakes, in *Proc. Earthquake Ground Motion Estimation in Eastern North America*, R.K. McGuire and J.F. Schneider, Editors, Electric Power Research Institute, Palo Alto, California.

Kanamori, H. and D.L. Anderson (1975). Theoretical bases of some empirical relations in seismology, *Bull. Seism. Soc. Am.* **65**, 1073–1095.

Kvamme, L.B. and R.A. Hansen (1991). Simultaneous inversion for seismic moment and Q in Norway (in preparation).

McGarr, A. (1984). Scaling of ground motion parameters, state of stress, and focal depth, *J. Geophys. Res.* **89**, 6969–6979.

McGarr, A. (1986). Some observations indicating complications in the nature of earthquake scaling, *Earthquake Source Mechanics*, Geophysical Monograph 37 (Maurice Ewing 6), 217–225.

Mykkeltveit, S., F. Ringdal, T. Kværna, and R.W. Alewine (1990). Application of regional arrays in seismic verification research, *Bull. Seism. Soc. Am.* **80**, (in press).

Nuttli, O.W. (1983a). Average seismic source-parameter relations for mid-plate earthquakes, *Bull. Seism. Soc. Am.* **73**, 519–545.

Nuttli, O.W. (1983b). Empirical magnitude and spectral scaling relations for mid-plate and plate-margin earthquakes. *Tectonophysics* **93**, 207–223.

Sereno, T.J, S.R. Bratt, and T.C. Bache (1988). Simultaneous inversion of regional wave spectra for attenuation and seismic moment in Scandinavia, *J. Geophys. Res.* **93**, 2019–2035.

Sommerville, P.G., J.P. McLaren, L.J. LeFevre, R.W. Burger, and D.V. Helmberger (1987). Comparison of source scaling relations of eastern and western North American earthquakes, *Bull. Seism. Soc. Am.* **77**, 322–346.

Event	Year	Date	Hour	Data	M_L	No	M_0 (Nm)	No
A_0	1986	Feb 05	17.53.35	hf-sp	4.8	1	$6.5 \cdot 10^{15}$	2
A_1			20.23.15	hf-sp	2.2	1	$4.7 \cdot 10^{12}$	1
A_2			23.35.42	hf-sp	1.8	1	$2.5 \cdot 10^{12}$	1
A_3		Feb 06	06.19.51	hf-sp	1.8	1	$1.4 \cdot 10^{12}$	1
A_4		Feb 10	12.31.36	hf-sp	1.4	1	$1.5 \cdot 10^{12}$	1
A_5		Feb 13	13.39.01	sp	2.0	1	$3.1 \cdot 10^{12}$	1
A_6		Feb 13	19.03.50	sp	2.0	1	$3.5 \cdot 10^{12}$	1
B_0	1989	Jan 23	14.06.29	hf-sp	4.9	6	$4.3 \cdot 10^{16}$	6
B_1			14.35.21	hf-sp	1.6	1	$2.6 \cdot 10^{12}$	1
B_2			15.57.27	hf-sp	1.9	5	$2.8 \cdot 10^{12}$	4
B_3			16.40.31	hf-sp	2.8	4	$2.6 \cdot 10^{13}$	4
B_4			21.38.05	hf-sp	2.5	6	$1.3 \cdot 10^{13}$	6
B_5		Jan 25	23.07.36	hf-sp	1.5	4	$1.2 \cdot 10^{12}$	3
B_6		Jan 26	10.01.43	hf-sp	1.6	4	$1.8 \cdot 10^{12}$	2

Table 2.2.1. Events analyzed in this study, with event code, year, date, origin time, NORESS data channels, local magnitude (M_L), number of records used in estimating M_L, predetermined seismic moments (Nm), and number of records used in estimating M_0.

Event	M_0 (Nm)	f_0 (Hz)	σ_r/σ_i	σ (MPa)
A_0	$(1.8 \cdot 10^{16})$	2.19	(1.00)	10.4
A_1	$2.1 \cdot 10^{13}$	18.34	0.60	6.3
A_2	$8.1 \cdot 10^{12}$	24.64	0.56	5.9
A_3	$3.4 \cdot 10^{12}$	32.50	0.53	5.5
A_4	$4.2 \cdot 10^{12}$	30.30	0.54	5.6
A_5	$1.2 \cdot 10^{13}$	22.05	0.58	6.0
A_6	$1.2 \cdot 10^{13}$	21.77	0.58	6.1
B_0	$(7.0 \cdot 10^{16})$	1.53	(1.00)	23.4
B_1	$4.9 \cdot 10^{12}$	18.96	0.13	3.1
B_2	$3.9 \cdot 10^{12}$	20.03	0.13	3.0
B_3	$8.2 \cdot 10^{13}$	9.00	0.24	5.7
B_4	$3.9 \cdot 10^{13}$	10.99	0.21	4.8
B_5	$1.3 \cdot 10^{12}$	26.78	0.10	2.4
B_6	$1.8 \cdot 10^{12}$	24.76	0.11	2.5

Table 2.1.2. Results from the present source scaling inversion analysis, with event code, seismic moment (not determined for A_0 and B_0), corner frequency, stress drop ratios, and stress drops when using equation (5) for determining the Brune (1970, 1971) stress drop for the reference event (1 MPa is 10 bars).

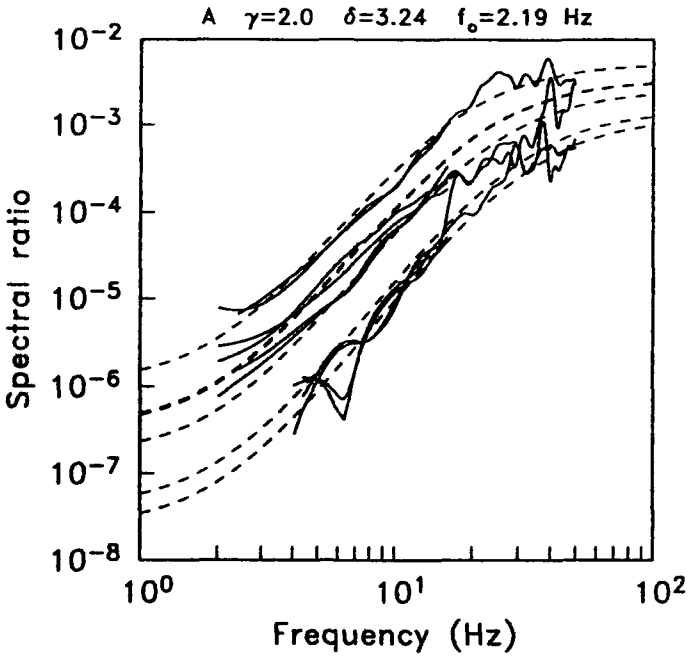

Fig. 2.1.1. Observed spectral ratios for event sequence *A* (fully drawn lines) together with theoretical ones (dashed lines) for the set of parameters (see top label) that gives the best fit, including also an adjustment of the moment ratios. Numerical values for this solution are given in Table 2.1.2.

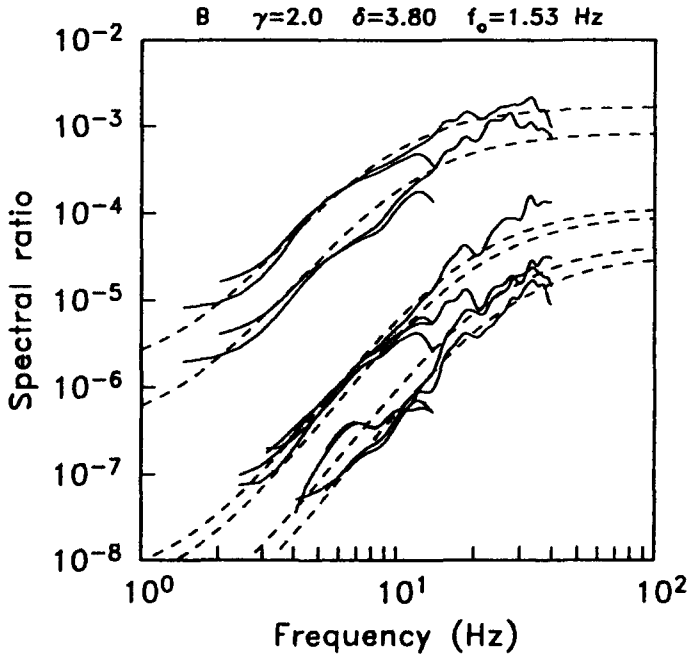

Fig. 2.1.2. Spectral ratios as in Figure 2.1.1, but for earthquake sequence *B*.

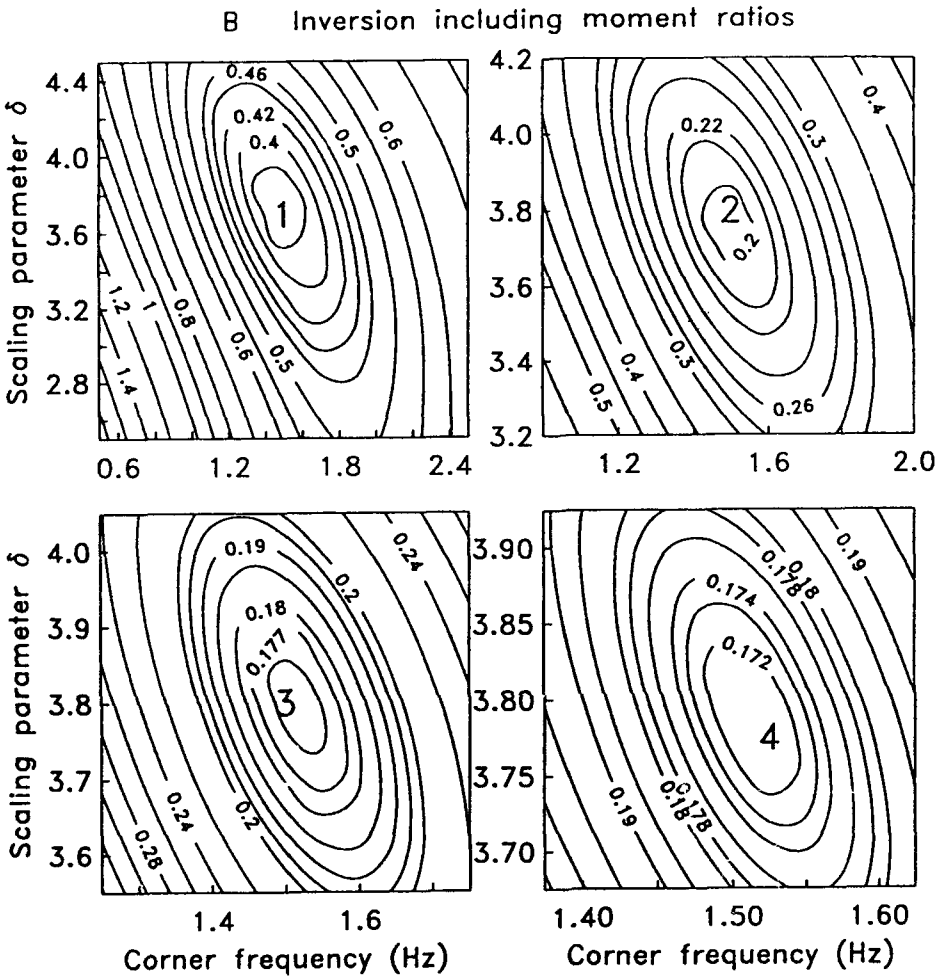

Fig. 2.1.3. Contour diagrams of root-mean-square (RMS) deviations between computed and observed spectral ratios for event sequence B, as a function of reference event corner frequency $f_{0,r}$ and the scaling parameter δ. An ω^2 source model (γ of 2) is assumed here, and the four diagrams cover the first four iterations, where moment ratios are adjusted simultaneously. The numbers 1 to 4 in each frame indicate iteration number and also the locations of the minima.

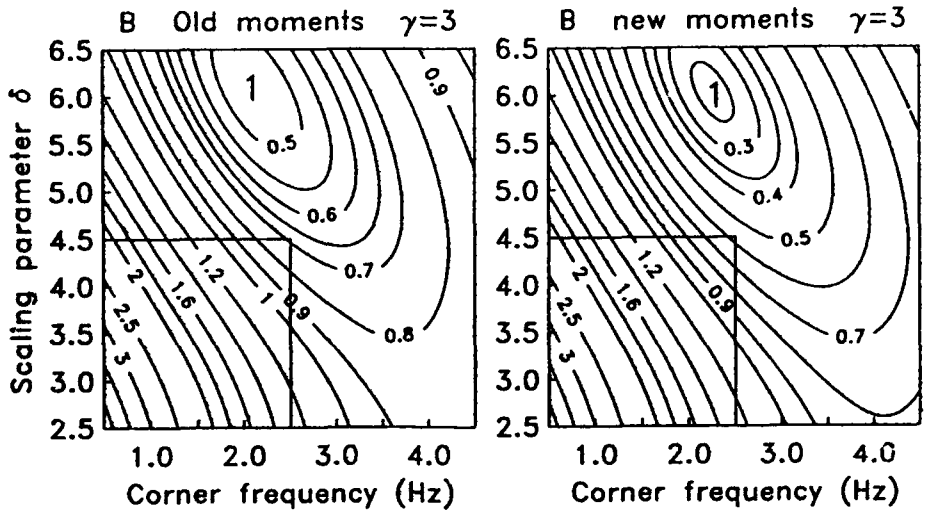

Fig. 2.1.4. Contour diagrams as for Figure 3.1.2, but for an ω^3 source model (γ of 3). The parameter ranges covered here are twice as large as the earlier ranges, which are indicated by the boxes in the lower-left corners of each frame.

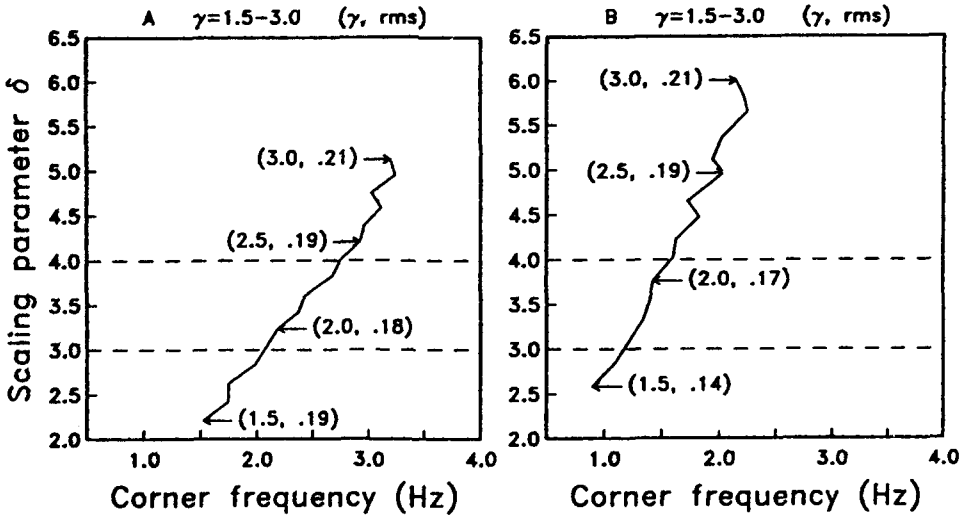

Fig. 2.1.5. Trajectories of source scaling inversion solutions when the source spectral shape parameter γ is allowed to vary from 1.5 to 3.0, in steps of 0.1. The values in the parentheses are γ and resulting RMS value corresponding to that solution, and the two dashed lines indicate the initial range considered for the parameter δ (3 is CSD, 4 is ISD). The left frame is for earthquake sequence *A* and the right one is for *B*.

2.2 P-wave focusing effects at NORSAR for Novaya Zemlya explosions

Introduction

It is now well established that significant improvements in P-wave detectability of weak seismic events can be achieved by taking advantage of receiver focusing effects of P-waves. Such effects appear to originate from upper mantle heterogeneities underneath the receiver, and are strongly dependent upon incoming azimuth and angle of incidence of the wavefront. Thus, at any given site, P-wave focusing is expected to be strong for certain epicentral regions, and weak for others, causing highly variable sensitivity for P-wave detection of signals from different source regions.

One of the most well-known examples of P-wave focusing is the remarkable detection performance of the NORESS array for Semipalatinsk explosions (Ringdal, 1990). NORESS is located at a site (06C02) within the large NORSAR array that has especially favorable focusing effects for P-waves from the Semipalatinsk region, and detectability has been further amplified through the array gain of 14–16 dB in the frequency band (2–4 Hz) of highest signal-to-noise ratio. On the other hand, for many other source areas, the focusing effects at the NORESS site are far less favorable, and the array detection performance is correspondingly lower.

In this paper we study the P-wave focusing effects across NORSAR for Novaya Zemlya explosions, and give some preliminary comments on the results achieved so far.

NORSAR P-wave recordings of Novaya Zemlya explosions

A number of underground nuclear explosions have been conducted at Novaya Zemlya during the 20 years of NORSAR operation. Because of the proximity of NORSAR to this test site (20 degrees) and the excellent P-wave propagation characteristics, the recorded signals have usually been so strong that they have exceeded the dynamic range of the NORSAR digital recording system. In fact, even the smallest explosion reported by Lilwall and Marshall (1986), (9 October 1977, $m_b = 4.51$) was in this category. Fig. 2.2.1 shows NORSAR recordings (7 SP seismometers, 1 per subarray) for this event. It can be noted that two of the data channels are clipped (02C01 and 03C01). In the latter case (03C01) the amount of clipping is very significant.

This example shows that for NORSAR seismometers located at sites with favorable receiver focusing effects, even very small explosions ($m_b > 4.0$) at Novaya Zemlya produce high amplitude recordings. While this is a disadvantage for studying focusing effects and other waveform features, it clearly implies that there is a very significant potential for exploiting these effects in achieving detectability at low magnitude levels.

Among the presumed explosions at Novaya Zemlya recorded by NORSAR, we have found only two events that are suitable for an amplitude pattern study (Events 2 and 3 of Table 2.2.1).

The location estimates in Table 2.2.1 of these two events (2 and 3) are approximate, but both explosions are from the Northern test site. The m_b values have been estimated as world-wide equivalent, by comparing NORSAR recordings to Event 1 (9 October 1977).

Figures 2.2.2 and 2.2.3 show NORSAR P-wave recordings of events 2 and 3, using the same instrument selection as for Event 1 (Figure 2.2.1). We note that on Figure 2.2.2, the background (microseismic) noise level is very high, but the signal is still clearly visible on some traces (notably 03C01). On Figure 2.2.3, the general amplitude pattern is similar to the other two events, again with 02C01 and 03C01 showing the strongest signals.

NORSAR amplitude patterns

In practice, detectability is determined by the signal-to-noise ratio in the "best" frequency band. For NORSAR recordings of Novaya Zemlya explosions, the 2.5–4.5 Hz band is near optimum, and Figure 2.2.4 shows the data from Figure 2.2.2 after applying this filter. The amplitude pattern in Figure 2.2.4a (given by the scaling factors to the left of each trace) shows an order of magnitude variation across the 60 km aperture array. From Figure 2.2.4b it can be seen that the noise levels at the different sites are similar, thus the signal amplitude pattern reflects true differences in P-wave detectability.

There are also significant amplitude variations within NORSAR subarrays (typical diameter 8–10 km), although naturally not as great as across the entire NORSAR array. Figures 2.2.5 and 2.2.6 show as examples unfiltered data for event 3 within the two best subarrays (02C and 03C). Note that the pattern is generally stable within subarray 02C, while at 03C the previously selected site (03C01) stands out as having far stronger signal than the others.

Figure 2.2.7 gives an overall view of NORSAR P-wave amplitude levels for Novaya Zemlya explosions as a function of seismometer location. It is clear that there are many sites with very favorable focusing effects, in particular 03C01. Compared to the NORESS site (06C02), there is an order of magnitude difference.

Detectability considerations

Across the large NORSAR array, the coherency of the signals from Novaya Zemlya is far too low to allow any meaningful improvement in signal-to-noise ratio through standard array processing. In fact, the NORSAR array beam has a lower SNR than the best single sensors for this region.

Thus, when considering seismic events in the regional distance range, the

main benefit of having full NORSAR data available is to obtain location estimates for small events, and, very importantly, to identify sites with particularly strong signals for a given region of interest. It is easy (taking appropriate reservations in view of the limited data available) to make first-order estimates of what could be achieved in this way. E.g., by simple SNR scaling, we have found that the seismometer 03C01 would record detectable signals for Novaya Zemlya explosions at the northern test site of m_b = 2.0–2.5 during normal noise conditions. With a small array of 6–10 instruments at that site (diameter ca 1000 m), it is projected that a further improvement of 0.5 m_b units could be achieved. This is based on NORESS noise structure experience, and would imply a threshold below m_b = 2.0 for such a small array. Again, it is emphasized that further studies are necessary before the potential for such low level detection can be confidently established.

F. Ringdal

References

Lilwall, R.C. and P.D. Marshall (1986). Body Wave Magnitudes and Locations of Soviet Underground Explosions at the Novaya Zemlya Test Site, *AWRE Report No. 0 17/86*, AWRE, MOD(PE), Blacknest, United Kingdom.

Ringdal, F. (1990). Teleseismic event detection using the NORESS array, with special reference to low-yield Semipalatinsk explosions, *Bull. Seism. Soc. Am.*, Special Issue, in press.

Event 1	9 Oct 1977	73.414°N		54.935°E		m_b = 4.51	O.T. 10.59.58.1
Event 2	15 Nov 1978	73	°N	55	°E	m_b = 3.6	O.T. 08.30.00.0
Event 3	26 Aug 1984	73	°N	55	°E	m_b = 3.8	O.T. 03.30.00.0

Table 2.2.1. Presumed explosions at Novaya Zemlya analyzed in this study.

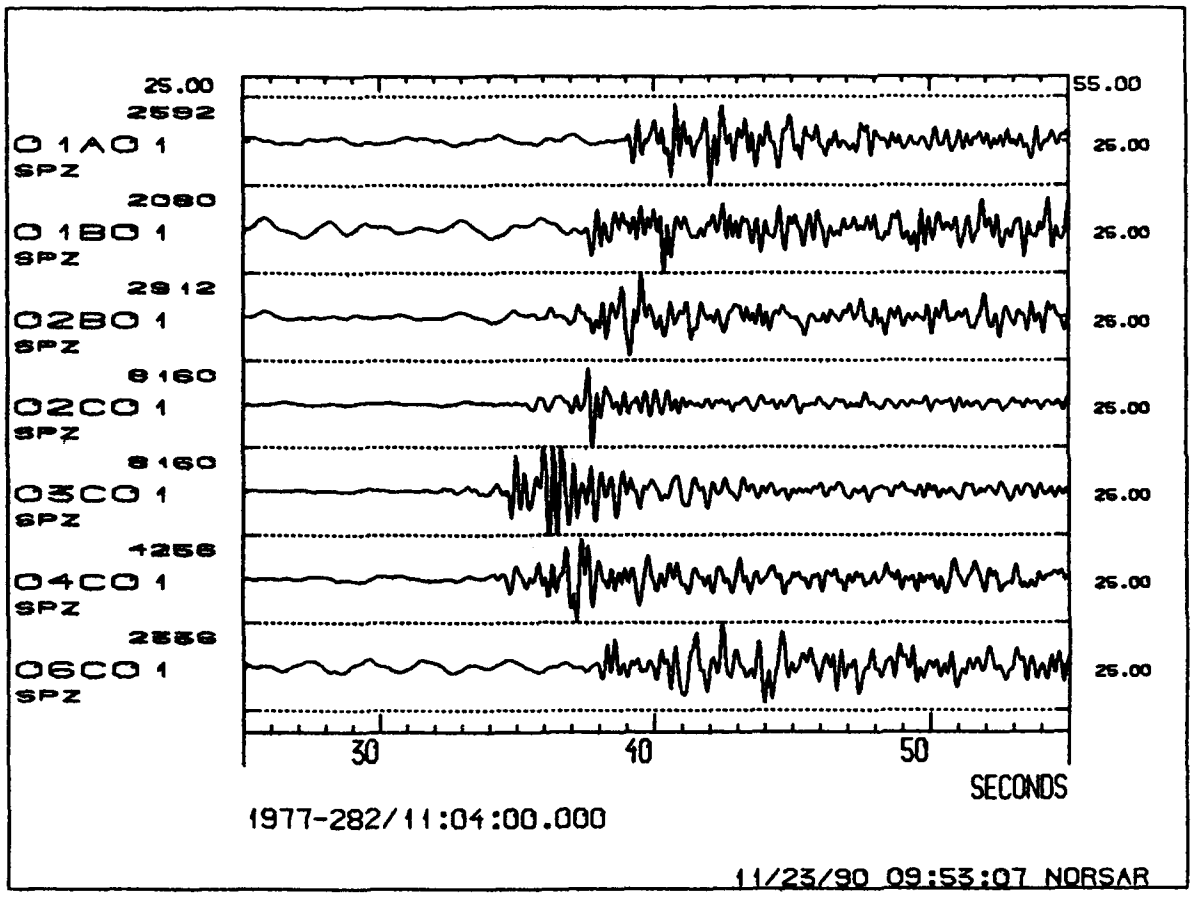

Fig. 2.2.1. NORSAR unfiltered recordings (one seismometer for each of 7 subarrays) for the Novaya Zemlya underground nuclear explosion of 9 October 1977 (Event 1 in Table 2.2.1). The scaling factors are shown to the left of each trace. Note that even though this explosion was very small ($m_b \approx 4.5$), the recorded signal was strong enough to saturate the NORSAR digital recording system at sites 02C01 and 03C01.

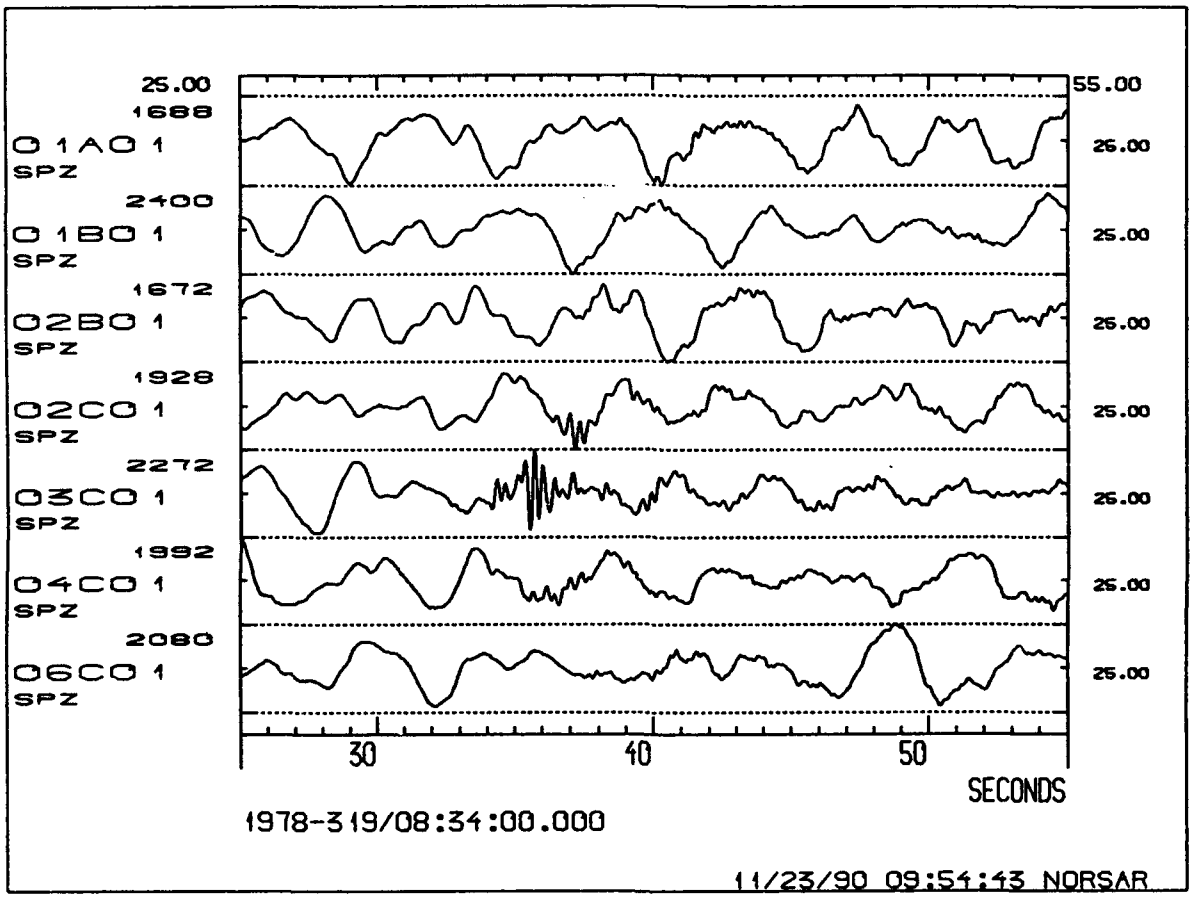

Fig. 2.2.2. Same as Fig. 2.2.1, but for Event 2 ($m_b \approx 3.6$) in Table 2.2.1. Note that in spite of very strong background noise, the signal is clearly visible at sites 02C01 and 03C01, even on the unfiltered recordings.

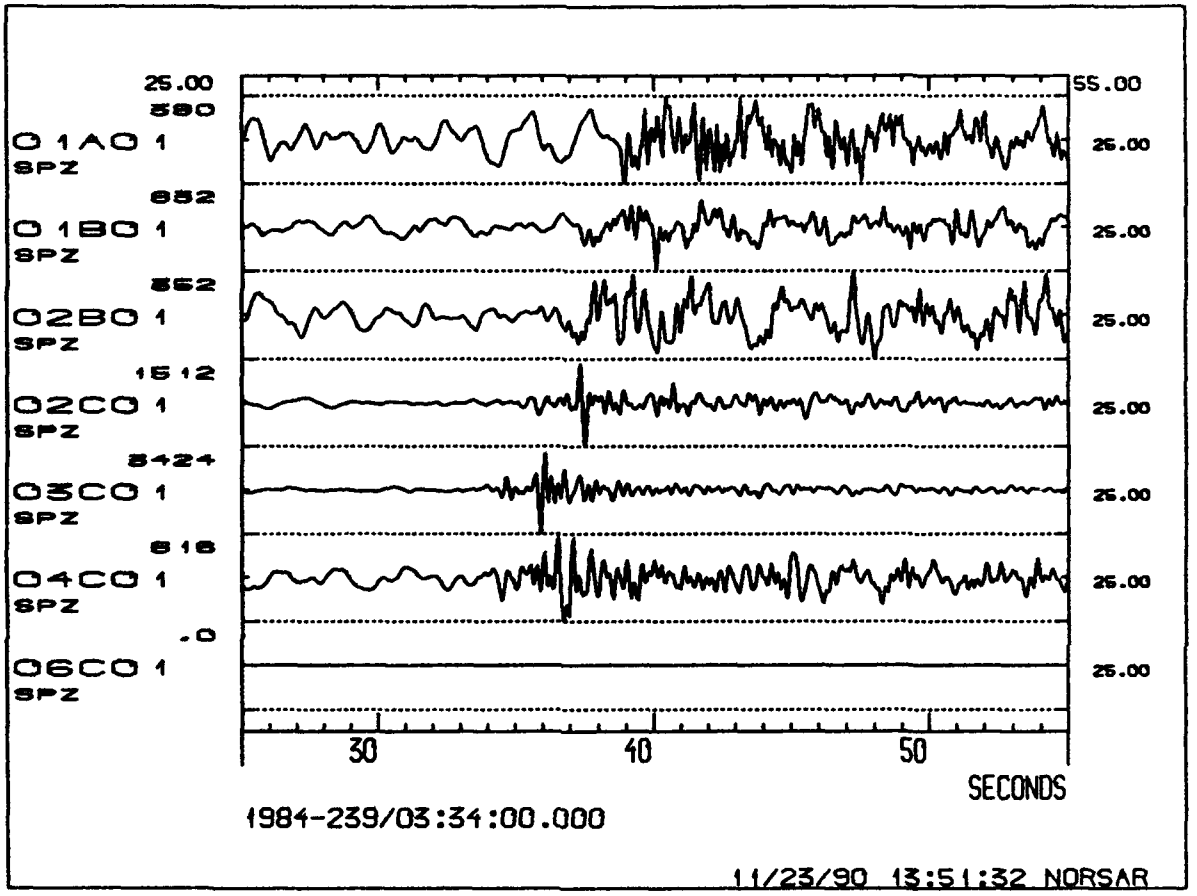

Fig. 2.2.3. Same as Fig. 2.2.1, but for Event 3 ($m_b \approx 3.8$) in Table 2.2.1. Note that the background noise in this case is much lower than on Fig. 2.2.2. Again sites 02C and 03C have the strongest signals.

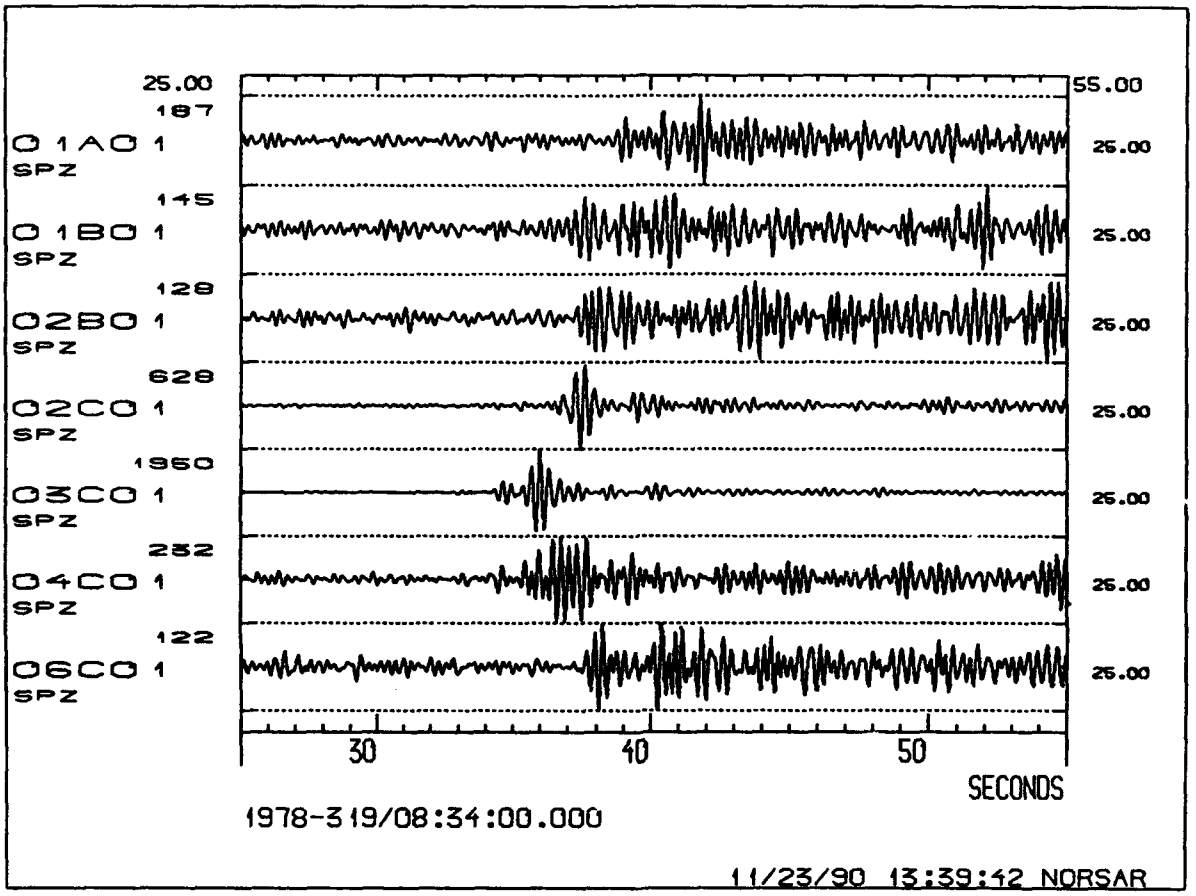

Fig. 2.2.4a. Filtered recordings (2.5–4.5 Hz) of the data shown in Fig. 2.2.2. Note that the signal can be seen on all traces, but with maximum amplitudes varying by more than an order of magnitude (see scaling factors to the left of each trace).

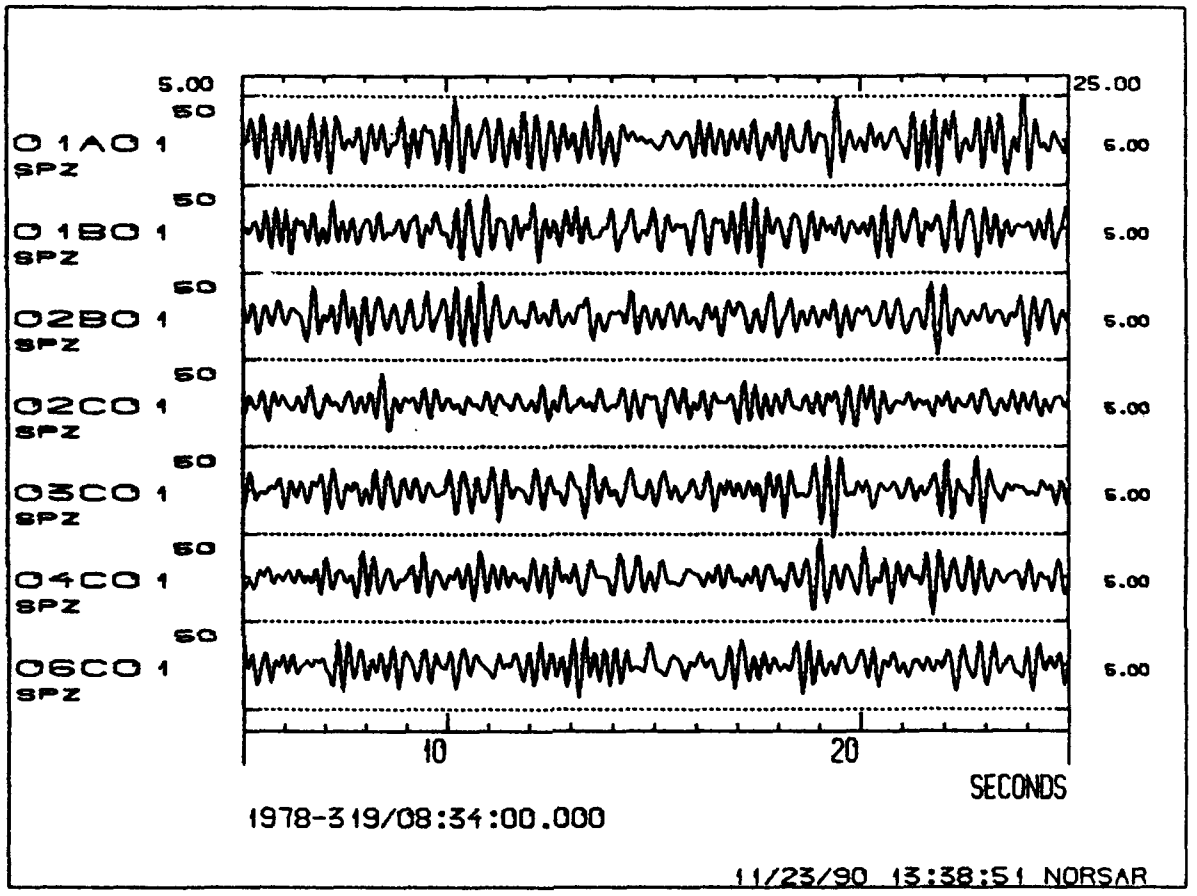

Fig. 2.2.4b. Noise data (2.5–4.5 Hz) preceding the signal shown in Fig. 2.2.4a. All traces have the same scale. Note that the noise levels at different sites are similar, thus the amplitude variation in Fig. 2.2.4a reflects true differences in P-wave detectability of Novaya Zemlya explosions.

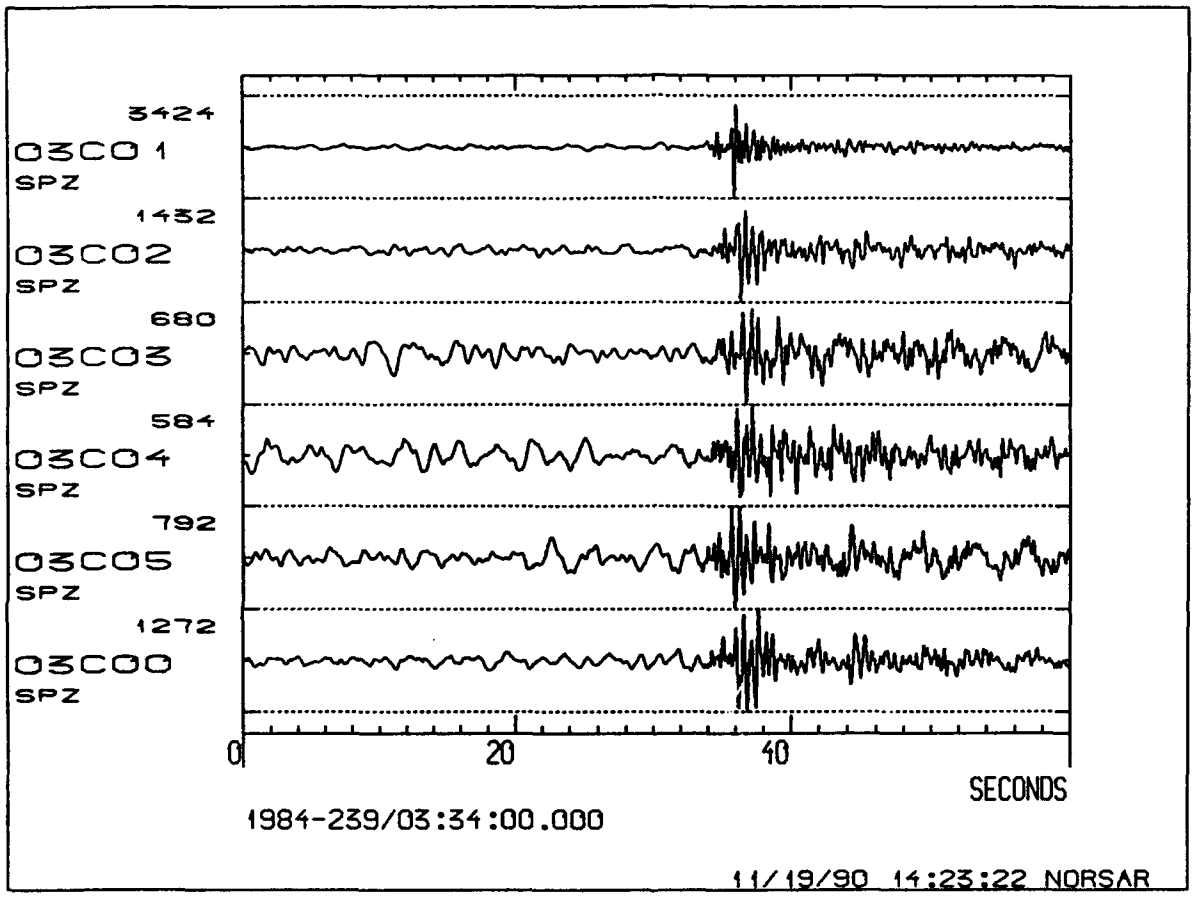

Fig. 2.2.5. P-wave amplitude variation within subarray 03C for Event 3 (unfiltered data). There is a factor of 6 in variation from the weakest to the strongest signal.

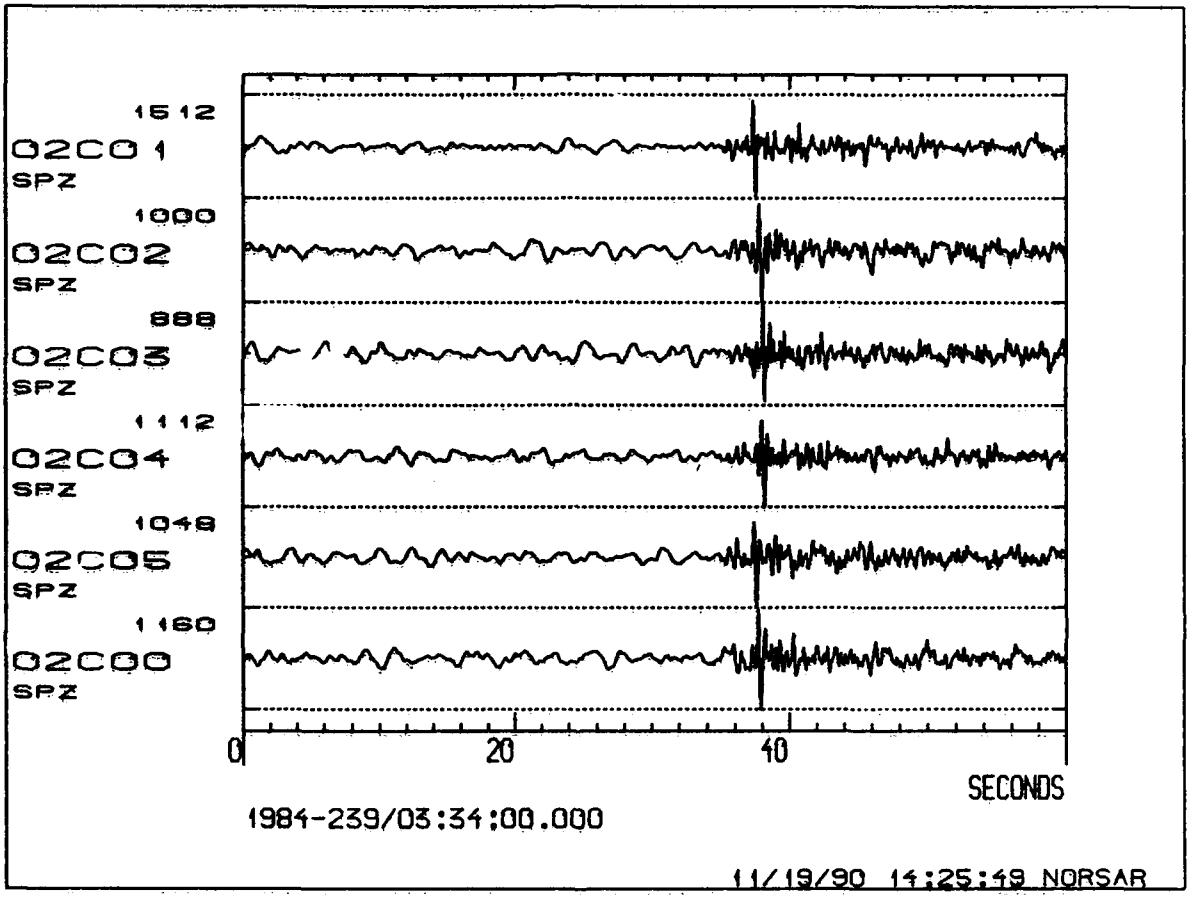

Fig. 2.2.6. P-wave amplitude variation within subarray 02C for Event 3 (unfiltered data). Note that both the amplitudes and waveform shapes are similar within this subarray, in contrast to subarray 03C (Fig. 2.2.5).

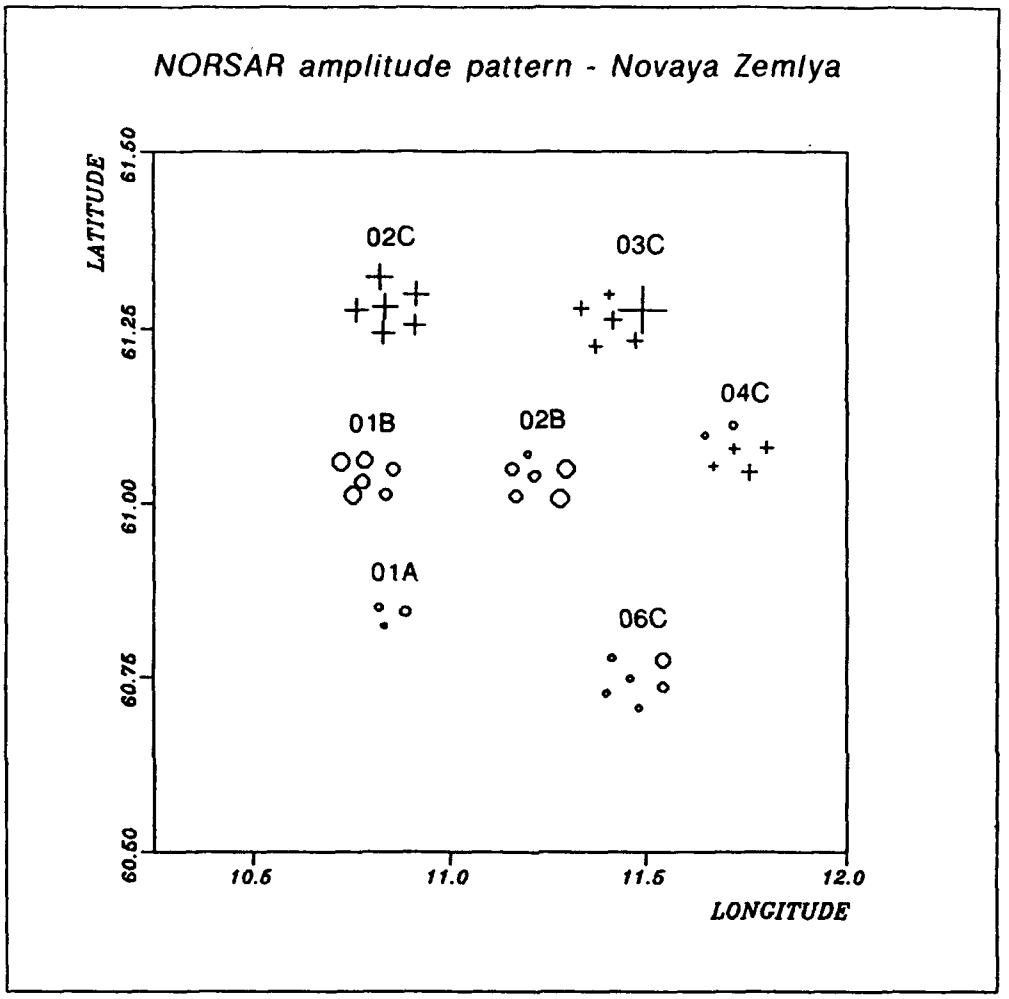

Fig. 2.2.7. P-wave magnitude bias relative to average NORSAR m_b for individual sites within the array. Symbol sizes are proportional to m_b bias, with plusses indicating positive bias values. Note the high positive bias for all sites within subarray 02C, and the especially high bias value at 03C01. The range of the bias values is from +0.9 (03C01) to -0.3 (01B05).

2.3 Wavefield extrapolation of array data

A major consideration in selecting the NORESS array site has been the high amplification of short-period P signals from directions to the East. From the analysis of data from large arrays it is well-known that the amplitude anomalies are associated with significant time residuals (Berteussen, 1976). It is desirable and possible to calibrate the times and amplitudes of specific phases at NORESS and similar arrays, but it would be an advantage both from a scientific and from a practical point of view to base the calibration and interpolation of seismic anomalies on a physically acceptable model of subsurface structure. As a first step toward that goal, we describe an experiment to extrapolate the observed wavefield at the surface down onto the subsurface. Downward extrapolation is common in processing seismic reflection data where the procedure is part of a migration process. The experiment we describe here differs from the usual reflection methods in two important aspects: (1) The time and amplitude anomalies are the result of forward scattering, rather than backward scattering as in reflection seismology. Downward extrapolation of the forward scattered wavefield has sometimes been called holography (Troitskiy *et al*, 1981); (2) The wavefield at the Earth's surface is sampled on a more or less irregular grid (c.f. the NORSAR array configuration). This precludes the effective use of Fourier transform methods. However, the elastodynamic representation theorem can be used to formulate wavefield extrapolation as an inverse problem independent of how the field is sampled. A range of methods is then available to solve this problem.

The inverse problem

Let the objective of downward extrapolation be to determine the field on subsurface S. The field at the Earth's surface in $\underline{x}$ is given by (c.f. Doornbos, 1988):

$$u_i(\underline{x},t) = \int_S \{T^i_{jk}(\underline{\xi},\underline{x},t) * u_j(\underline{\xi},t) - G^i_j(\underline{\xi},\underline{x},t) * \tau_{jk}(\underline{\xi},t)\} n_k \, dS \qquad (1)$$

Here $\underline{\xi}$ is a point on S with upward normal $\underline{n}$, the displacement and stress fields are denoted by u_j and τ_{jk}, respectively, and the Green's function and its associated stress tensor by G^i_j and T^i_{jk}.

Although it is customary to simplify equation (1) to a Kirchhoff integral under the assumption of acoustic waves, we use here a less restrictive far field approximation:

$$\begin{aligned} u_j(\underline{\xi},t) &= A_{in}(\underline{\xi})\, s_j(\underline{\xi})\, f(t - T_{in}) \\ G^i_j(\underline{\xi},\underline{x},t) &= A_G(\underline{\xi};\underline{x}) s_i(\underline{x};\underline{\xi})\, s_j(\underline{\xi};\underline{x})\, \delta(t - T_G) \end{aligned} \qquad (2)$$

where $T_{in} = T(\underline{\xi}), T_G = T(\underline{\xi};\underline{x})$, and the unit vectors $\underline{s}$ indicate the direction of particle motion in $\underline{\xi}$ and $\underline{x}$. Thus if $\underline{\nu}$ is a unit wave motion vector, then

$\underline{s} \cdot \underline{\nu} = 1$ for P, and $\underline{s} \cdot \underline{\nu} = 0$ for S waves. Substituting the asymptotic forms (2), assuming the amplitude factors A_{in} and A_G to be real, and disregarding time and amplitude anomalies, reduces equation (1) to a representation of the reference field:

$$\underline{u}^0(\underline{x}, t) = \int_S \underline{s}(\underline{x}; \underline{\xi}) B^0(\underline{\xi}; \underline{x}) \dot{f}(t - T^0)\, dS \tag{3}$$

where

$$T^0 = T_{in}(\underline{\xi}) + T_G(\underline{\xi}; \underline{x}) \tag{4}$$

$$B(\underline{\xi}; \underline{x}) = A_{in}(\underline{\xi})\, A_G(\underline{\xi}; \underline{x})\, R(\underline{\xi}; \underline{x}) \tag{5}$$

The factor $R(\underline{\xi}; \underline{x})$ depends on the incident and scattered wave modes. We will be concerned with P to P scattering. Then if subsurface S is embedded in an isotropic region with Lamè constants λ and μ and P velocity α:

$$R = \frac{1}{\alpha} \{\lambda - 2\mu(\underline{\nu} \cdot \underline{\nu}')\} \{(\underline{\nu}' \cdot \underline{n}) - (\underline{\nu} \cdot \underline{n})\} \tag{6}$$

Based on equation (3), the actually observed wavefield $\underline{u}(\underline{x}, t)$ will now be written as a perturbation of an initial estimate at subsurface S:

$$\underline{u}(\underline{x}, t) = \int_S \underline{s}\, (1 + \delta B)\, B\, \dot{f}(t - T - \delta T)\, dS \tag{7}$$

Here the amplitude and time perturbations δB and δT are unknown, but B, T and $f(t)$ are assumed known. Note that B and T need not be equal to B^0 and T^0 of equation (3). In general, B and T should be chosen such that the perturbations δB and δT are relatively small. In practice, values for B and T can be obtained from the results of downward extrapolating the wavefield to a level slightly above S. The waveform $f(t)$ is obtained from the array beam, assuming that the beam provides an estimate of the reference signal $\underline{u}^0(t)$ and noting that $u^0(t) \sim f(t - T^0)$. The representation (7) is physically meaningful if the perturbations are associated with topography of S and/or laterally varying structure below S (provided this structure does not produce caustics below S).

Using equation (7) and the approximation for the modified reference field:

$$\underline{u}'(\underline{x}, t) = \int_S \underline{s}\, B\, \dot{f}(t - t)\, dS \tag{8}$$

We can pose a linearized inverse problem in 3 different forms:

(a) Born approximation in time domain:

$$\begin{aligned} \delta\underline{u}(\underline{x}, t) &= \underline{u}(\underline{x}, t) - \underline{u}'(\underline{x}, t) \\ &\simeq \int_S \underline{s}\, B\{\delta B\, \dot{f}(t - T) - \delta T\, \ddot{f}(t - T)\, dS \end{aligned} \tag{9}$$

(b) Born approximation in frequency domain:

$$\delta \underline{u}(\underline{x}, w) \simeq -iw\, F(w) \int_S \underline{s}\, B\, e^{iwT} (\delta B + iw\delta T)\, dS \qquad (10)$$

(c) Rytov approximation:

$$ln \frac{\underline{U}(\underline{x}, w)}{\underline{U'}(\underline{x}, w)} \simeq -iw \frac{F(w)}{\underline{U'}(\underline{x}, w)} \int_S \underline{s}\, B\, e^{iwT} (\delta B + iw\delta T)\, dS \qquad (11)$$

Synthetic data

We have synthesized the surface displacement $\underline{u}(\underline{x}, t)$ from prescribed time and amplitude anomalies at depth. The spatial sampling of $\underline{u}(\underline{x}, t)$ was chosen so as to simulate the recordings of 132 short-period channels in the NORSAR array. The array beam signal from a nuclear explosion in E. Kazakh was used to get the basic waveform $f(t)$ and the direction of wave propagation $\underline{\nu}$. Downward extrapolation was then done in 3 different ways, by inverting equations (9), (10) and (11), respectively. The time domain method (a) used the first 3 seconds of the low-pass filtered P pulse resampled at 5 Hz. The frequency domain methods (b) and (c) used 6 frequencies of the same pulse, in the band 0.6 – 2.1 Hz.

Figure 2.3.1 pictures an anomaly at 100 km depth used in one of the experiments. In this example the anomaly equals a time delay with maximum 0.7 seconds. The resulting time and amplitude patterns at the NORSAR array site are shown in Figures 2.3.2 and 2.3.3. The time residuals are reduced in relation to the pattern at 100 km depth, but the amplitudes fluctuate by about a factor of 2. Inversion of these data was started at 20 km depth, and continued downward with a 5 km depth step. For the purpose of inversion, the subsurface area at each depth was divided in cells, the size of which is increasing with distance from the central ray. The reconstructed pattern at 100 km depth is shown in Figure 2.3.4 and 2.3.5, where we have used the Rytov method (c). There are outliers along the boundaries of the grid where data coverage is poor. There is also a time offset of about 0.2 s. However, the principal features of the time residual pattern are well recovered. On the other hand, the amplitudes fluctuate by about a factor of 2 in contrast to the starting model; we interpret this to mean that the surface data are primarily constraining the time perturbations at depths.

Explosion P wave from E. Kazakh

Figure 2.3.6 shows the P wave on the C-ring of NORSAR, from a nuclear explosion in E. Kazakh. The time residuals vary by more than 0.5 s, and the amplitudes vary by about a factor of 5 (Figures 2.3.7 and 2.3.8). The data from the complete array were used to reconstruct the residual time and amplitude pattern at depth. Results for 100 km depth are shown in Figures

2.3.9 and 2.3.10. From the results for synthetic data we expect solutions for the residual times to be more reliable than those for the amplitudes. The variation of the residual times is about twice as large as at the Earth's surface. Disregarding the poorly constrained outliers along the boundaries of the grid, the results suggest an extensive deep-seated region of low velocity to the NE from NORSAR (note that the center of the maps 2.3.9 and 2.3.10 is already displaced to the NE from the array center). In this connection it should also be noted that the optimum depth of subsurface S is actually another unknown of the inverse problem. Several error criteria may be used to determine this depth. In Figure 2.3.11 we have plotted the RMS error of time residuals left unexplained by the subsurface solution, in per cent of the observed RMS residual. Inversion of the synthetic data reduces the RMS error to very small values for depths larger than about 40 km. Inversion of the explosion data leaves a more significant part of the residuals unexplained, but there is a broad minimum in the range 100–130 km. It is of course desirable to delineate the structure in more detail; inversion of the data from many more events is needed to provide this detail.

E. Ødegaard, Univ. of Oslo
D.J. Doornbos, Univ. of Oslo

References

Berteussen, K.-A. (1976): The origin of slowness and azimuth anomalies at large arrays, *Bull. Seism. Soc. Am.*, 66, 719–741.

Doornbos, D.J. (1988): Multiple scattering by topographic relief with application to the core-mantle boundary, *Geophys. J.*, 92, 465–478.

Troitskiy, P., E.S. Husebye and A. Nikolaev (1981): Lithospheric studies based on holographic principles, *Nature*, 294, 618–623.

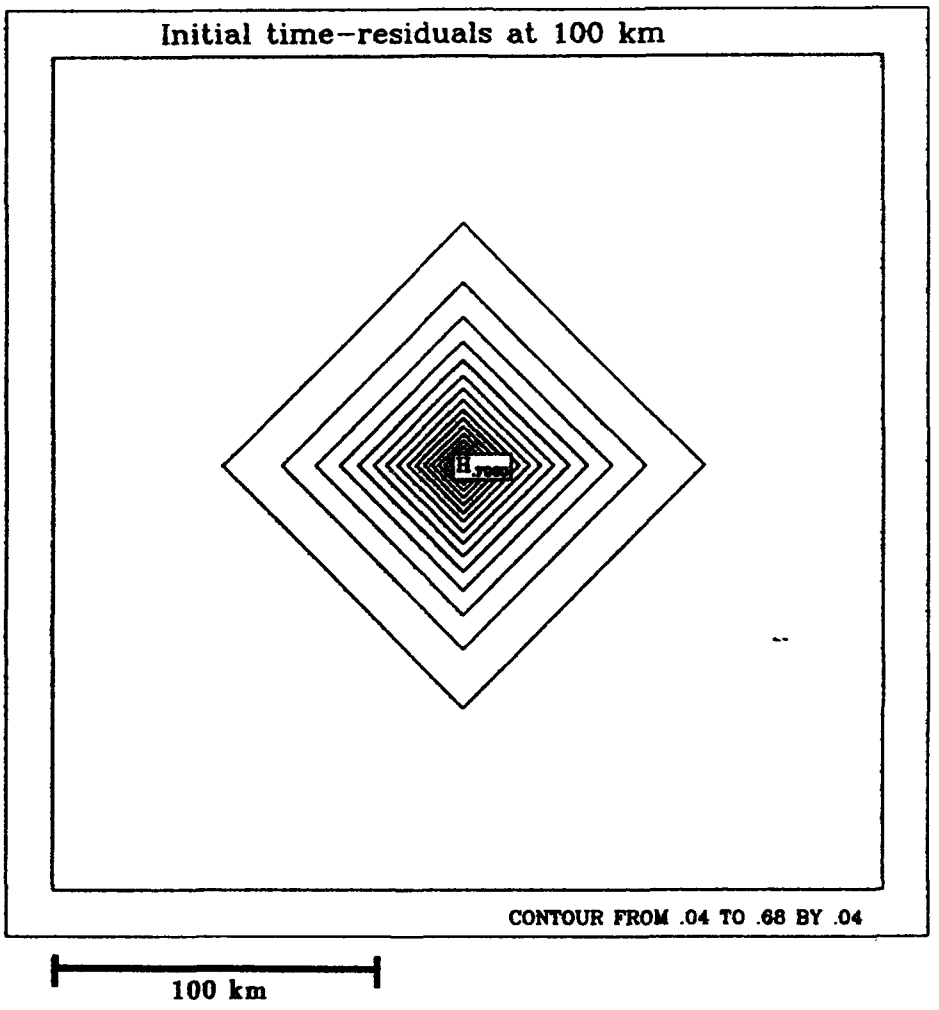

Fig. 2.3.1. Contour map of travel time delays at 100 km depth. The center of the map is at 60.992°N, 12.134°E (NE from the NORSAR array center). The incident ray slowness and propagation azimuth are 0.076 s/km and 255 deg.

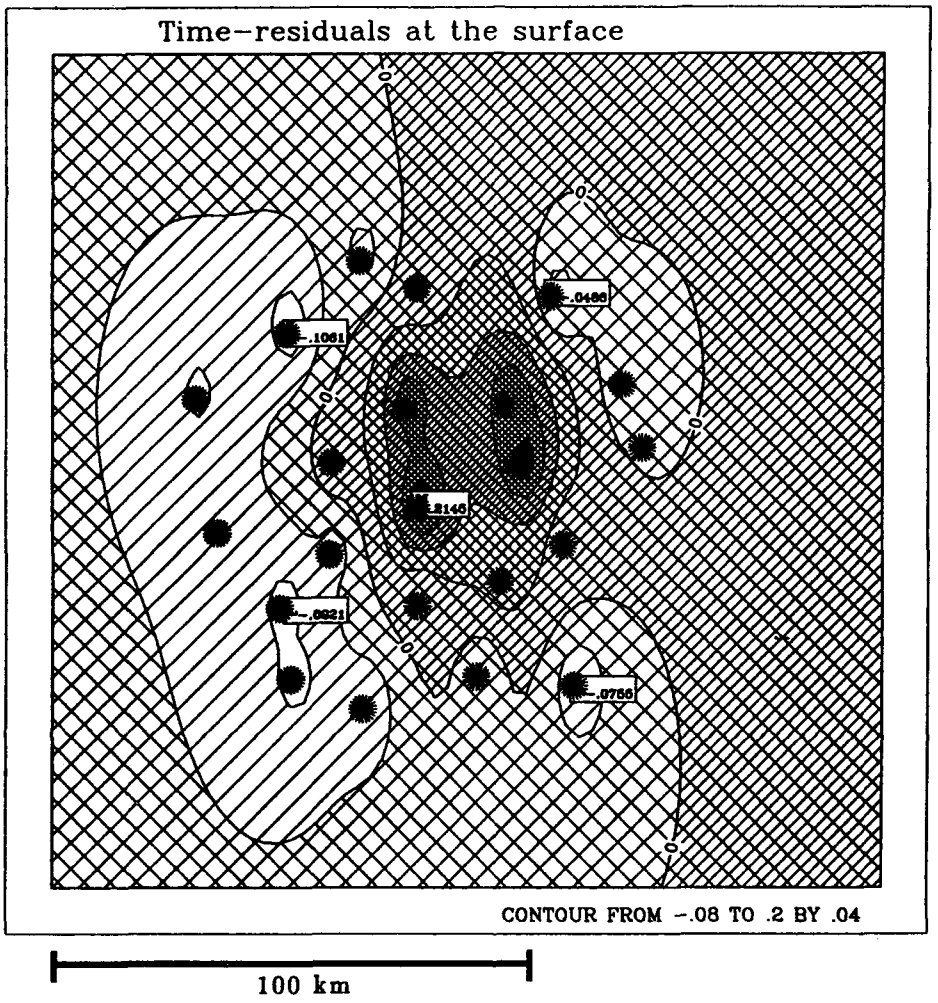

Fig. 2.3.2. Travel time residuals at the Earth's surface, caused by the anomaly of Fig. 2.3.1. The NORSAR subarray centers are indicated by stars.

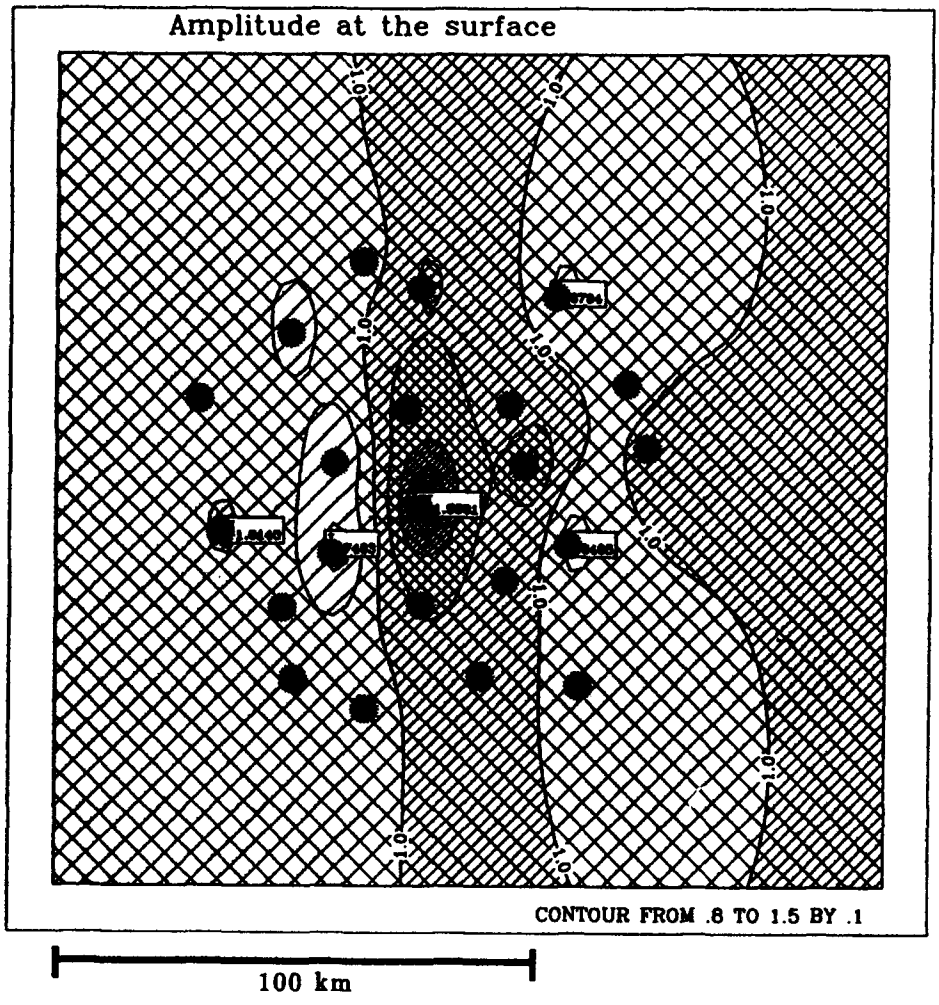

Fig. 2.3.3. Amplitude pattern at the Earth's surface, caused by the anomaly of Fig. 2.3.1. Amplitude factors relative to the reference value 1.

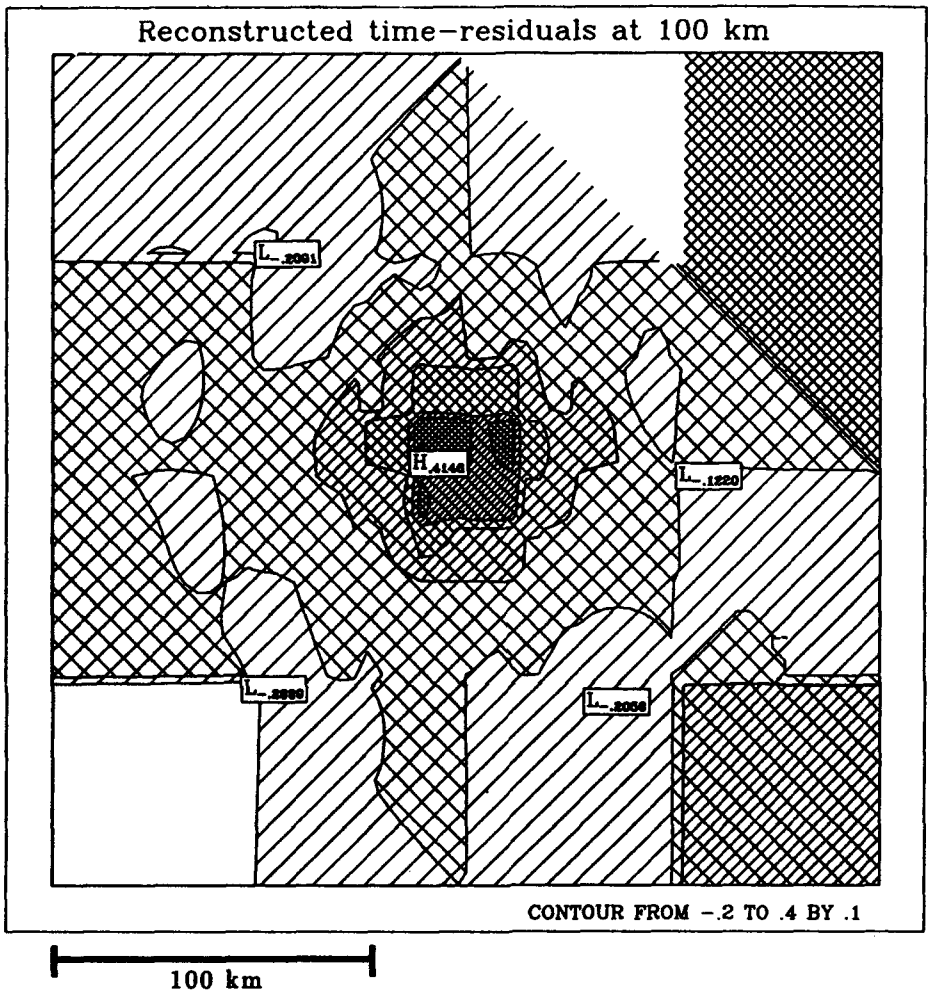

Fig. 2.3.4. Reconstructed time residuals at 100 km depth. the map covers the same area as Fig. 2.3.1.

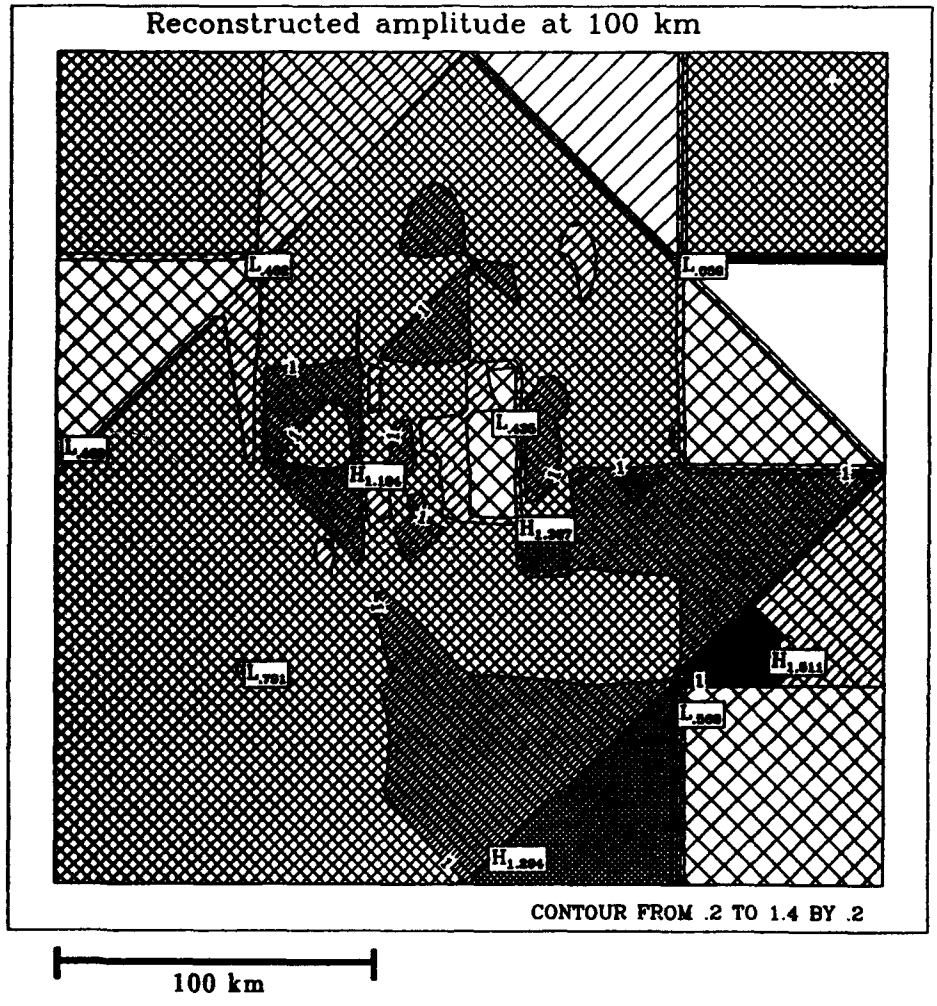

Fig. 2.3.5. Reconstructed amplitude factors at 100 km depth. The map covers the same area as Fig. 2.3.1.

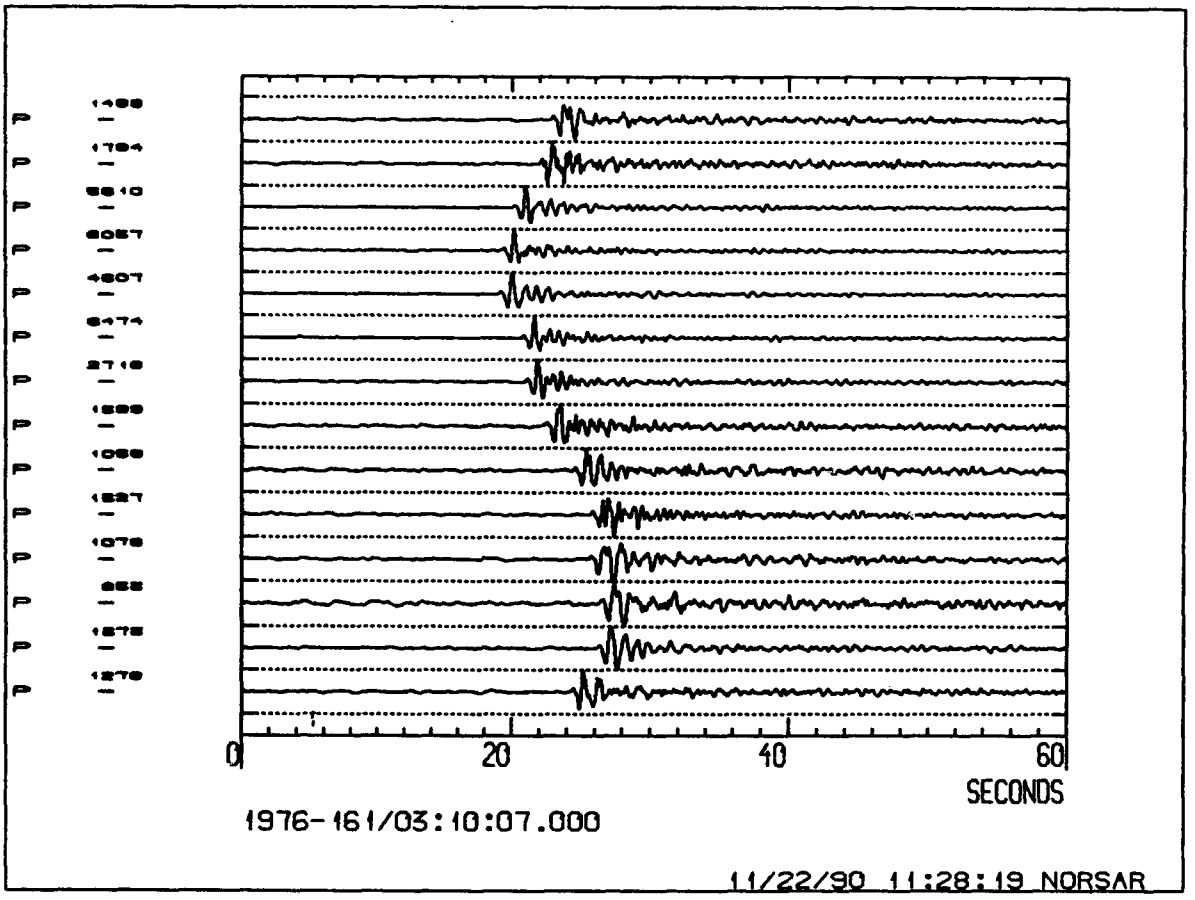

Fig. 2.3.6. NORSAR subarray beams at C01–C14. Scaling factors to the left. The P wave is from a nuclear explosion in E. Kazakh, in 1976. Start time of the records underneath.

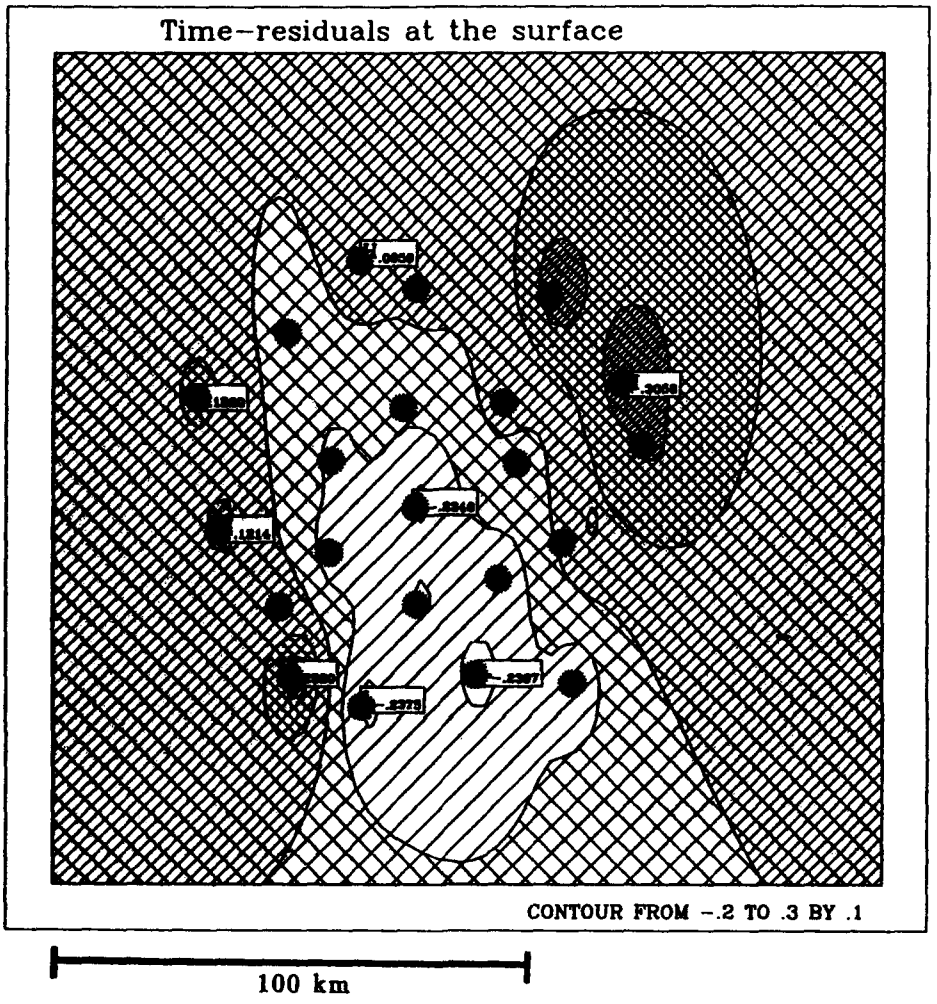

Fig. 2.3.7. Travel time residuals at NORSAR, of P wave from E. Kazakh nuclear explosion (Fig. 2.3.6).

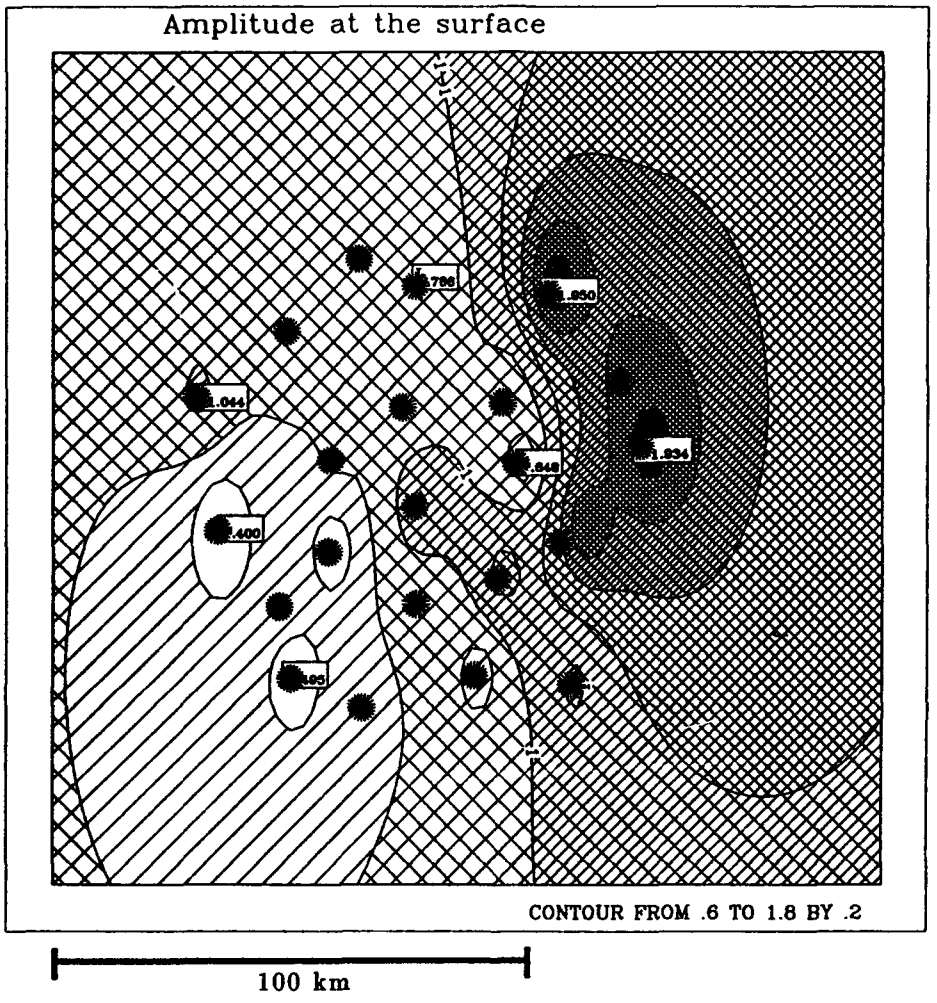

Fig. 2.3.8. Amplitude factors at NORSAR, of P wave from E. Kazakh nuclear explosion (Fig. 2.3.6).

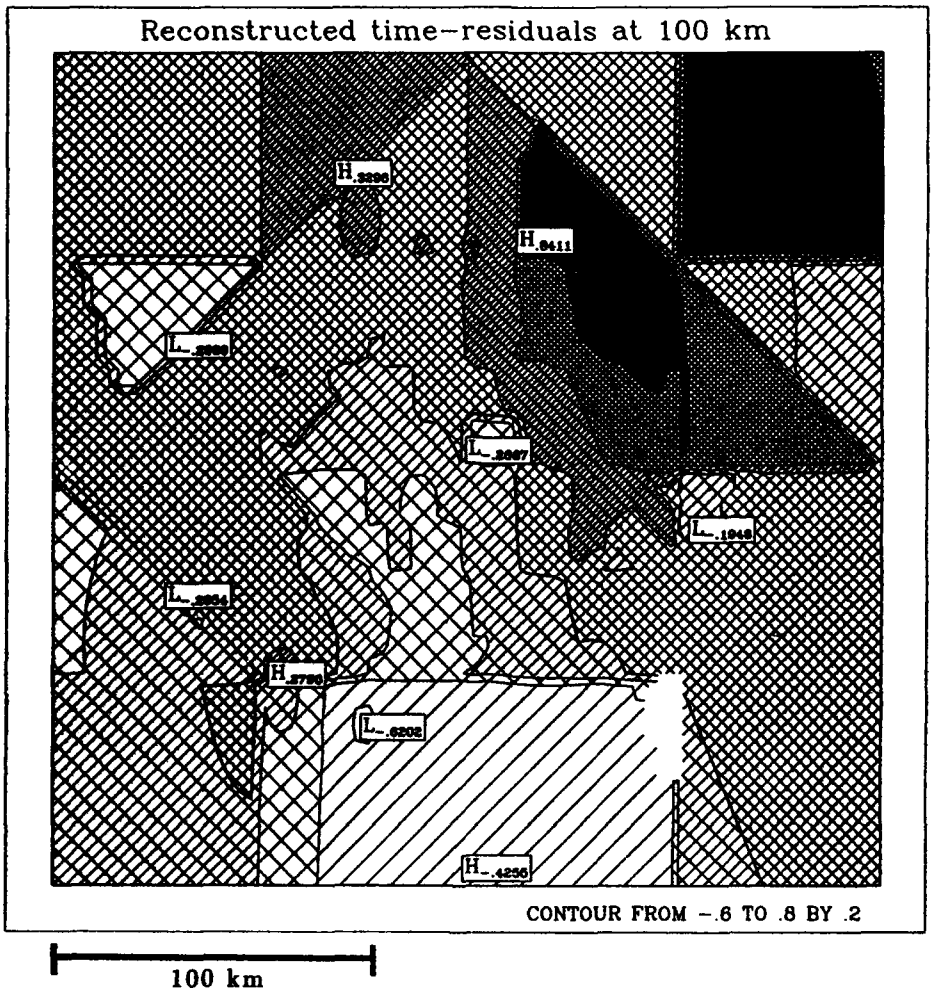

Fig. 2.3.9. Reconstructed time residuals at 100 km depth. The map center is at 60.992°N, 12.174°E (as in Fig. 2.3.1.

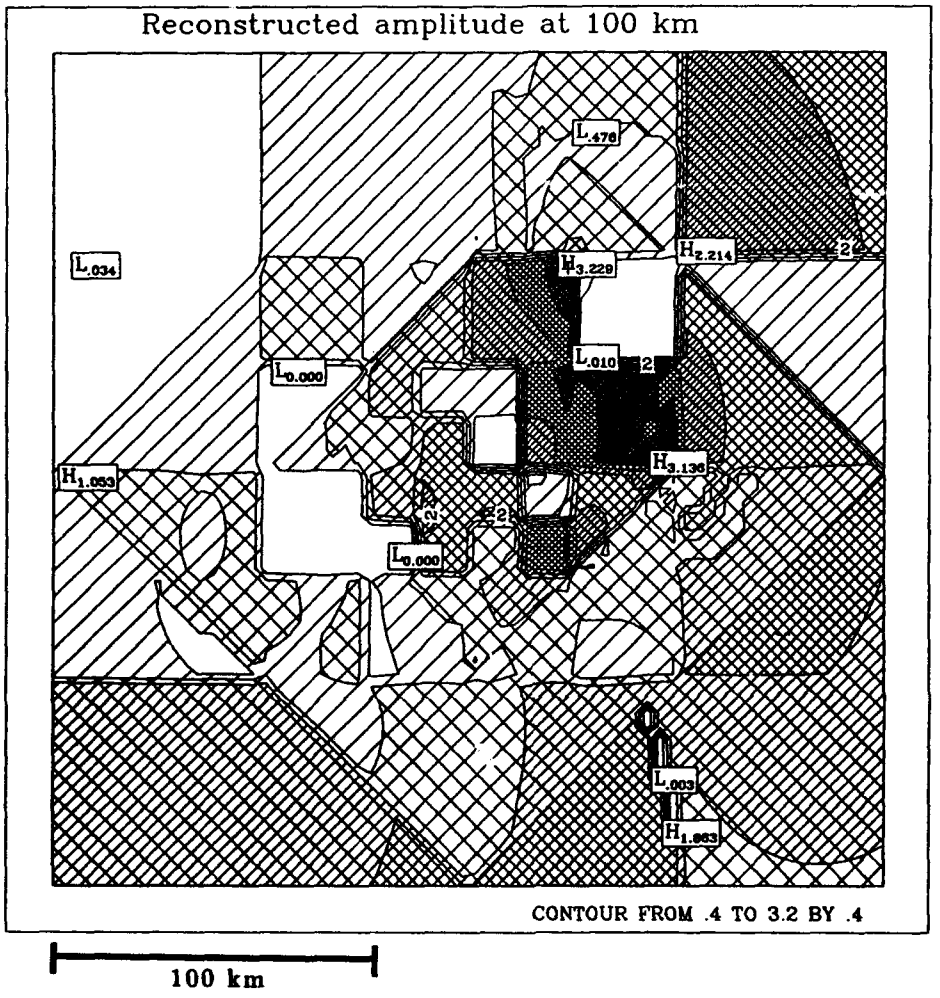

Fig. 2.3.10. Reconstructed amplitude pattern at 100 km depth. The map covers the same area as Fig. 2.3.9.

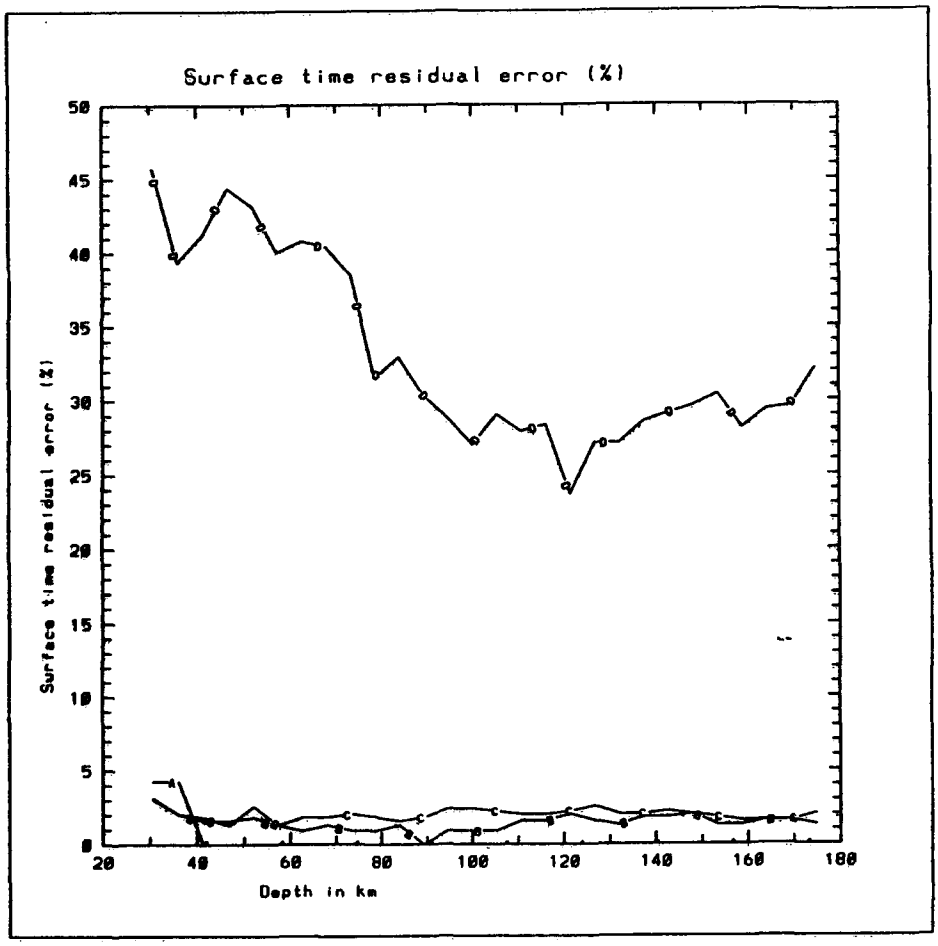

Fig. 2.3.11. RMS residual time error after correction for reconstructed time and amplitude models at depth. Values in per cent of RMS residual with respect to the reference model. A, B and C: Downward extrapolation of synthetic data. D: Downward extrapolation of P wave from nuclear explosion in E. Kazakh (Fig. 2.3.6).

2.4 The seismicity of Norway and surrounding areas

Introduction

Norway, the epicontinental North Sea and Barents Sea, and the Norwegian continental margin are characterized by low-to-intermediate seismicity (Kvamme and Hansen, 1989, Hansen *et al*, 1989; Bungum *et al*, 1991). The geology of the areas south of 62°N, and in particular the northern North Sea, has been widely investigated as a result of hydrocarbon exploration. The areas north of 62°N have been extensively investigated as well, although not in as much detail as further south. The regional geology and tectonic setting in all of these areas are therefore now relatively well understood (e.g. Spencer *et al*, 1984, 1986; Glennie, 1986).

Norway and its surrounding areas, in particular the northern continental margin, have until recently been relatively poorly covered in terms of seismic instrumentation (Husebye *et al*, 1975, 1978; Bungum and Fyen, 1980). In the last decade the situation has been much improved, however, through the installation of new regional and local networks (Bungum *et al*, 1986). This increased number of stations has resulted in more detailed delineation of seismicity patterns as well as improved focal mechanism solutions. Such information can in turn be correlated with geologic information.

One of the incentives for the improvements in our knowledge of the seismotectonics of Norway and the Norwegian continental shelf has been the need for better and more reliable earthquake hazard analyses for offshore industrial installations. These goals have been pursued through the installation of local microearthquake networks (Bungum *et al*, 1986; Kvamme and Hansen, 1989; Havskov *et al*, 1991), and through research studies specifically aimed at earthquake hazard and loading (Bungum and Selnes, 1988). For offshore Norway, known in great detail geologically, such networks and seismicity studies are moreover contributing significantly to our understanding of deep structures and large-scale features such as the Viking Graben.

Another important incentive for investigating the natural seismicity of Norway and surrounding areas is that the nuclear explosion monitoring programs need the best possible background information about the seismicity, not only in the areas where such explosions could take place, but also in the areas within local and regional distance from the monitoring stations (Richards, 1988). In the new *Intelligent Monitoring System* (Bache *et al*, 1990; Bratt *et al*, 1990) now installed at NORSAR such background seismicity can be displayed as overlays. For this purpose, three different catalogues have been prepared, covering the three time periods 1880–1954, 1955–1979 and 1980–1989, shown in Figures 2.4.1–2.4.3, respectively. The purpose of this presentation is to document these catalogues, and to outline briefly their seismotectonic context.

Earthquake data

Even though the seismicity of Norway is moderate, historical records show (Bungum and Selnes, 1988) that earthquakes strong enough to be felt clearly over several hundred kilometers have occurred repeatedly, particularly along the west coast. Systematic collection of macroseismic questionnaires was initiated in the 1880's at the Bergen Museum, and such data have been collected more or less uninterrupted for these areas ever since (Muir Wood *et al*, 1988). This has provided, in spite of a sparse population, a good basis for a major reassessment performed recently of the historical seismicity in Norway and surrounding areas (Ambraseys, 1985; Muir Wood and Woo, 1987). This reassessment has primarily included macroseismic intensity maps ("felt areas"), evaluated in a consistent way for this time period by going back to the original data for all of the earthquakes. From this felt area information similarly consistent magnitudes (M_S) have been evaluated, which in turn have been very important for assessments of earthquake hazard in these areas (Bungum and Selnes, 1988).

This historical earthquake catalogue has been updated to the end of 1989 by including all events that could be evaluated on the basis of felt effects. In addition, information on the regional earthquake distribution in Fennoscandia has now been available for several tens of years based on data from global networks of seismological stations. The earlier global networks, however, provided rather poor coverage in this area where the seismicity is low-to-intermediate (Bungum *et al*, 1986; Bungum *et al*, 1991). Only for the time period since 1963 do these networks become important for this region, and then first of all for the area north of 70°N (Sykes, 1967). After about 1980, microearthquake networks were also installed in northwestern Europe (Bungum *et al*, 1986; Havskov *et al*, 1991), and major improvements were again possible.

The historical data are limited by the shortcomings of any macroseismic catalogue in less populated areas, and in particular for offshore areas. Similar limitations in the global network solutions occur because very few earthquakes have been large enough to be detected by a sufficient number of stations. These limitations have been overcome in part in the present work by collecting a very large number of epicentral solutions from a variety of reporting agencies, and then carefully screening this data base so as to increase resolution while maintaining accuracy (Bungum and Selnes, 1988; Bungum *et al*, 1991). One of the most robust sorting criterion in this respect was found to be the number of stations and/or readings used in computing the epicenters.

Other sorting criteria included reporting agency (not equally reliable), magnitude, macroseismic information, various precision estimates (including consistency between different reports for the same event), in addition to number of stations and readings used in the solutions. A time dependent combination of these criteria has been used when selecting events for the seismicity

maps in Figures 2.4.1–2.4.3. Those maps include, in addition to earlier data, very significant contributions resulting from the increased microearthquake coverage during the 1980's (Bungum *et al.*, 1986), including the most recent data from the networks and stations in northern Norway (Kvamme and Hansen, 1989).

In Figures 2.4.1–2.4.3, there are some patterns of seismicity that appear clearer than reported before, especially when compared with the structural information. In addition to the Mid-Atlantic Ridge, the seismicity follows broadly the continental margin from Svalbard to the northern North Sea. Some concentrations of earthquakes also are found in the coastal areas of western and northern Norway as well as in the Viking Graben, the Central Graben and the Oslo Graben. In addition, significant earthquake activity is confined to a large area in the eastern Lofoten Basin west of the Senja Fracture Zone and possibly also to a small area near the intersection between the Vøring Plateau Escarpment and a set of parallel faults tied to the East Jan Mayen Fracture Zone. We also note the presence of relatively well-defined zones in Sweden (Slunga *et al*, 1984) and in Finland (Ahjos *et al*, 1984). These zones have significantly lower recurrence rates, however.

Because of the particular properties of the data bases used in this analysis, and the way they have been combined, we have chosen to break the seismicity data into three different time periods, as follows:

- *Figure 2.4.1*: 1880–1954, consisting mostly of the felt (historical) earthquakes, with a few additional instrumental network locations.
- *Figure 2.4.2*: 1955–1979, consisting mostly of instrumentally located earthquakes from a variety of reporting agencies.
- *Figure 2.4.3*: 1980–1989, consisting mostly of locations based on new microearthquake networks.

The earthquake magnitudes used in these catalogues are mostly M_S for the first one, m_b for the second, and M_L for the third. The M_S scale is here tied to the "felt area" A_{IV} (for MSK intensity IV) and A_{III} (for intensity III) as developed by (Muir Wood and Woo, 1987).

The following relationship has been developed between M_S and M_L (Bungum and Selnes, 1988):

$$M_S = 0.85M_L + 0.60 \qquad (1)$$

This magnitude relationship, developed for events in the M_L range 3 to 5, is used in most cases when earthquakes from different catalogues are used together. The catalogues also contain many reported body wave magnitudes m_b (Figure 2.2.2), but with relationships to M_L and M_S which are more uncertain.

Earthquake location precisions

The seismicity information presented in this paper covers almost 200 years. In the beginning of this time period Norway was sparsely populated, limiting the possibilities for gathering earthquake information, while for the last few years the country has been very well covered with seismic stations, arrays and networks. The earthquake location precisions therefore necessarily also vary considerably. In this presentation of the earthquake catalogues we discuss three different time periods, and the main reason for this separation is that the three time periods also represent different levels of precision (as well as different detectability levels), as outlined in the following:

The first time period (1800–1954, Figure 2.4.1) consists primarily of macroseismically determined epicenters, and all of those have recently (as mentioned above) been reevaluated in a consistent way, including tuning of locations using recent instrumentally located (and macroseismically surveyed) template earthquakes (Muir Wood and Woo, 1987). Location uncertainties can still be quite large, however, usually in the range 20–60 km, and up to 100 km in particular cases. It should be noted here that large (macroseismically located) earthquakes often may have larger uncertainties than smaller ones. For the few instrumentally located earthquakes during this time period, the uncertainties are assessed to be of the same size as for the macroseismically located ones. This catalogue of historical earthquakes has been found to be complete since about 1880 down to M_S 4.0 south of 65°N and down to M_S 4.5 further north (Muir Wood and Woo, 1987).

The second time period (1955–1979, Figure 2.4.2) contains earthquake reports that are more inhomogeneous, consisting of locations reported by a variety of seismological agencies. With a fairly large number of events in the data base, it was generally not possible for us to go back to the original readings for these events. The sorting and screening criteria discussed above, however, were designed first of all to ensure the best possible quality in the locations, which partly conflicts with the criteria that would provide the best possible completeness. The resulting location uncertainties are estimated to be in the range 20–25 km for most of the events, but also less than 10 km in some cases.

The third and last time period (1980–1989, Figure 2.4.3) contains again data that are more homogeneous, with completeness down to about M_L 2.0 for the areas south of 65°N . These locations are based on recordings from the relatively dense microseismic networks installed in the area since the beginning of the 1980s. We have in this case been actively involved in much of the earthquake location work (e.g., Bungum *et al*, 1986), and most of the readings are also available to us. This makes it easier to assess location uncertainties, found to be less than 15 km in most cases, and often less than 5 km.

All of the earthquake locations based on instrumental data are obtained using an essentially continental crustal model. Biased errors are still not found

to be significant, however, because most of the offshore seismicity is close to the coast (with a reasonable azimuthal coverage of stations), and because readings from stations in Great Britain (including Scotland and the Shetland Islands) and from ocean-bottom seismographs routinely are used in the locations. For the events large enough to provide readings at teleseismic distances, the azimuthal coverage is even better.

Regional patterns of seismicity

In the areas south of 63°N, the offshore seismicity is more or less confined to the shelf edge to the northwest and to the Viking Graben and the Central Graben to the west and southwest. In the Central Graben, the earthquakes are quite small, but nevertheless occur along a convincing lineation. The events in the Viking Graben are larger and more frequent, including a widely felt M_S 5.3 earthquake in 1927. Some seismic activity is also found in the Oslo Rift. Presently only very small earthquakes occur there (Bungum and Fyen, 1980), but one of magnitude M_S 5.4 occurred on October 23, 1904, and another of M_S 4.4 on March 6, 1953. Another seismically active area is west of Jutland in the Norwegian-Danish Basin, possibly related to the Fjerritslev-Tornquist Zone or the Fennoscandian Border Zone. The areas south of 63°N with the highest earthquake activity, however, are the coastal areas between 59 and 63°N, including an offshore extension into the northern North Sea.

The area between 63 and 70°N includes the location (near 66.5°N, 14.5°E) of the largest known (M_S 5.8 in 1819) historical earthquake in northwestern Europe (Bungum and Selnes, 1988). It is seen fro the seismicity maps that this area along the Nordland coast is still quite active. One of the most prominent features is the zone of seismic activity that runs parallel to the shelf edge from 64°N, 6°E, continuing into the Lofoten Islands.

For the area between 70 and 78°N, the most obvious feature (the spreading ridge excluded) is the seismicity that seems to be limited by the series of faults and fracture zones that parallels the shelf edge between northern Norway and Svalbard. The most prominent of these is the Senja Fracture Zone, along which we find a well-defined seismic activity (see also Kvamme and Hansen, 1989). A broad zone of seismicity in the eastern Lofoten Basin (cf. Husebye *et al*, 1975) now seems to be even more clearly defined than before. Further north, the Svalbard region also shows significant earthquake activity in some areas (Mitchell *et al*, 1989). Further south, events have been located along the Senja Fracture Zone and eastwards to the Ringvassøy-Loppa Fault Complex. The Senja Fracture Zone is known to be quite active, separating the oceanic crust to the west from the continental crust to the east.

For a more in-depth study of the seismicity and seismotectonics of Norway and surrounding areas, including focal mechanism solutions (stress patterns) and focal depths, we refer to Bungum *et al* (1991).

Conclusions

The new historical and instrumental earthquake catalogues presented here have been organized to cover the time periods 1880–1954, 1955–1979 and 1980–1989. These catalogues have given us a much improved picture of the distribution of earthquakes both in time, space and magnitude. The seismicity follows on a regional basis various geologic structures such as fault zones and complexes, grabens, fracture zones, shelf and margin areas.

H. Bungum
A. Alsaker

References

Ahjos, T., J. Saari, E. Penttila and H. Korhonen (1984). Earthquakes seismic hazard in Finland, *Eng. Geology* **20**, 1–12.

Ambraseys, N.N. (1985). The seismicity of western Scandinavia, *Earthq. Eng. and Structural Dynamics* **13**, 361–399.

Bache, T.C., S.R. Bratt, J. Wang, R.M. Fung, C. Kobryn and J. Given (1990). The Intelligent Monitoring System, *Bull. Seism. Soc. Am.*, Special Issue, in press.

Bratt, S.R., H.J. Swanger, R.J. Stead, F. Ryall and T.C. Bache (1990). Initial results from the Intelligent Monitoring System, *Bull. Seism. Soc. Am.*, Special Issue, in press.

Bungum, H., A. Alsaker, L.B. Kvamme and R.A. Hansen (1991). Seismicity and seismotectonics of Norway and surrounding continental shelf areas, *J. Geophys. Res.*, in press.

Bungum, H. and J. Fyen (1980). Hypocentral distribution, focal mechanisms, and tectonic implications of Fennoscandian earthquakes, 1954–1978, *Geol. Fören. Sth. Förh.* **101**, 261–273.

Bungum, H., J. Havskov, B.K. Hokland and R. Newmark (1986). Contemporary seismicity of northwest Europe. *Ann. Geophysicae* **48**, 567–576.

Bungum, H. and P.B. Selnes (eds.) (1988). ELOCS: Earthquake Loading on the Norwegian Continental Shelf, *Summary Report*, 38 pp., Norwegian Geotechnical Institute (Oslo), NTNF/NORSAR (Kjeller) and Principia Mechanica Ltd. (London).

Glennie, K.W. (ed.) (1986). *Introduction to the Petroleum Geology of the North Sea*, 2nd ed., 278 pp., Blackwell Scientific Publications, Oxford.

Hansen, R.A., H. Bungum, and A. Alsaker (1989). Three recent larger earthquakes offshore Norway, *Terra Nova* **1**, 284–295.

Havskov, J., C.D. Lindholm and R.A. Hansen (1989). Temporal variations in North Sea seismicity, in *Earthquakes at North Atlantic Passive Margins: Neotectonics and Postglacial Rebound*, edited by S. Gregersen and P.W. Basham, 413–427, Kluwer Academic Publishers.

Havskov, J., H. Bungum and L.B. Kvamme (1991): The Norwegian regional network and data center operation. *Phys. Earth Planet Int.*, in press.

Husebye, E.S., H. Bungum, J. Fyen, and H. Gjøystdal (1978). Earthquake activity in Fennoscandia between 1497 and 1975 and intraplate tectonics, *Nor. Geol. Tidsskr.* **58**, 51–68.

Husebye, E.S., H. Gjøystdal, H. Bungum, and O. Eldholm (1975). The seismicity of the Norwegian and Greenland Seas and adjacent continental shelf areas, *Tectonophysics* **26**, 55–70.

Kvamme, L. and R.A. Hansen (1989). The seismicity in the continental margin areas of northern Norway, in *Earthquakes at North Atlantic Passive Margins: Neotectonics and Postglacial Rebound*, edited by S. Gregersen and P.W. Basham, 429–440, Kluwer Academic Publishers.

Mitchell, B.J., H. Bungum, W.W. Chan and P.B. Mitchell (1990). Seismicity and present-day tectonics of Svalbard, *Geophys. J. Int.* **102**, 139–149.

Muir Wood, R., and G. Woo (1987). The historical seismicity of the Norwegian continental shelf, *ELOCS (Earthquake Loading on the Norwegian Continental Shelf) Report 2-1*, 124 pp., Norwegian Geotechnical Institute (Oslo), NTNF/NORSAR (Kjeller) and Principia Mechanica Ltd. (London).

Muir Wood, R., G. Woo and H. Bungum (1988). The history of earthquakes in the Northern North Sea, in *Historical Seismograms and Earthquakes of the World*, edited by W.H.K. Lee, H. Meyers and K. Shimazaki, 297–306, Academic Press, San Diego.

Richards, P. (1988). Seismic methods for verifying test ban treaties, in *Nuclear Arms Technologies in the 1990s*, D. Schroeder and D. Hafemeister (Editors), AIP Conference Proceedings 178, 54–108, American Institute of Physics, New York.

Slunga, R., P. Norrman, and A.-C. Glans (1984). Baltic Shield seismicity, the results of a regional network, *Geophys. Res. Lett.* **11**, 1247–1250.

Spencer, A.M. et al (eds.) (1984). *Petroleum Geology of the North European Margin*, 436 pp., Norwegian Petroleum Society, Graham and Trotman, London.

Spencer, A.M. et al (eds.) (1986). *Habitat of Hydrocarbons on the Norwegian Continental Shelf*, 354 pp., Norwegian Petroleum Society, Graham and Trotman, London.

Sykes, L.R. (1967). Mechanism of earthquakes and nature of faulting on the mid-oceanic ridge, *J. Geophys. Res.* **72**, 2131–2151.

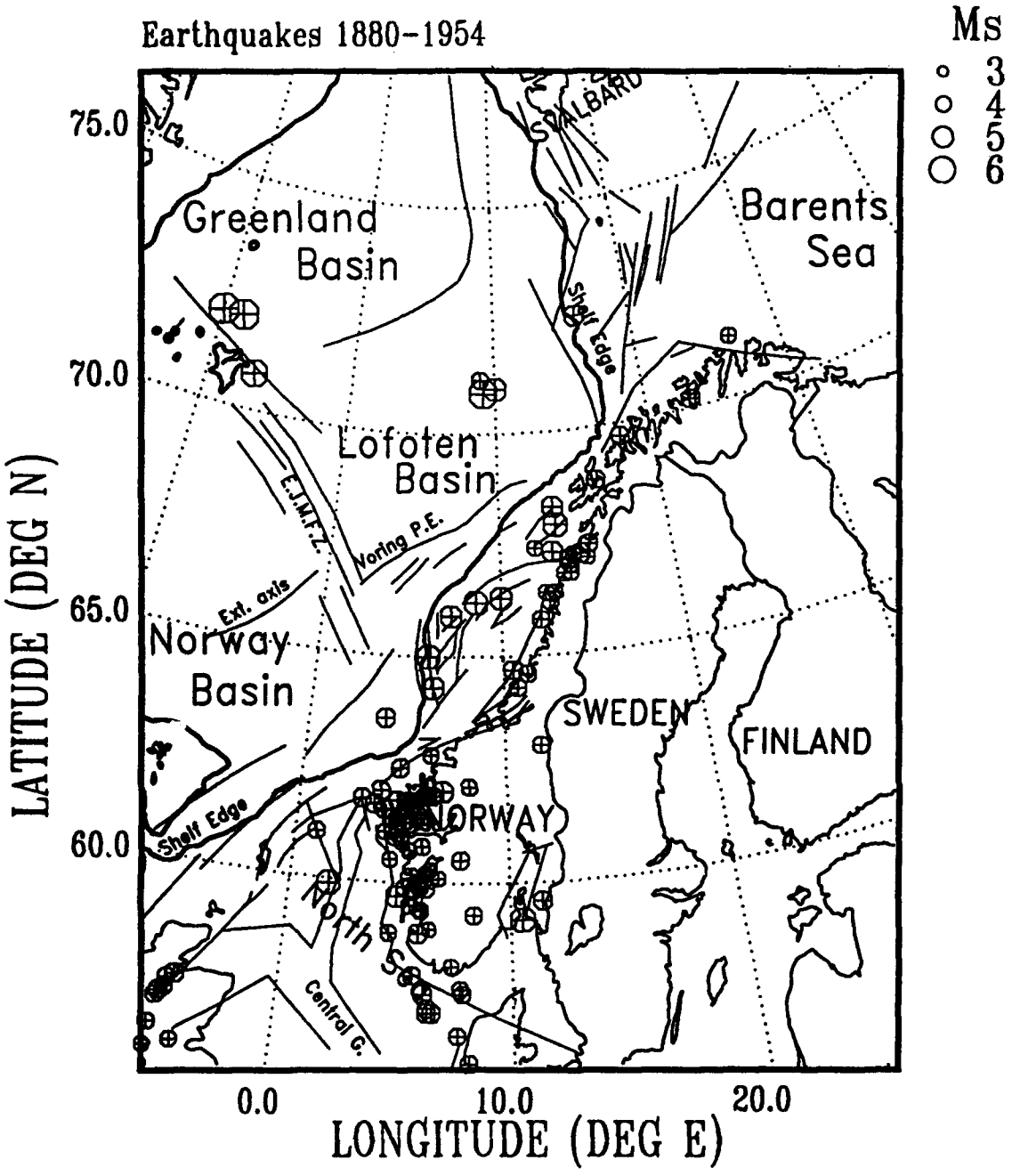

Fig. 2.4.1. Seismicity of Norway and surrounding areas for the time period 1880–1954. Magnitude is predominantly M_S.

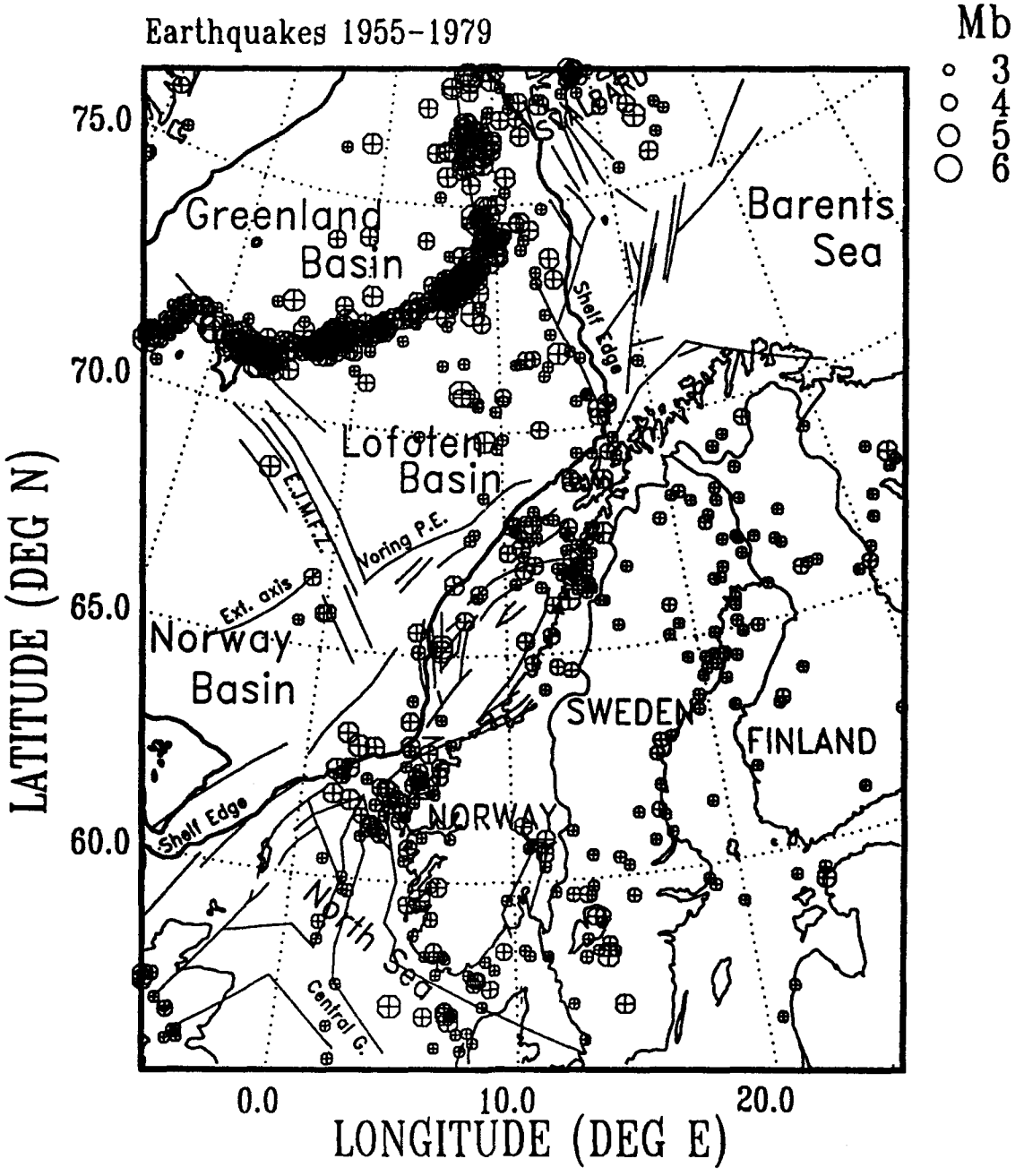

Fig. 2.4.2. Seismicity of Norway and surrounding areas for the time period 1955–1979. Magnitude is predominantly m_b.

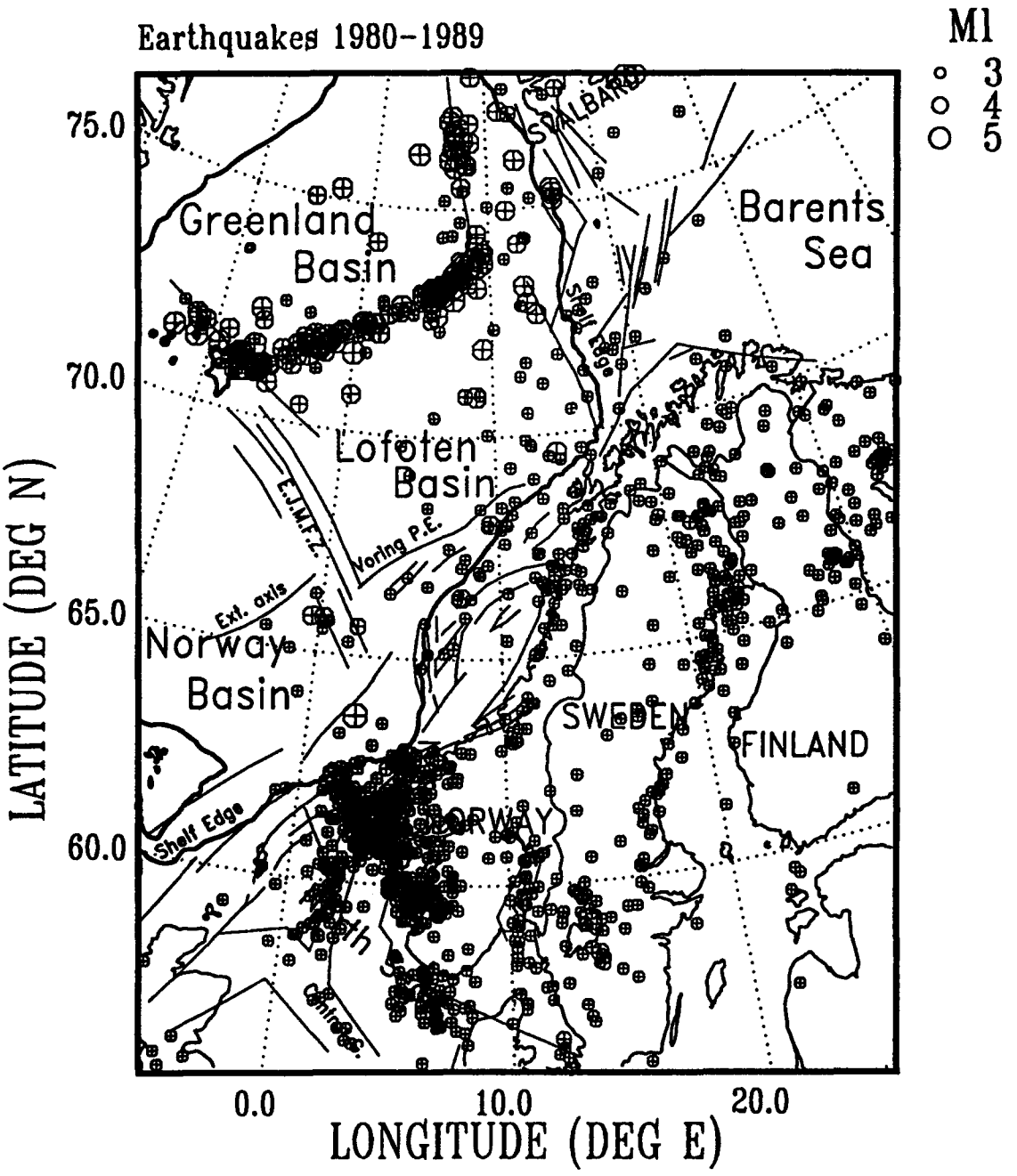

Fig. 2.4.3. Seismicity of Norway and surrounding areas for the time period 1980–1989. Magnitude is predominantly M_L.

2.5 Report on the symposium entitled "Regional Seismic Arrays and Nuclear Test Ban Verification" held in Oslo, Norway, 14–17 February 1990

During 14–17 February 1990 NORSAR hosted an international symposium entitled "Regional Seismic Arrays and Nuclear Test Ban Verification". The symposium was attended by 76 scientists and representatives from 21 countries, including a large number of seismologists participating in the work of the Conference on Disarmament's Group of Scientific Experts (GSE) in Geneva.

The purpose of the symposium was to assess the state-of-the-art of research on regional seismic arrays and associated topics. In particular, the symposium focused upon the advanced regional arrays NORESS and ARCESS in Norway and their associated data processing facilities, in the light of the potential of such arrays to provide a much improved monitoring capability for a future comprehensive nuclear test ban treaty. During a three-day scientific symposium, a number of presentations were given on topics relevant to this issue. A special session was devoted to summarizing the experience and discussing further plans for the on-going international GSE experiment (GSETT-2).

In this paper, we give a brief review of some of the results presented during the scientific symposium. The majority of the papers presented will be published in a special issue of the *Bulletin of the Seismological Society of America*, scheduled to appear in December 1990. Authors and titles of the 28 papers of the special issue are given in the Appendix.

Development of regional arrays

Reviews of recent developments with regard to regional seismic arrays are presented for NORESS and ARCESS in Norway [1], GERESS in the Federal Republic of Germany [2] and FINESA in Finland [3]. Paper [1] summarizes the design considerations leading to the establishment of the first regional array, NORESS, and describes how the success of this new array concept motivated the deployment of additional arrays of this type. The paper documents the basic signal processing techniques used in real-time data analysis for regional arrays, and demonstrates the excellent detection performance of such arrays at regional distances (less than 2000 km). It is shown that NORESS and ARCESS are capable of detecting seismic events of magnitude 2.5 with 90 per cent probability, if these events occur within 1000 km distance, whereas global teleseismic networks have much higher event detection thresholds. The FINESA array is also documented to have an excellent performance [3], and together, these three arrays are capable of locating weak seismic events in Fennoscandia very accurately (typically to within 10–20 km). The GERESS array currently under development shows many of the same excellent features [2], and will contribute further to an excellent regional coverage of large parts of Northern Europe.

Processing of data from a network of regional arrays

Recent technological advances have allowed very sophisticated processing techniques to be applied in detecting, locating and identifying seismic events using a network of seismic arrays and single stations, and this is highlighted by the development of the Intelligent Monitoring System (IMS) [4],[5]. Two of the goals for this system are (1) to demonstrate the monitoring performance and capability of the system for small events at regional distances and (2) to explore the promise of an expert-systems approach for providing improved monitoring performance as experience accumulates. The first operational version, described in [4], processes data from NORESS and ARCESS, whereas later versions will be expanded to networks including both arrays and single stations. The IMS is ambitious in exploring and integrating many new computer technologies, and the validity of the concept is documented in an evaluation of its initial operational performance [5].

Signal analysis methods

A number of presentations addressed methods for processing seismic signals recorded by arrays as well as three-component stations. It was demonstrated that both types of stations can provide information very useful in phase identification, azimuth estimation and estimating the apparent velocity of detected phases. From theoretical considerations as well as from experimental comparison [12],[24],[14] arrays are shown to be superior in this regard at low signal-to-noise ratios, although the precision e.g. of azimuth estimates is influenced by a number of factors, including phase type, frequency of the signal and systematic bias caused by earth heterogeneities [14],[17], [24]. A very promising approach, discussed in [16] is that of joint analysis of 3-component and array data.

Signal detection methods are discussed in several papers. In [11], a system for on-line detection and signal analysis is presented as applied to a Soviet 3-component station in Kazakhstan. In [13], a detection technique is described using NORESS array and 3-component data. A statistical approach, using adaptive techniques, to detection processing and estimation is presented in [7]. A new approach to obtain precise relative location estimates of seismic events, using high frequency recordings, is presented in [23].

Source identification

Traditionally, seismic discrimination research has focused on distinguishing between earthquakes and underground nuclear explosions. Under a Comprehensive Test Ban Treaty, emphasis will be on detecting and identifying *weak* seismic events, and a third category, large chemical explosions for industrial purposes (e.g. mining work) will become important to consider. In [10], a very promising method is applied to NORESS data to discriminate between earthquakes and ripple-fired quarry blasts (mining events consisting of several explosions closely grouped in space and time). Using spectral characteristics of the signals, an "automatic" discriminant is proposed computing the likelihood that ripple firing occurred in each given case.

In [8], a novel approach making use of artificial neural networks is used to develop a classification procedure between earthquakes and mining explosions. Also in this approach, the spectral characteristics of the signals form the basis for the discriminants. The neural network appears to improve in particular the classification of outliers in the population, and reduce the number of uncertain events. Application of neural networks in improving seismic processing performance is also addressed in [9].

Of considerable interest for source identification is also the method proposed in [15], applying transfer functions to transform e.g. between recordings of presumed single explosions and ripple-fired explosions, and also between recordings at different NORESS sensors for a given event. This gives promise to improve the coherence of seismic phases recorded at an array, with ensuing implications for improved source parameter estimation. In [6], a case-based reasoning approach to event identification is discussed, and a waveform envelope matching technique is applied to a set of Western Norway earthquakes and explosions.

Detection thresholds and in-country networks

While regional arrays were originally designed to enhance the capabilities for detecting and characterizing weak seismic events at regional distances, they have also been found very effective in the teleseismic distance range. As an example, published yields of Soviet underground nuclear explosions at Semipalatinsk have been used to evaluate the NORESS detection threshold, in terms of explosive yield for events at this test site [20]. The threshold for detection at NORESS is estimated to be as low as 0.1 kt, assuming full coupling and normal noise conditions. It is pointed out that NORESS has particularly favorable conditions for detecting small events from this test site, and that the seismic identification threshold necessarily will be higher than the detection threshold.

Data from new Global Seismic Network stations in the Soviet Union, installed as a cooperative project between American and Soviet scientists, have

been applied in several studies to address problems relevant to an in-country monitoring network. Seismic noise levels at these stations are analyzed in [18], and found to be higher than at NORESS in the band 1-20 Hz, with maximum difference ranging from 7 to 25 dB, depending on the station. However, significant noise reduction can be achieved by borehole deployment.

Using data from stations in the USSR, the frequency-dependent attenuation of regional seismic phases has been studied in [21]. Attenuation characteristics are found to be similar to those observed in Scandinavia, but with an absolute Pn amplitude almost a factor of 2 higher in eastern Kazakhstan for a fixed Lg magnitude.

Recordings of Semipalatinsk nuclear explosions at the new Global Seismic Network stations in the Soviet Union, together with data from stations in China have been analyzed in [19] and it is shown that RMS Lg can be measured at widely separated stations with a remarkable degree of consistency. The standard deviation of the differences between pairs of stations is as low as 0.03–0.04 in logarithmic units, and reliable measurements may be made at magnitude (m_b) down to about 4.0 for stations situated about 1500 km away from Semipalatinsk. The importance of this observation in terms of supplying yield estimates for nuclear explosions down to and even below one kiloton is pointed out.

Earth structure, wave propagation, scattering

Several of the papers were devoted to studies of general problems in seismology and geophysics, in areas relevant to the seismic monitoring issue. The structure of the crust and upper mantle in parts of northern Eurasia is addressed in papers [22], [25] and [27]. All three papers are specifically making use of regional array data. Seismic wave propagation and scattering are addressed in a number of papers, e.g. [13], [24], [26], [27], [28].

Conclusion

The Oslo symposium demonstrated the considerable progress in the field of seismic monitoring during recent years. It particularly highlighted the technological advances in seismic instrumentation, data communication and computer processing, as exemplified by the development of advanced regional seismic arrays with very sophisticated automatic and interactive signal processing facilities. The presentations at the scientific symposium show that these technological advances are accompanied by considerable scientific progress, although much work remains in order to fully exploit the potential offered by regional arrays in a seismic monitoring context.

F. Ringdal
S. Mykkeltveit

Appendix

List of papers given during the 1990 Oslo Symposium on Regional Seismic Arrays and Nuclear Test Ban Verification, to appear in a special issue of *The Bulletin of the Seismological Society of America*

References

[1] Svein Mykkeltveit[1], Frode Ringdal[1], Tormod Kværna[1] and Ralph W. Alewine[2] — [1] NORSAR, Norway, and [2] DARPA, USA: "Application of Regional Arrays in Seismic Verification Research"

[2] Hans-Peter Harjes — Ruhr Univ., Fed. Rep. of Germany: "Design and Siting of a New Regional Array in Central Europe"

[3] Marja Uski — University of Helsinki, Finland: "Event Detection and Location Performance of the FINESA Array in Finland"

[4] Thomas C. Bache[1], Steven R. Bratt[1], James Wang[1], Robert M. Fung[2], Cris Kobryn[1] and Jeffrey W. Given[1] — [1] Science Applications International Corp., USA, and [2] Advanced Decision Systems, USA: "The Intelligent Monitoring System"

[5] Steven R. Bratt, Henry J. Swanger, Richard J. Stead, Floriana Ryall and Thomas C. Bache — Science Applications International Corp., USA: "Initial Results from the Intelligent Monitoring System"

[6] Douglas R. Baumgardt and Gregory B. Young — ENSCO, Inc., USA: "Regional Seismic Waveform Discriminants and Case-based Event Identification using Regional Arrays"

[7] A. Kushnir[1], V. Laphsin[1], V. Pinsky[1], and J. Fyen[2] — [1] Inst. of Physics of the Earth, USSR, and [2] NORSAR, Norway: "Statistically Optimal Event Detection using Small Array Data"

[8] Paul Dysart[1] and Jay Pulli[2] — [1] Science Applications International Corp., USA, and [2] Radix Systems, Inc., USA: "Regional Seismic Event Classification at the NORESS Array: Seismological Measurements and the Use of Trained Neural Networks"

[9] Kenneth R. Anderson — BBN, USA: "Programming as a Geophysical Inverse Problem"

[10] Michael A.H. Hedlin, J. Bernard Minster and John A. Orcutt — Scripps Inst. of Oceanography, UCSD, USA: "An Automatic Means to Discriminate between Earthquakes and Quarry Blasts"

[11] O.K. Kedrov and V.M. Ovtchinnikov — Inst. of Earth Physics, USSR: "An On-Line Analysis System for Three-Component Seismic Data: Method and Preliminary Results"

[12] David B. Harris -- Lawrence Livermore National Laboratory, USA: "Comparison of the Direction Estimation Performance of High-Frequency Seismic Arrays and Three-Component Stations"

[13] S.C. Bannister, E.S. Husebye and B.O. Ruud — University of Oslo, Norway: "Teleseismic P Coda Analyzed by Three-Component and Array Techniques: Deterministic Location of Topographic P-to-Rg Scattering near the NORESS Array"

[14] Anne Suteau-Henson — Science Applications International Corp., USA: "Estimating Azimuth and Slowness from Three-Component and Array Stations"

[15] Zoltan A. Der, M.R. Hirano and Robert H. Shumway — ENSCO, Inc., USA: "Coherent Processing of Regional Signals at Small Seismic Arrays"

[16] D.C. Jepsen and B.L.N. Kennett — Australian National University, Canberra, Australia: "Three-component Analysis of Regional Seismograms"

[17] Dorthe Bame, Marianne C. Walck and Kathie L. Hiebert-Dodd — Sandia National Laboratory, USA: "Azimuth Estimation Capabilities of the NORESS Regional Seismic Array"

[18] Holly K. Given — Scripps Inst. of Oceanography, UCSD, USA: "Variations in Broadband Seismic Noise at IRIS/IDA Stations in the USSR with Impications for Event Detection"

[19] Roger A. Hansen[1], Frode Ringdal[1] and Paul G. Richards[2] — [1] NORSAR, Norway, and [2] Lamont-Doherty Geological Observatory, USA: "The Stability of RMS Lg Measurements and their Potential for Accurate Estimation of the Yields of Soviet Underground Nuclear Explosions"

[20] Frode Ringdal — NORSAR, Norway: "Teleseismic Event Detection using the NORESS Array, with Special Reference to Low-Yield Semipalatinsk Explosions"

[21] Thomas J. Sereno, Jr. — Science Applications International Corp., USA: "Frequency-Dependent Attenuation in Eastern Kazakhstan and Implications for Seismic Detection Thresholds in the Soviet Union"

[22] Vladimir Ryaboy — Science Applications International Corp., USA: "Upper Mantle Structure along a Profile from Oslo (NORESS) to Helsinki to Leningrad, based on Explosion Seismology"

[23] Hans Israelsson — Science Applications International Corp., USA: "Correlation of Waveforms from Closely Spaced Regional Arrays"

[24] E. Ødegaard[1], D.J. Doornbos[1] and T. Kværna[2] — [1] University of Oslo, Norway, and [2] NORSAR, Norway: "Surface Topographic Effect at Arrays and Three-Component Stations"

[25] Kristin S. Vogfjord and Charles A. Langston — Penn State Univ., USA: "Analysis of Regional Events Recorded at NORESS"

[26] I. Gupta, C.S. Lynnes, T.W. McElfresh and R.A. Wagner — Teledyne Geotech, USA: "F-K Analysis of NORESS Array and Single-Station Data to Identify Sources of Near-Receiver and Near-Source Scattering"

[27] Douglas R. Baumgardt — ENSCO, Inc., USA: "Investigation of Teleseismic Lg Blockage and Scattering using Regional Arrays"

[28] Anton M. Dainty and M. Nafi Toksoz — Earth Resources Lab., MIT, USA: "Array Analysis of Seismic Scattering"

2.6 Summaries of Quarterly Technical Reports Submitted

During the current fiscal year (FY90), three quarterly technical reports were submitted on this contract. The abstracts of these papers are given in the following.

2.6.1 The stability of RMS Lg measurements and their potential for accurate estimation of the yields of Soviet underground nuclear explosions — R.A. Hansen[1], F. Ringdal[1] and P.G. Richards[2] ([1] NTNF/NORSAR, Kjeller, Norway, and [2] Lamont-Doherty Geol. Obs., Columbia Univ., New York, USA)

Data on underground nuclear explosions have recently become available from modern digital seismic stations installed within the Soviet Union and China. Observations of root mean square (RMS) Lg-wave signals for Soviet underground nuclear explosions at the Shagan River test site in East Kazakhstan show that the relative amplitudes of the RMS signals, at stations in Norway, the U.S.S.R. and China, are very similar for different explosions, the standard deviation of the differences being only about 0.03 in logarithmic units (i.e., magnitude units).

This is consistent with earlier observations comparing NORSAR and Graefenberg array data, and the observed scatter is significantly lower than has been reported for Lg data from Nevada Test Site explosions. In view of the excellent correspondence found by Nuttli (1986) and Patton (1988) for Lg versus yield at Nevada, this indicates that RMS Lg has a potential for yield estimation with very high accuracy at Shagan River.

Our study has shown that: (a) selected stations in the U.S.S.R. and China, situated at regional distances, provide a much improved signal-to-noise ratio of the Lg phase for events at Shagan River, as compared to NORSAR array data; (b) the scaling of RMS Lg amplitudes between different sized events recorded at the same single station site appears to be consistent with that of NORSAR, indicating a remarkable degree of precision in single station measurements of Lg signal; (c) RMS Lg amplitude measurements for the best of these stations may be made at 1.5 to 2.0 magnitude units lower than at NORSAR or Graefenberg, allowing a much lower threshold for Lg based yield determinations; and (d) the P-wave detection capabilities of these single stations do not match those of the NORESS and ARCESS arrays, thus teleseismic signals continue to be important for the detection of small nuclear explosions.

Our conclusion is that Lg signals appear to provide an excellent basis for supplying estimates of the yields of nuclear explosions even down to below one kiloton, when such signals are recorded at high-quality digital in-country

seismic stations, and when calibrated by access to independent (non-seismic) yield information for a few nuclear explosions at the test sites of interest. In the context of monitoring a low yield threshold test ban treaty, it will, in addition, be important to take into consideration various environmental conditions in the testing area, such as the possible presence of cavities, and to devise appropriate procedures for on-site observations in this regard.

2.6.2 The M_L scale in Norway — A. Alsaker, L.B. Kvamme, R.A. Hansen, A. Dahle and H. Bungum (NTNF/NORSAR, Kjeller, Norway)

A new low magnitude M_L scale has been developed for Norway, based on a regression analysis of synthesized Wood-Anderson records. The scale is applicable for distances up to more than 1000 km, and the data used comprise 741 short-period recordings at 21 seismic stations from 195 earthquakes in the magnitude range 1 to 5 occurring in and around Norway over the last 20 years. Magnitude corrections for distance have been evaluated in terms of a geometrical spreading term a and an anelastic attenuation term b, and the significant regional crustal differences in the area under investigation made it desirable to develop these for several subsets of the data base. The results for a are generally found to be around the commonly found value of 1.0 (using the L_g phase), while the b-values are found to be around 0.0008, consistent with the weak, intraplate attenuation expected for Norway. Compared to interplate California, this difference in attenuation represents more than one magnitude unit at a distance of 1000 km.

New M_L scales are commonly tied to Richter's original definition at the standard reference hypocentral distance of 100 km. The significantly weaker L_g wave attenuation in Norway, however, requires a smaller reference distance. We have chosen a value of 60 km, based on an overall assessment of regional coverage, focal depths and quality of the data. The resulting M_L formula for Norway reads

$$M_L = log A_{wa} + a\, log(R/60) + b\,(R-60) + 2.68 + S \qquad (1)$$

where A_{wa} is synthesized Wood-Anderson amplitude (in mm), R is hypocentral distance (in km), and S is a station correction term that for all 21 stations is found to lie within the range $\pm$ 0.22. When using the entire data base the spreading term a equals 1.02, and the anelastic attenuation term b equals 0.00080. When only strictly continental ray paths are selected, the a-value decreases to 0.91 while the b-value increases to 0.00087, a difference which on the average accounts for less than 0.1 magnitude units. While all values used in the regressions have been derived for vertical amplitudes, a separate analysis has shown that these are not significantly different from the horizontal ones, and the new scale is therefore applicable to both. In order to facilitate

the practical use of this new M_L scale, a relation has also been established between observed seismogram amplitudes (corrected for instrument response) and the synthesized Wood-Anderson amplitudes. This relation reads $log A_{wa} = 0.925\ log A_{obs} - 2.32$.

The new M_L scale magnitudes for the events analyzed are in fairly good agreement with those calculated from a previously used relation developed by Båth for Sweden. The new values are, however, systematically about 0.4 magnitude units lower, which is mostly due to the combined effect of a reference distance less than 100 km and a Wood-Anderson magnification of 2080 instead of the earlier value of 2800. The new M_L values have also regressively been related to a data set of M_s values, yielding the relation $M_s = 0.83 M_L + 1.09$.

2.6.3 Application of regional arrays in seismic verification research — S. Mykkeltveit[1], F. Ringdal[1], T. Kværna[1] and R.W. Alewine[2] ([1] NTNF/NORSAR, Kjeller, Norway, and [2] DARPA/NMRO, Virginia, USA)

The paper gives an account of the work related to the development of the NORESS concept of a regional array. The array design considerations and objectives are reviewed, and a description is given of the NORESS and ARCESS array facilities in Norway with their field installations, data transmission lines and data receiving center functions.

The automatic signal detection processing of NORESS data applies multiple narrow-band frequency filters in parallel and forms array beams from selected subgeometries. The detection algorithm is based on computing the STA/LTA ratio for each beam individually, and a detection is declared whenever this ratio exceeds a given threshold. It is explained how the beam deployment and the individual threshold values can be tuned to ensure that the interesting phase arrivals are not missed, but at the same time avoiding coda detections.

For each detected signal, frequency-wavenumber analysis is invoked to determine arrival azimuth and apparent velocity. Currently, a broad band estimator is used, and it is demonstrated that use of this algorithm increases the stability of the azimuth and apparent velocity estimates, relative to narrow band methods. Local and regional events are automatically located on the basis of identification and association of P- and S-wave arrivals. The uncertainty in the arrival azimuth is the limiting factor in accurately determining single-array event locations, and it is shown that this uncertainty is as large as 10°–15° for Pn phases from certain regions.

In order to further investigate the potential of the NORESS concept, work was initiated towards installing a network of regional arrays in the northern

Europe area. This involved the deployment of the ARCESS array in northern Norway, and the installation of the FINESA array in Finland in cooperation with the University of Helsinki. Data from these three arrays have been used jointly in a location estimation scheme. It is shown that for events in the Fennoscandian region of magnitude typically around 2.5 and for which at least one phase is detected by each array, location estimates can be obtained automatically that deviate from published network locations by only 16 km on the average.

In the future, it is anticipated that additional arrays and single stations in the northern Europe area will contribute real-time data to NORSAR for analysis jointly with existing arrays. The first additional data to become available will be from the GERESS array, which will be established in the Federal Republic of Germany in 1990. Future perspectives also include the use of expert system technology in the data analysis, and the IMS system already in operation represents the initial attempt in this regard. A summary is given of problem areas where further work is needed in order to fully exploit the regional array concept.

Prof. Thomas Ahrens
Seismological Lab, 252-21
Division of Geological & Planetary Sciences
California Institute of Technology
Pasadena, CA 91125

Prof. Charles B. Archambeau
CIRES
University of Colorado
Boulder, CO 80309

Dr. Thomas C. Bache, Jr.
Science Applications Int'l Corp.
10260 Campus Point Drive
San Diego, CA 92121 (2 copies)

Prof. Muawia Barazangi
Institute for the Study of the Continent
Cornell University
Ithaca, NY 14853

Dr. Douglas R. Baumgardt
ENSCO, Inc
5400 Port Royal Road
Springfield, VA 22151-2388

Prof. Jonathan Berger
IGPP, A-025
Scripps Institution of Oceanography
University of California, San Diego
La Jolla, CA 92093

Dr. Lawrence J. Burdick
Woodward-Clyde Consultants
566 El Dorado Street
Pasadena, CA 91109-3245

Dr. Jerry Carter
Center for Seismic Studies
1300 North 17th St., Suite 1450
Arlington, VA 22209-2308

Dr. Karl Coyner
New England Research, Inc.
76 Olcott Drive
White River Junction, VT 05001

Prof. Vernon F. Cormier
Department of Geology & Geophysics
U-45, Room 207
The University of Connecticut
Storrs, CT 06268

Professor Anton W. Dainty
Earth Resources Laboratory
Massachusetts Institute of Technology
42 Carleton Street
Cambridge, MA 02142

Prof. Steven Day
Department of Geological Sciences
San Diego State University
San Diego, CA 92182

Dr. Zoltan A. Der
ENSCO, Inc.
5400 Port Royal Road
Springfield, VA 22151-2388

Prof. John Ferguson
Center for Lithospheric Studies
The University of Texas at Dallas
P.O. Box 830688
Richardson, TX 75083-0688

Dr. Mark D. Fisk
Mission Research Corporation
735 State Street
P. O. Drawer 719
Santa Barbara, CA 93102

Prof. Stanley Flatte
Applied Sciences Building
University of California
Santa Cruz, CA 95064

Dr. Alexander Florence
SRI International
333 Ravenswood Avenue
Menlo Park, CA 94025-3493

Prof. Henry L. Gray
Vice Provost and Dean
Department of Statistical Sciences
Southern Methodist University
Dallas, TX 75275

Dr. Indra Gupta
Teledyne Geotech
314 Montgomery Street
Alexandria, VA 22314

Prof. David G. Harkrider
Seismological Laboratory
Division of Geological & Planetary Sciences
California Institute of Technology
Pasadena, CA 91125

Prof. Donald V. Helmberger
Seismological Laboratory
Division of Geological & Planetary Sciences
California Institute of Technology
Pasadena, CA 91125

Prof. Eugene Herrin
Institute for the Study of Earth and Man
Geophysical Laboratory
Southern Methodist University
Dallas, TX 75275

Prof. Bryan Isacks
Cornell University
Department of Geological Sciences
SNEE Hall
Ithaca, NY 14850

Dr. Rong-Song Jih
Teledyne Geotech
314 Montgomery Street
Alexandria, VA 22314

Prof. Lane R. Johnson
Seismographic Station
University of California
Berkeley, CA 94720

Dr. Richard LaCoss
MIT-Lincoln Laboratory
M-200B
P. O. Box 73
Lexington, MA 02173-0073 (3 copies)

Prof Fred K. Lamb
University of Illinois at Urbana-Champaign
Department of Physics
1110 West Green Street
Urbana, IL 61801

Prof. Charles A. Langston
Geosciences Department
403 Deike Building
The Pennsylvania State University
University Park, PA 16802

Prof. Thorne Lay
Institute of Tectonics
Earth Science Board
University of California, Santa Cruz
Santa Cruz, CA 95064

Prof. Arthur Lerner-Lam
Lamont-Doherty Geological Observatory
of Columbia University
Palisades, NY 10964

Dr. Christopher Lynnes
Teledyne Geotech
314 Montgomery Street
Alexandria, VA 22314

Professor Peter E. Malin
Department of Geology
Old Chemistry Building
Duke University
Durham, NC 27706

Dr. Randolph Martin, III
New England Research, Inc.
76 Olcott Drive
White River Junction, VT 05001

Prof. Thomas V. McEvilly
Seismographic Station
University of California
Berkeley, CA 94720

Dr. Keith L. McLaughlin
S-CUBED
A Division of Maxwell Laboratory
P.O. Box 1620
La Jolla, CA 92038-1620

Prof. William Menke
Lamont-Doherty Geological Observatory
of Columbia University
Palisades, NY 10964

Stephen Miller
SRI International
333 Ravenswood Avenue
Box AF 116
Menlo Park, CA 94025-3493

Prof. Bernard Minster
IGPP, A-025
Scripps Institute of Oceanography
University of California, San Diego
La Jolla, CA 92093

Prof. Brian J. Mitchell
Department of Earth & Atmospheric Sciences
St. Louis University
St. Louis, MO 63156

Mr. Jack Murphy
S-CUBED, A Division of Maxwell Laboratory
11800 Sunrise Valley Drive
Suite 1212
Reston, VA 22091 (2 copies)

Prof. John A. Orcutt
IGPP, A-025
Scripps Institute of Oceanography
University of California, San Diego
La Jolla, CA 92093

Prof. Keith Priestley
University of Cambridge
Bullard Labs, Dept. of Earth Sciences
Madingley Rise, Madingley Rd.
Cambridge CB3 OEZ, ENGLAND

Dr. Jay J. Pulli
Radix Systems, Inc.
2 Taft Court, Suite 203
Rockville, MD 20850

Prof. Paul G. Richards
Lamont Doherty Geological Observatory
of Columbia University
Palisades, NY 10964

Dr. Wilmer Rivers
Teledyne Geotech
314 Montgomery Street
Alexandria, VA 22314

Prof. Charles G. Sammis
Center for Earth Sciences
University of Southern California
University Park
Los Angeles, CA 90089-0741

Prof. Christopher H. Scholz
Lamont-Doherty Geological Observatory
of Columbia University
Palisades, NY 10964

Thomas J. Sereno, Jr.
Science Application Int'l Corp.
10260 Campus Point Drive
San Diego, CA 92121

Prof. David G. Simpson
Lamont-Doherty Geological Observatory
of Columbia University
Palisades, NY 10964

Dr. Jeffrey Stevens
S-CUBED
A Division of Maxwell Laboratory
P.O. Box 1620
La Jolla, CA 92038-1620

Prof. Brian Stump
Institute for the Study of Earth & Man
Geophysical Laboratory
Southern Methodist University
Dallas, TX 75275

Prof. Jeremiah Sullivan
University of Illinois at Urbana-Champaign
Department of Physics
1110 West Green Street
Urbana, IL 61801

Prof. Clifford Thurber
University of Wisconsin-Madison
Department of Geology & Geophysics
1215 West Dayton Street
Madison, WS 53706

Prof. M. Nafi Toksoz
Earth Resources Lab
Massachusetts Institute of Technology
42 Carleton Street
Cambridge, MA 02142

Prof. John E. Vidale
University of California at Santa Cruz
Seismological Laboratory
Santa Cruz, CA 95064

Prof. Terry C. Wallace
Department of Geosciences
Building #77
University of Arizona
Tucson, AZ 85721

Dr. William Wortman
Mission Research Corporation
735 State Street
P. O. Drawer 719
Santa Barbara. CA 93102

OTHERS (UNITED STATES)

Dr. Monem Abdel-Gawad
Rockwell International Science Center
1049 Camino Dos Rios
Thousand Oaks, CA 91360

Prof. Keiiti Aki
Center for Earth Sciences
University of Southern California
University Park
Los Angeles, CA 90089-0741

Prof. Shelton S. Alexander
Geosciences Department
403 Deike Building
The Pennsylvania State University
University Park, PA 16802

Dr. Kenneth Anderson
BBNSTC
Mail Stop 14/1B
Cambridge, MA 02238

Dr. Ralph Archuleta
Department of Geological Sciences
University of California at Santa Barbara
Santa Barbara, CA 93102

Dr. Jeff Barker
Department of Geological Sciences
State University of New York
at Binghamton
Vestal, NY 13901

Dr. Susan Beck
Department of Geosciences
Bldg. # 77
University of Arizona
Tucson, AZ 85721

Dr. T.J. Bennett
S-CUBED
A Division of Maxwell Laboratory
11800 Sunrise Valley Drive, Suite 1212
Reston, VA 22091

Mr. William J. Best
907 Westwood Drive
Vienna, VA 22180

Dr. N. Biswas
Geophysical Institute
University of Alaska
Fairbanks, AK 99701

Dr. G.A. Bollinger
Department of Geological Sciences
Virginia Polytechnical Institute
21044 Derring Hall
Blacksburg, VA 24061

Dr. Stephen Bratt
Center for Seismic Studies
1300 North 17th Street
Suite 1450
Arlington, VA 22209

Michael Browne
Teledyne Geotech
3401 Shiloh Road
Garland, TX 75041

Mr. Roy Burger
1221 Serry Road
Schenectady, NY 12309

Dr. Robert Burridge
Schlumberger-Doll Research Center
Old Quarry Road
Ridgefield, CT 06877

Dr. W. Winston Chan
Teledyne Geotech
314 Montgomery Street
Alexandria, VA 22314-1581

Dr. Theodore Cherry
Science Horizons, Inc.
710 Encinitas Blvd., Suite 200
Encinitas, CA 92024 (2 copies)

Prof. Jon F. Claerbout
Department of Geophysics
Stanford University
Stanford, CA 94305

Prof. Robert W. Clayton
Seismological Laboratory
Division of Geological & Planetary Sciences
California Institute of Technology
Pasadena, CA 91125

Prof. F. A. Dahlen
Geological and Geophysical Sciences
Princeton University
Princeton, NJ 08544-0636

Mr. Charles Doll
Earth Resources Laboratory
Massachusetts Institute of Technology
42 Carleton St.
Cambridge, MA 02142

Prof. Adam Dziewonski
Hoffman Laboratory
Harvard University
20 Oxford St
Cambridge, MA 02138

Prof. John Ebel
Department of Geology & Geophysics
Boston College
Chestnut Hill, MA 02167

Eric Fielding
SNEE Hall
INSTOC
Cornell University
Ithaca, NY 14853

Dr. John Foley
GL/LWH
Hanscom AFB, MA 01731-5000

Prof. Donald Forsyth
Department of Geological Sciences
Brown University
Providence, RI 02912

Dr. Cliff Frolich
Institute of Geophysics
8701 North Mopac
Austin, TX 78759

Dr. Anthony Gangi
Texas A&M University
Department of Geophysics
College Station, TX 77843

Dr. Freeman Gilbert
IGPP, A-025
Scripps Institute of Oceanography
University of California
La Jolla, CA 92093

Mr. Edward Giller
Pacific Sierra Research Corp.
1401 Wilson Boulevard
Arlington, VA 22209

Dr. Jeffrey W. Given
SAIC
10260 Campus Point Drive
San Diego, CA 92121

Prof. Stephen Grand
University of Texas at Austin
Department of Geological Sciences
Austin, TX 78713-7909

Prof. Roy Greenfield
Geosciences Department
403 Deike Building
The Pennsylvania State University
University Park, PA 16802

Dan N. Hagedorn
Battelle
Pacific Northwest Laboratories
Battelle Boulevard
Richland, WA 99352

Dr. James Hannon
Lawrence Livermore National Laboratory
P. O. Box 808
Livermore, CA 94550

Prof. Robert B. Herrmann
Dept. of Earth & Atmospheric Sciences
St. Louis University
St. Louis, MO 63156

Ms. Heidi Houston
Seismological Laboratory
University of California
Santa Cruz, CA 95064

Kevin Hutchenson
Department of Earth Sciences
St. Louis University
3507 Laclede
St. Louis, MO 63103

Dr. Hans Israelsson
Center for Seismic Studies
1300 N. 17th Street, Suite 1450
Arlington, VA 22209-2308

Prof. Thomas H. Jordan
Department of Earth, Atmospheric
and Planetary Sciences
Massachusetts Institute of Technology
Cambridge, MA 02139

Prof. Alan Kafka
Department of Geology & Geophysics
Boston College
Chestnut Hill, MA 02167

Robert C. Kemerait
ENSCO, Inc.
445 Pineda Court
Melbourne, FL 32940

William Kikendall
Teledyne Geotech
3401 Shiloh Road
Garland, TX 75041

Prof. Leon Knopoff
University of California
Institute of Geophysics & Planetary Physics
Los Angeles, CA 90024

Prof. L. Timothy Long
School of Geophysical Sciences
Georgia Institute of Technology
Atlanta, GA 30332

Dr. Gary McCartor
Department of Physics
Southern Methodist University
Dallas, TX 75275

Prof. Art McGarr
Mail Stop 977
Geological Survey
345 Middlefield Rd.
Menlo Park, CA 94025

Dr. George Mellman
Sierra Geophysics
11255 Kirkland Way
Kirkland, WA 98033

Prof. John Nabelek
College of Oceanography
Oregon State University
Corvallis, OR 97331

Prof. Geza Nagy
University of California, San Diego
Department of Ames, M.S. B-010
La Jolla, CA 92093

Dr. Keith K. Nakanishi
Lawrence Livermore National Laboratory
L-205
P. O. Box 808
Livermore, CA 94550

Dr. Bao Nguyen
GL/LWH
Hanscom AFB, MA 01731-5000

Prof. Amos Nur
Department of Geophysics
Stanford University
Stanford, CA 94305

Prof. Jack Oliver
Department of Geology
Cornell University
Ithaca, NY 14850

Dr. Kenneth Olsen
P. O. Box 1273
Linwood, WA 98046-1273

Howard J. Patton
Lawrence Livermore National Laboratory
L-205
P. O. Box 808
Livermore, CA 94550

Prof. Robert Phinney
Geological & Geophysical Sciences
Princeton University
Princeton, NJ 08544-0636

Dr. Paul Pomeroy
Rondout Associates
P.O. Box 224
Stone Ridge, NY 12484

Dr. Jay Pulli
RADIX System, Inc.
2 Taft Court, Suite 203
Rockville, MD 20850

Dr. Norton Rimer
S-CUBED
A Division of Maxwell Laboratory
P.O. Box 1620
La Jolla, CA 92038-1620

Prof. Larry J. Ruff
Department of Geological Sciences
1006 C.C. Little Building
University of Michigan
Ann Arbor, MI 48109-1063

Dr. Richard Sailor
TASC Inc.
55 Walkers Brook Drive
Reading, MA 01867

Dr. Susan Schwartz
Institute of Tectonics
1156 High St.
Santa Cruz, CA 95064

John Sherwin
Teledyne Geotech
3401 Shiloh Road
Garland, TX 75041

Dr. Matthew Sibol
Virginia Tech
Seismological Observatory
4044 Derring Hall
Blacksburg, VA 24061-0420

Dr. Albert Smith
Lawrence Livermore National Laboratory
L-205
P. O. Box 808
Livermore, CA 94550

Prof. Robert Smith
Department of Geophysics
University of Utah
1400 East 2nd South
Salt Lake City, UT 84112

Dr. Stewart W. Smith
Geophysics AK-50
University of Washington
Seattle, WA 98195

Donald L. Springer
Lawrence Livermore National Laboratory
L-205
P. O. Box 808
Livermore, CA 94550

Dr. George Sutton
Rondout Associates
P.O. Box 224
Stone Ridge, NY 12484

Prof. L. Sykes
Lamont-Doherty Geological Observatory
of Columbia University
Palisades, NY 10964

Prof. Pradeep Talwani
Department of Geological Sciences
University of South Carolina
Columbia, SC 29208

Dr. David Taylor
ENSCO, Inc.
445 Pineda Court
Melbourne, FL 32940

Dr. Steven R. Taylor
Lawrence Livermore National Laboratory
L-205
P. O. Box 808
Livermore, CA 94550

Professor Ta-Liang Teng
Center for Earth Sciences
University of Southern California
University Park
Los Angeles, CA 90089-0741

Dr. R.B. Tittmann
Rockwell International Science Center
1049 Camino Dos Rios
P.O. Box 1085
Thousand Oaks, CA 91360

Dr. Gregory van der Vink
IRIS, Inc.
1616 North Fort Myer Drive
Suite 1440
Arlington, VA 22209

Professor Daniel Walker
University of Hawaii
Institute of Geophysics
Honolulu, HI 96822

William R. Walter
Seismological Laboratory
University of Nevada
Reno, NV 89557

Dr. Raymond Willeman
GL/LWH
Hanscom AFB, MA 01731-5000

Dr. Gregory Wojcik
Weidlinger Associates
4410 El Camino Real
Suite 110
Los Altos, CA 94022

Dr. Lorraine Wolf
GL/LWH
Hanscom AFB, MA 01731-5000

Prof. Francis T. Wu
Department of Geological Sciences
State University of New York
at Binghamton
Vestal, NY 13901

Dr. Gregory B. Young
ENSCO, Inc.
5400 Port Royal Road
Springfield, VA 22151-2388

Dr. Eileen Vergino
Lawrence Livermore National Laboratory
L-205
P. O. Box 808
Livermore, CA 94550

J. J. Zucca
Lawrence Livermore National Laboratory
P. O. Box 808
Livermore, CA 94550

GOVERNMENT

Dr. Ralph Alewine III
DARPA/NMRO
1400 Wilson Boulevard
Arlington, VA 22209-2308

Mr. James C. Battis
GL/LWH
Hanscom AFB, MA 01731-5000

Dr. Robert Blandford
AFTAC/TT
Center for Seismic Studies
1300 North 17th St., Suite 1450
Arlington, VA 22209-2308

Eric Chael
Division 9241
Sandia Laboratory
Albuquerque, NM 87185

Dr. John J. Cipar
GL/LWH
Hanscom AFB, MA 01731-5000

Cecil Davis
Group P-15, Mail Stop D406
P.O. Box 1663
Los Alamos National Laboratory
Los Alamos, NM 87544

Mr. Jeff Duncan
Office of Congressman Markey
2133 Rayburn House Bldg.
Washington, DC 20515

Dr. Jack Evernden
USGS - Earthquake Studies
345 Middlefield Road
Menlo Park, CA 94025

Art Frankel
USGS
922 National Center
Reston, VA 22092

Dr. Dale Glover
DIA/DT-1B
Washington, DC 20301

Dr. T. Hanks
USGS
Nat'l Earthquake Research Center
345 Middlefield Road
Menlo Park, CA 94025

Paul Johnson
ESS-4, Mail Stop J979
Los Alamos National Laboratory
Los Alamos, NM 87545

Janet Johnston
GL/LWH
Hanscom AFB, MA 01731-5000

Dr. Katharine Kadinsky-Cade
GL/LWH
Hanscom AFB, MA 01731-5000

Ms. Ann Kerr
IGPP, A-025
Scripps Institute of Oceanography
University of California, San Diego
La Jolla, CA 92093

Dr. Max Koontz
US Dept of Energy/DP 5
Forrestal Building
1000 Independence Avenue
Washington, DC 20585

Dr. W.H.K. Lee
Office of Earthquakes, Volcanoes,
& Engineering
345 Middlefield Road
Menlo Park, CA 94025

Dr. William Leith
U.S. Geological Survey
Mail Stop 928
Reston, VA 22092

Dr. Richard Lewis
Director, Earthquake Engineering & Geophysics
U.S. Army Corps of Engineers
Box 631
Vicksburg, MS 39180

James F. Lewkowicz
GL/LWH
Hanscom AFB, MA 01731-5000

Mr. Alfred Lieberman
ACDA/VI-OA'State Department Bldg
Room 5726
320 - 21st Street, NW
Washington, DC 20451

Stephen Mangino
GL/LWH
Hanscom AFB, MA 01731-5000

Dr. Robert Masse
Box 25046, Mail Stop 967
Denver Federal Center
Denver, CO 80225

Art McGarr
U.S. Geological Survey, MS-977
345 Middlefield Road
Menlo Park, CA 94025

Richard Morrow
ACDA/VI, Room 5741
320 21st Street N.W
Washington, DC 20451

Dr. Carl Newton
Los Alamos National Laboratory
P.O. Box 1663
Mail Stop C335, Group ESS-3
Los Alamos, NM 87545

Dr. Kenneth H. Olsen
Los Alamos Scientific Laboratory
P. O. Box 1663
Mail Stop D-406
Los Alamos, NM 87545

Mr. Chris Paine
Office of Senator Kennedy
SR 315
United States Senate
Washington, DC 20510

Colonel Jerry J. Perrizo
AFOSR/NP, Building 410
Bolling AFB
Washington, DC 20332-6448

Dr. Frank F. Pilotte
HQ AFTAC/TT
Patrick AFB, FL 32925-6001

Katie Poley
CIA-ACIS/TMC
Room 4X16NHB
Washington, DC 20505

Mr. Jack Rachlin
U.S. Geological Survey
Geology, Rm 3 C136
Mail Stop 928 National Center
Reston, VA 22092

Dr. Robert Reinke
WL/NTESG
Kirtland AFB, NM 87117-6008

Dr. Byron Ristvet
HQ DNA, Nevada Operations Office
Attn: NVCG
P.O. Box 98539
Las Vegas, NV 89193

Dr. George Rothe
HQ AFTAC/TTR
Patrick AFB, FL 32925-6001

Dr. Alan S. Ryall, Jr.
DARPA/NMRO
1400 Wilson Boulevard
Arlington, VA 22209-2308

Dr. Michael Shore
Defense Nuclear Agency/SPSS
6801 Telegraph Road
Alexandria, VA 22310

Mr. Charles L. Taylor
GL/LWG
Hanscom AFB, MA 01731-5000

Dr. Larry Turnbull
CIA-OSWR/NED
Washington, DC 20505

Dr. Thomas Weaver
Los Alamos National Laboratory
P.O. Box 1663, Mail Stop C335
Los Alamos, NM 87545

GL/SULL
Research Library
Hanscom AFB , MA 01731-5000 (2 copies)

Secretary of the Air Force
(SAFRD)
Washington, DC 20330

Office of the Secretary Defense
DDR & E
Washington, DC 20330

HQ DNA
Attn: Technical Library
Washington, DC 20305

DARPA/RMO/RETRIEVAL
1400 Wilson Boulevard
Arlington, VA 22209

DARPA/RMO/Security Office
1400 Wilson Boulevard
Arlington, VA 22209

Geophysics Laboratory
Attn: XO
Hanscom AFB, MA 01731-5000

Geophysics Laboratory
Attn: LW
Hanscom AFB, MA 01731-5000

DARPA/PM
1400 Wilson Boulevard
Arlington, VA 22209

Defense Technical Information Center
Cameron Station
Alexandria, VA 22314 (5 copies)

Defense Intelligence Agency
Directorate for Scientific & Technical Intelligence
Attn: DT1B
Washington, DC 20340-6158

AFTAC/CA
(STINFO)
Patrick AFB, FL 32925-6001

TACTEC
Battelle Memorial Institute
505 King Avenue
Columbus, OH 43201 (Final Report Only)

CONTRACTORS (FOREIGN)

Dr. Ramon Cabre, S.J.
Observatorio San Calixto
Casilla 5939
La Paz, Bolivia

Prof. Hans-Peter Harjes
Institute for Geophysik
Ruhr University/Bochum
P.O. Box 102148
4630 Bochum 1, FRG

Prof. Eystein Husebye
NTNF/NORSAR
P.O. Box 51
N-2007 Kjeller, NORWAY

Prof. Brian L.N. Kennett
Research School of Earth Sciences
Institute of Advanced Studies
G.P.O. Box 4
Canberra 2601, AUSTRALIA

Dr. Bernard Massinon
Societe Radiomana
27 rue Claude Bernard
75005 Paris, FRANCE (2 Copies)

Dr. Pierre Mecheler
Societe Radiomana
27 rue Claude Bernard
75005 Paris, FRANCE

Dr. Svein Mykkeltveit
NTNF/NORSAR
P.O. Box 51
N-2007 Kjeller, NORWAY (3 copies)

FOREIGN (OTHERS)

Dr. Peter Basham
Earth Physics Branch
Geological Survey of Canada
1 Observatory Crescent
Ottawa, Ontario, CANADA K1A 0Y3

Dr. Eduard Berg
Institute of Geophysics
University of Hawaii
Honolulu, HI 96822

Dr. Michel Bouchon
I.R.I.G.M.-B.P. 68
38402 St. Martin D'Heres
Cedex, FRANCE

Dr. Hilmar Bungum
NTNF/NORSAR
P.O. Box 51
N-2007 Kjeller, NORWAY

Dr. Michel Campillo
Observatoire de Grenoble
I.R.I.G.M.-B.P. 53
38041 Grenoble, FRANCE

Dr. Kin Yip Chun
Geophysics Division
Physics Department
University of Toronto
Ontario, CANADA M5S 1A7

Dr. Alan Douglas
Ministry of Defense
Blacknest, Brimpton
Reading RG7-4RS, UNITED KINGDOM

Dr. Roger Hansen
NTNF/NORSAR
P.O. Box 51
N-2007 Kjeller, NORWAY

Dr. Manfred Henger
Federal Institute for Geosciences & Nat'l Res.
Postfach 510153
D-3000 Hanover 51, FRG

Ms. Eva Johannisson
Senior Research Officer
National Defense Research Inst.
P.O. Box 27322
S-102 54 Stockholm, SWEDEN

Dr Fekadu Kebede
Geophysical Observatory, Science Faculty
Addis Ababa University
P. O. Box 1176
Addis Ababa, ETHIOPIA

Dr. Tormod Kvaerna
NTNF/NORSAR
P.O. Box 51
N-2007 Kjeller, NORWAY

Dr. Peter Marshall
Procurement Executive
Ministry of Defense
Blacknest, Brimpton
Reading FG7-4RS, UNITED KINGDOM

Prof. Ari Ben-Menahem
Department of Applied Mathematics
Weizman Institute of Science
Rehovot, ISRAEL 951729

Dr. Robert North
Geophysics Division
Geological Survey of Canada
1 Observatory Crescent
Ottawa, Ontario, CANADA K1A 0Y3

Dr. Frode Ringdal
NTNF/NORSAR
P.O. Box 51
N-2007 Kjeller, NORWAY

Dr. Jorg Schlittenhardt
Federal Institute for Geosciences & Nat'l Res.
Postfach 510153
D-3000 Hannover 51, FEDERAL REPUBLIC OF GERMANY

Universita Degli Studi Di Trieste
Facolta Di Ingegneria
Istituto Di Miniere E. Geofisica Applicata, Trieste, ITALY